MONOGRAPH

No. 2

1996

ERKKI LOUKOLA

Simulation of a test embankment on a clay foundation according to critical state models

MONOGRAPHS
of the
Boreal Environment Research

MONOGRAPHS OF THE BOREAL ENVIRONMENT RESEARCH

2

Erkki Loukola

Simulation of a test embankment on a clay foundation according to critical state models

Yhteenveto: Savikerrokselle rakennetun koepenkereen simulointi kriittisen tilan malleilla

FINNISH ENVIRONMENT INSTITUTE, FINLAND
Helsinki 1996

Contents

Simulation of a test embankment on a clay foundation according to critical state models

Erkki Loukola

Loukola, E. 1996. Simulation of a test embankment on a clay foundation according to critical state models. Monographs of the Boreal Environment Research. Monograph No. 2, 1996.

This report presents the second part of a study aimed at solving the problems involved in constructing an earth dam on a thick clay deposit in conjunction with regulation of the River Taasianjoki. The first part of the study concerned cracking of the dam and discussed how this could be prevented. The properties of the foundation were investigated at Helsinki University of Technology. In the second part, the investigations are supplemented mainly with drained triaxial tests, and the models of the critical state are applied to the whole body of research data. All the tests and calculations of the second part were made by the author at the National Board of Waters and the Environment (later as the Finnish Environment Institute).

The behaviour of the soil layers was studied with the aid of in situ and laboratory tests. A test embankment was constructed at the site in 1980, and its settlement was monitored for fifteen years. The dry-crust clay used for the test embankment was extracted from an area adjacent to the test embankment. The laboratory studies comprised investigations of the dam material, in situ dry-crust clay and the underlying clay layer. The test embankment material was studied in the laboratory with samples taken from the test embankment. According to the laboratory tests, the materials largely obey the models based on the theory of the critical state. The soft clay layers show the greatest deviation from the models, as the samples underwent continuous volumetric strain when submitted to triaxial compression. The values for the dry-crust clay and the embankment material differed from those predicted by the model in failure stress, probably due to the differences between intact and restructured clays and to the high scatter. The dry-crust clay layer had dried and cracked in situ and was thus difficult to study. The samples taken from the test embankment behaved somewhat differently from those taken from the in situ dry-crust layer. The information produced by the study about the behaviour of different soil layers was sufficiently reliable for it to be applied in developing reference data for the critical state parameters of clay deposits in Finland. A few studies with critical state models have been conducted on soft layers and dry-crust clay in Finland, but the use of test embankments is still imperative in the planning of large dams on thick clay deposits. The critical state theory has shown its usefulness in determining the stress and strain of the dam foundation. However, other techniques must still be used to study the behaviour of the dam structure, e.g. those applied in the first part of this research project, in which the relationship of the stresses and strains of the dam material determined in the laboratory can be applied directly to simulation calculation.

Keywords: Clay foundation, critical state model, test embankment.

1 Introduction

In many countries, e.g. the USA, Canada and the UK, dams on clay foundations have been geotechnically simulated with a finite element method. A clay-foundation dam was first simulated with the finite element method in Finland in 1985, in the course of the present research project (Loukola 1985).

Planning for the Taasia reservoir and dam began at the National Board of Waters in 1979. The author was involved in the project as designer of the dam. He drew up the plans for the site investigations and the laboratory tests conducted with the National Board of Waters and was further responsible for the practical work on site and in the laboratory. For the laboratory work the project was joined by Helsinki University of Technology. The location of the study area and a map of the dam area are shown in Fig. 1. The dam was to cross a soft-bottomed river valley, where the soil is predominantly clay. Owing to the great thickness of the clay deposit, 0–35 m, the design of the dam involved many problems. These were resolved with field and laboratory studies and a test embankment.

Most of the laboratory studies for the first part of the project on the foundation were undertaken by the laboratory of soil mechanics and foundation engineering of Helsinki University of Technology (Lojander 1980, Casagrande 1980, Kallio 1980, Pitkänen 1982). Lojander made triaxial and oedometer tests on samples taken from sites at which the test embankment was later built. Casagrande performed tests to determine various mechanical parameters. His samples were collected from the other side of the dam site. Kallio made oedometer tests on the samples of Casagrande. Pitkänen undertook supplementary investigations on an inferred softer layer within the deep clay stratum and concluded that it did not exist. She also collected settlement test data on the foundation and assessed settlement of the test embankment with conventional methods.

The technical research office of the National Board of Waters investigated the dry-crust clay to be used in the dam. A test embankment was constructed at the site of the proposed dam in autumn 1980 to check the computational methods used and to plan the dam seal-off. Conventional slope stability and settlement calculations were used in the design of the dam and the test embankment. The set-

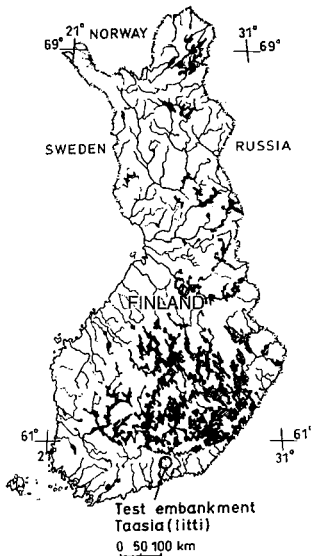

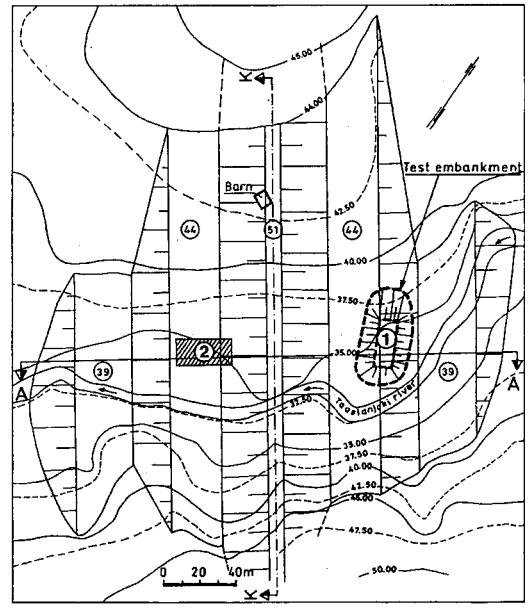

① Area studied and monitored in 1979 - 1995
② Area studied in 1980 - 1982

Fig. 1. Location of Taasia test embankment and map of dam area.

tlement and especially the cracking of the dam were also studied with finite element calculations. The computer programs were developed at the University of Alberta, Canada (Eisenstein and Krishnayya 1972, Krishnayya 1973a, 1973b).

The first part of the study, conducted using the finite element method, dealt with the investigations and research undertaken by the National Board of Waters before 1985 (Loukola 1985). The present report combines the results of these earlier investigations with the supplementary investigations made by the National Board of Waters (from 1986, the National Board of Waters and the Environment) in 1985–1995. On 1.3.1995 the Name of the Board was changed to the Finnish Environment Agency and in 1996 to the Finnish Environment Institute. The latter involved laboratory studies on soil layers and dam material, and simulation calculations applying elastic and critical state models. The author was responsible for the practical laboratory work and all the calculations.

The studies aimed to solve the key problems involved in the planning of the Taasia earth dam. The crucial question was settlement of the clay layers under the weight of the dam and the effect of settlement on the dam structure. As the dam was to rest partly on bedrock and partly on a thick clay deposit, stress would become concentrated. Thus tensional stress would develop, leading to cracking of the structure. In the first part of the study (Loukola 1985), the development of stress was simulated by taking the relationship of stresses and strains directly from a triaxial compression test as the basis of computation. In the present part of the study, models of critical state are applied, and the emphasis is on laboratory triaxial tests and simulation of the test embankment with elastic and critical state models.

Critical state models were applied to the Taasia test embankment for further study of the elastic and plastic behaviour of the test embankment and its foundation. The CRISP program were considered the most useful for this purpose. Most of the calculations are made with the 1990 version of CRISP. The results of CRISP were checked with the Z-soil program. Finally the 1994 version of CRISP was used. All the computer programs used apply finite element analysis to solve differential equations. As the finite element method was developed fairly recently it provides the best method for calculations of elastic and plastic deformations. It gives results showing the development of stresses and deformations in all parts of the calculation section.

As shown with the calculations, the models chosen gave reliable results for the test embankment settlement and pressures.

The set of computer programs used, CRISP-90, was developed at the University of Cambridge (Britto and Gunn 1987, 1990). The Z-soil model calculations were made with version PC 2.1 (Zace Services Ltd 1993). The CRISP-94 program is an improved version of CRISP-90.

Critical state models are based on an integrated theory which combines the strength and strain properties of clay. Here the Taasia clay was studied as normally consolidated and over consolidated, the latter in dry-crust and dam material. The dam material was studied in the laboratory with samples taken from the finished test embankment. Owing to the load of the test embankment, the clay deposits below the dry crust changed from the over-consolidated stress state to the normally consolidated stress state.

Critical state models have been applied to only very few real dam construction projects. Many test embankments around the world have, however, been studied with the finite element method (Leroueil et al. 1990), the critical state models in particular. These include a trial embankment at the MIT prediction symposium (Wroth 1977) and a centrifuge test (Almeida 1984). A more recent application was the EGAR road embankment in the UK (Pickles 1989). A test embankment simulation in Finland has been reported by Vepsäläinen et al. (1991).

Here the critical state models with coupled consolidation are applied to a test embankment constructed at the site of a proposed earth dam on a thick clay foundation. Various techniques were developed to test the correctness of the calculations in the whole section.

The theory of critical state coupled with Biot's consolidation theory explains what happens in a test embankment and dam foundation at the working stage better than the conventional stability and settlement approach. When the settlement and pore water pressure calculated with experimentally determined parameters are compared with the monitoring data on the test embankment, approximate values for the critical state parameters of the Taasia clay can be deduced. Three different sets of critical state soil models were used.

This thesis defines the critical state parameters

that can be used in the design of the proposed dam and, in particular, the settlement properties of the foundation, thus enabling the proper choice of embankment construction schedule to be made. Clay samples were taken from two adjacent layers of the test embankment foundation and from the test embankment itself and submitted to different laboratory tests. That way the behaviour of clay in the lightly over-consolidated state, in the natural, heavily over-consolidated state and in the compacted, over-consolidated state could be compared. In the final calculation the normally consolidated state was also considered.

Sensitivity analysis was used to determine the contribution of different parameters to the calculated value of test embankment settlement. The data on the Taasia clay are compared with those from other investigations of clay deposits.

The critical state theory is described in Chapter 2. The programs used are explained in Chapter 3. The construction of the test embankment and the laboratory and site investigations are dealt with in Chapter 4. The laboratory and site investigations include index properties, undrained strength properties and, particularly, strength and strain properties tested by triaxial and oedometer tests. Chapter 5 explains the calculations made in the study. The results are discussed in Chapter 6, which includes a comparison of the calculated results with measurements made on site, a sensitivity analysis, the influence of error factors and a comparison with other investigations. Conclusions are drawn in Chapter 7. The summary is given in Chapter 8.

2 Basic theories used in the models

2.1 The critical state models

The classical development of critical state models took place at the University of Cambridge, starting in the late 1950s (Roscoe et al. 1958, 1959, 1963, Roscoe and Poorooshasb 1963, Schofield and Wroth 1968, Roscoe and Burland 1968, Atkinson 1981, Atkinson and Bransby 1978, Houlsby et al. 1982, Wroth 1984, Houlsby 1985). The work done there showed that changes in effective stresses and volume changes in soils can be combined to build a general picture of soil behaviour.

Stress invariants

Soil behaviour as a function of the effective stresses has mainly been expressed by two invariants, the mean effective stress and the deviator stress, which, in three-dimensional space, are defined by equations (1) and (2)

$$p' = \frac{1}{3}(\sigma_1' + \sigma_2' + \sigma_3') \tag{1}$$

where

p' = mean effective stress
σ_1' = maximum effective principal stress
σ_2' = intermediate effective principal stress
σ_3' = minimum effective principal stress

$$q = \frac{1}{\sqrt{2}}[(\sigma_1 - \sigma_2)^2 + (\sigma_2 - \sigma_3)^2 + (\sigma_3 - \sigma_1)^2]^{1/2} \tag{2}$$

where

q = deviator stress
σ_1 = maximum principal stress
σ_2 = intermediate principal stress
σ_3 = minimum principal stress

The mean effective stress is one third of the first effective stress invariant I_1' (3)

$$I_1' = \sigma_x' + \sigma_y' + \sigma_z' \tag{3}$$

where

I_1' = first effective stress invariant
σ_x' = effective stress in x-direction
σ_y' = effective stress in y-direction
σ_z' = effective stress in z-direction

The deviator stress is related to the second invariant of the stress deviation J_2

$$q = \sqrt{3J_2} \tag{4}$$

where

J_2 = second invariant of stress deviation.
It is defined by equations (5) – (8)

$$J_2 = \frac{1}{2}(s_1^2 + s_2^2 + s_3^2) \tag{5}$$

where

$$s_1 = (2\sigma_1 - \sigma_2 - \sigma_3)/3 \tag{6}$$

$$s_2 = (2\sigma_2 - \sigma_1 - \sigma_3)/3 \tag{7}$$

$$s_3 = (2\sigma_3 - \sigma_1 - \sigma_2)/3 \quad (8)$$

where

s_1, s_2, s_3 = principal stress deviations

The invariants I_1 and J_2 are used in the Drucker-Prager criterion, which will be explained in conjunction with the Z-soil program.

In order to completely define a stress state, a third stress invariant is also needed. In tensor form it is defined by the equation (9)

$$J_3 = \frac{1}{3} s_{ij} s_{jk} s_{ki} \quad (9)$$

where

J_3 = the third invariant of stress deviation
s_{ij}, s_{jk} and s_{ki} are deviatoric stress tensors

The angular measure of the third invariant of the stress deviation J_3 is defined by equation (10) (Nayak and Zienkiewicz 1972)

$$\theta = \frac{1}{3} \sin^{-1} \left(\frac{-3\sqrt{3}}{2} \frac{J_3}{J_2^{3/2}}\right); \frac{\pi}{6} \geq \theta \geq -\frac{\pi}{6} \quad (10)$$

where

θ = the Lode angle

In soil modelling, the dependence of this third stress invariant is often neglected, for instance, for clays, but should be accounted for when dealing with non-cohesive coarse-grained soils.

In the stress state corresponding to the standard triaxial test ($\sigma_2 = \sigma_3$), the invariants p' and q are obtained from equations (11) and (12)

$$p' = \frac{\sigma_1' + 2\sigma_3'}{3} = \frac{\sigma_1 + 2\sigma_3}{3} - u \quad (11)$$

where

u = pore water pressure

$$q = \pm(\sigma_1 - \sigma_3) = (\sigma_1' - \sigma_3') \quad (12)$$

Strain invariants

The strain invariants generally used in soil modelling are the volumetric strain and the second deviatoric strain invariant (the shear strain). The volumetric strain, i.e. the first strain invariant, is given by equation (13)

$$\varepsilon_v = \varepsilon_x + \varepsilon_y + \varepsilon_z = \varepsilon_1 + \varepsilon_2 + \varepsilon_3 \quad (13)$$

where

ε_v = volumetric strain
ε_x = strain in x-direction
ε_y = strain in y-direction
ε_z = strain in z-direction
ε_1 = strain in direction of maximum principal stress
ε_2 = strain in direction of intermediate principal stress
ε_3 = strain in direction of minimum principal stress

Under the conditions of the triaxial test ($\varepsilon_2 = \varepsilon_3$), the volumetric strain is expressed by (14)

$$\varepsilon_v = \varepsilon_1 + 2\varepsilon_3 \quad (14)$$

The second deviatoric strain invariant (the shear strain) is given by the general equation (15)

$$\varepsilon_s = \frac{1}{3}\{2[(\varepsilon_x - \varepsilon_y)^2 + (\varepsilon_y + \varepsilon_z)^2 + (\varepsilon_z - \varepsilon_x)^2] + 3(\varepsilon_{s(yz)}^2 + \varepsilon_{s(zx)}^2 + \varepsilon_{s(xy)}^2)\}^{1/2} \quad (15)$$

where

ε_s = second deviatoric strain invariant (shear strain)
$\varepsilon_{s(yz)}$ = shear strain in yz-plane
$\varepsilon_{s(zx)}$ = shear strain in zx-plane
$\varepsilon_{s(xy)}$ = shear strain in xy-plane

In the case of the standard triaxial tests with strains in the principal directions, the second deviatoric strain invariant is given by equation (16)

$$\varepsilon_s = \frac{2}{3}(\varepsilon_1 - \varepsilon_3) \quad (16)$$

The critical state theory

In general, the critical state theory treats the stresses and strains in the triaxial (p',V,q)-space.

The specific volume V is obtained from equation (17)

$$V = 1 + e \tag{17}$$

where

V = specific volume
e = void ratio

According to the critical state theory, the behaviour of soils in the (p', V, q)-space is controlled by the stable state boundary surface (Fig. 2), in the inner side of which deformations are elastic. If the point representing the stress state is on the surface, the deformations are plastic.

In the p', q-plane the stable state boundary surface forms what is known as a yield locus. When a point representing the mechanical state of soil in the (p', V, q)-space moves on the stable state boundary surface, the yield locus moves in the p', q-plane. The strain continues until the stress reaches the critical state at which the soil yields without changes in stress ratio and volume (or void ratio).

Once the stresses reach the critical state, their ratio (q / p') reaches a constant value of M as shown by equation (18). In the $\ln(p')$, V-plane, the critical state is reached on line (19) (Schofield and Wroth 1968)

$$q = Mp' \tag{18}$$

$$V = \Gamma - \lambda \ln(p') \tag{19}$$

where

Γ determines the position of the critical state line in the $\ln(p')$, V-plane. Γ equals V when p' is 1 kPa (Fig. 3).

λ = parameter of total volumetric strain, or the absolute value of the slope of the critical state line

M = the ratio of stresses q and p' in the critical state as shown by equation (20)

$$M = \left(\frac{q}{p'}\right)_{cs} \tag{20}$$

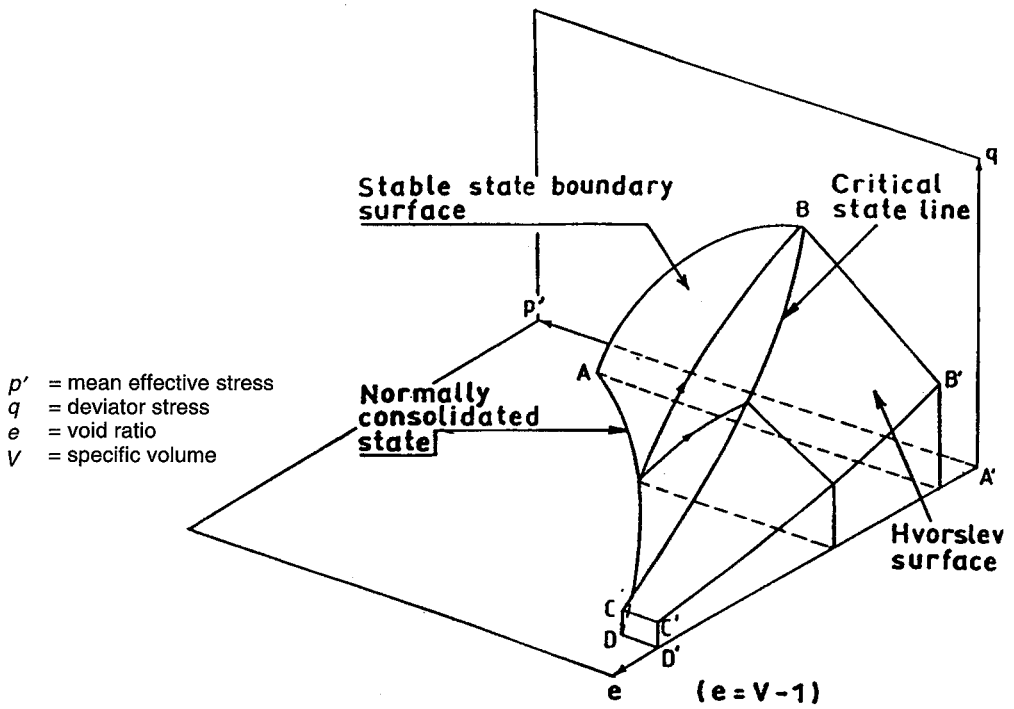

Fig. 2. Stable state boundary surface (Roscoe and Burland 1968).

According to equation (19), the relation between compression stresses and specific volume in the critical state is a straight line in the $\ln(p')$, V-plane. The straight lines of compression are important in other compression conditions, too.

The parameter M in triaxial compression is related to the friction angle ϕ_{cs}' as shown by equation (21) (Schofield and Wroth 1968)

$$M = \frac{6\sin\phi_{cs}'}{(3-\sin\phi_{cs}')} \tag{21}$$

where

ϕ_{cs}' = angle of friction between soil grains in the critical state.

In the $\varepsilon_s, \varepsilon_v$-plane the ratio of strain increments follows equation (22) in the critical state

$$\frac{\delta\varepsilon_v}{\delta\varepsilon_s} = 0 \tag{22}$$

According to the critical state theory, isotropic compression in the normally consolidated state, swell at the reduction in load, and compression in the over-consolidated state can be described with straight lines on the $\ln(p')$, V-plane as shown in Fig. 3

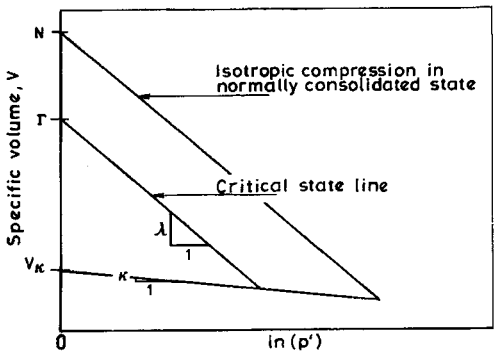

p' = mean effective stress

Fig. 3. Critical state line in ln (p'), V-coordinate system (Schofield and Wroth 1968).

Isotropic compression in the normally consolidated state is expressed by line (23) in the $\ln(p')$, V-plane

$$V = N - \lambda \ln(p') \tag{23}$$

where

N = V when p' = 1 kPa.

According to equations (19) and (23), the critical state line in the $\ln(p')$, V-plane is a straight line parallel to the consolidation line describing isotropic compression in the normally consolidated state. Likewise a straight line and parallel to the above lines is the line of anisotropic compression in the normally consolidated state [equation (24)]

$$V = V_\lambda - \lambda \ln(p') \tag{24}$$

where

V_λ = a general form of the parameters corresponding to parameter N in different states of anisotropy. One of them is K_o consolidation, which will be described later in this section.

Swell at the reduction in load and recompression in the over-consolidated state are described by the line defined by equation (25)

$$V = V_\kappa - \kappa \ln(p') \tag{25}$$

where

V_κ = V when p' = 1 kPa. The value of V_κ depends on the prevailing preconsolidation stress.

Equation (25) shows that the unloading/reloading relation is a straight line in the $\ln(p')$, V-plane.

Original Cam Clay

In the original Cam-Clay model the yield criterion obeys equation (26), (Fig. 4) (Schofield and Wroth 1968)

$$f = \frac{q}{Mp'} + \ln\left(\frac{p'}{p_u'}\right) - 1 = 0 \tag{26}$$

where

f = yield function
p_u' = p' at the intersection of the yield curve and critical state line.

a

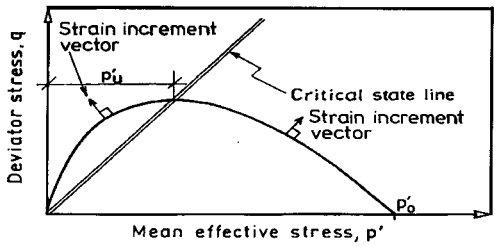

$$\frac{|q|}{Mp'}+\ln(\frac{p'}{p_u'})=1$$

(a) Cam-Clay (Schofield and Wroth 1968)

b

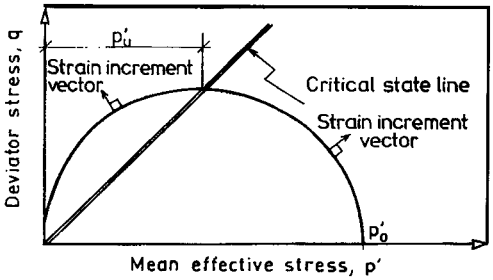

$$q^2+M^2p'^2=M^2p'p'_0$$

(b) Modified Cam-Clay (Roscoe and Burland 1968)

Fig. 4. Yield surfaces of critical state models. Models are included in CRISP-90.

The yield function is logarithmic, corresponding to a yield locus in the p',q-plane having its maximum at the critical state line for $p'=p_u'$ and intersecting the p'-axis at the preconsolidation pressure, p_o', see Fig. 4a.

It is assumed that the plastic strain vector is perpendicular to the yield loqus, see Fig. 4a. Thus equation (27) holds

$$\frac{dq}{dp'}=-\frac{d\varepsilon_v^p}{d\varepsilon_s^p} \tag{27}$$

corresponding to the associated plastic flow.

On the right-hand side of the maximum value of q the soil is said to be in a wet condition and on the left-hand side in a dry condition. In the former, the change in volume is positive, i.e. the material shrinks. In the dry condition, the change is negative, i.e. dilatation takes place.

In the $\ln(p'),V$-plane the yield surface and the critical state coincide at the intersection of the κ-line (equation 25) and the critical state line where the pair of equations, (28) and (29), hold (Schofield and Wroth 1968)

$$V+\kappa\ln(p')=V_u+\kappa\ln(p_u') \tag{28}$$

$$V_u=\Gamma-\lambda\ln(p_u') \tag{29}$$

By eliminating V_u and p_u' from these equations and from equation (26), the value of q can be calculated on the yield locus from equation (30)

$$|q|=\frac{Mp'}{\lambda-\kappa}[\Gamma+\lambda-\kappa-V-\lambda(\ln p')] \tag{30}$$

From equations (24) and (30), V_λ can be written in the form of equation (31)

$$V_\lambda=\Gamma+(\lambda-\kappa)(1-\frac{\eta}{M}) \tag{31}$$

where

$$\eta=\frac{q}{p'}$$

In isotropic consolidation $\eta = 0$. Equation (31) changes to the form (32)

$$V_\lambda=N=\Gamma+\lambda-\kappa \tag{32}$$

When equation (23) or (24) is differentiated, the change in total volume is found to follow equation (33)

$$\delta V=-\lambda\left(\frac{\delta p'}{p'}\right) \tag{33}$$

Differentiation of equation (25) gives equation (34)

$$\delta V^e=-\kappa\left(\frac{\delta p'}{p'}\right) \tag{34}$$

where

δV^e = elastic change in specific volume

The plastic change in specific volume is obtained from equation (35)

$$\delta V^p=\delta V-\delta V^e \tag{35}$$

where

δV = change in specific volume
δV^p = plastic change in specific volume

Equation (35) can be written (by applying (33) and (34)) as equation (36)

$$\delta V^p = (\kappa - \lambda)\left(\frac{\delta p'}{p'}\right) \tag{36}$$

From equation (30) and equations (32)–(36) equations (37) and (38) are derived for the plastic change in volume strain

$$\delta\varepsilon_v^p = \frac{-\delta V^p}{V} = (\lambda - \kappa)\frac{\delta p'}{V p'} \tag{37}$$

$$\delta\varepsilon_v^p = \frac{\lambda - \kappa}{MVp'}[(M - \frac{q}{p'})\delta p' + \delta q] \tag{38}$$

where

$\delta\varepsilon_v{}^p$ = plastic change in volume strain

As equation (37) can be applied when $p' = p_o'$ equation (39) is derived

$$\delta p_o' = \delta\varepsilon_v{}^p V p_o' / (\lambda - \kappa) \tag{39}$$

Equation (39) shows that the preconsolidation pressure p_o' can be used as the hardening parameter of the yield locus. As the yield locus expands during consolidation or during shearing with different stress ratios or stress paths, the preconsolidation pressure p_o' show the size of the yield locus.

As p_o' is only a function of plastic change in volume strain, the hardening is called volumetric hardening.

One of the fundamental features of the Cam-Clay model is that yield obeys the condition of normality. As the vector of the plastic strain increment is always normal to the yield locus, equation (40) holds

$$\frac{d\varepsilon_v^p}{d\varepsilon_s^p} = M - \frac{q}{p'} \tag{40}$$

where

ε_s^p = plastic shear strain

By solving equation (40) for $d\varepsilon_s^p$, equation (41) can be obtained

$$\delta\varepsilon_s^p = \frac{1}{[M - (q/p')]}\delta\varepsilon_v^p \tag{41}$$

Modified Cam Clay

The Modified Cam-Clay model, which differs from the original model in the equation of the yield locus, was developed at the University of Cambridge to eliminate drawbacks found in the original Cam-Clay model (Roscoe and Burland 1968).

In the Modified Cam-Clay model, the yield locus in the p', q-plane is an ellipse, see Fig. 4b. Its equation is expressed in the form (42)

$$f = M^2 p'(p' - p_o') + q^2 = 0 \tag{42}$$

where

p_o' = the preconsolidation pressure, i.e. the intersection of the stable state boundary surface and the p'-axis in the p', q-plane.

This yield locus has its maximum at the critical state at which the ellipse is symmetrical. The value of p' at the critical state is half of p_o'.

In the Modified Cam-Clay model the difference given by equation (32) in the original Cam-Clay model

$$N - \Gamma = \lambda - \kappa \tag{32bis}$$

changes into (43)

$$N - \Gamma = (\lambda - \kappa)\ln 2 \tag{43}$$

The work equations

When an element of soil is subjected to a stress-increment (p', q) it undergoes strain-increments $\delta\varepsilon_v$ and $\delta\varepsilon_s$. The work dissipated is expressed by equation (44) (original Cam Clay)

$$\delta W = p'\delta\varepsilon_v + q\delta\varepsilon_s \tag{44}$$

where

δW = dissipated work

For the plastic strain the dissipated work follows equation (45) (Roscoe et al. 1963) (original Cam Clay)

$$\delta W = Mp'\delta\varepsilon \tag{45}$$

For the plastic-strain increment ratio, equation (46) applies

$$\Psi = \frac{\delta\varepsilon_v}{\delta\varepsilon_s} = M - \eta \tag{46}$$

where

Ψ = plastic-strain increment ratio

For the Modified Cam-Clay model the work equation becomes (47)

$$\delta W = p'\sqrt{(d\varepsilon_v)^2 + M^2(d\varepsilon_s)^2} \tag{47}$$

It leads to equation (48)

$$\Psi = \frac{\delta\varepsilon_v}{\delta\varepsilon_s} = \frac{M^2 - \eta^2}{2\eta} \tag{48}$$

In the normally consolidated state the soil elements in deep soil layers are in the K_o-condition, where radial strains (ε_3) are zero. In such a state the value of Ψ = 3/2. By solving equation (48), equation (49) can be obtained for the compressive side

$$\eta_{K_o} = -\frac{3}{2} + \sqrt{(\frac{3}{2})^2 + M^2} \tag{49}$$

As (48) will be substituted into the basic equations, equations (50), (51) and (52) can be obtained (Roscoe and Burland 1968)

$$d\varepsilon_v^p = \frac{\lambda - \kappa}{V}(\frac{dp'}{p'} + \frac{2\eta d\eta}{M^2 + \eta^2}) \tag{50}$$

$$d\varepsilon_v = \frac{\lambda}{V}[\frac{dp'}{p'} + (1 - \frac{\kappa}{\lambda})\frac{2\eta d\eta}{M^2 + \eta^2}] \tag{51}$$

$$d\varepsilon_s^p = \frac{\lambda - \kappa}{V}(\frac{dp'}{p'} + \frac{2\eta d\eta}{M^2 + \eta^2})\frac{2\eta}{M^2 - \eta^2} \tag{52}$$

2.2 Soil modelling within the theory of elasticity

The theory of elasticity has its basis in Hooke's law. As the varved clay structure is mainly horizontal, Hooke's law has been extended to apply to cross anisotropic material. The associated soil fabric and stress history lead to one set of properties for the $x-z$ (or h) -plane and to another set for vertical directions (v or y) and coupling between the horizontal and vertical directions. The basic equations are (53–58)

$$\varepsilon_x^e = \frac{1}{E_h}\sigma_x - \frac{\nu_{vh}}{E_v}\sigma_y - \frac{\nu_{hh}}{E_h}\sigma_z \tag{53}$$

$$\varepsilon_y^e = -\frac{\nu_{hv}}{E_h}\sigma_x + \frac{1}{E_v}\sigma_y - \frac{\nu_{hv}}{E_h}\sigma_z \tag{54}$$

$$\varepsilon_z^e = -\frac{\nu_{hh}}{E_h}\sigma_x - \frac{\nu_{vh}}{E_v}\sigma_y + \frac{1}{E_h}\sigma_z \tag{55}$$

$$\varepsilon_{s(xy)} = \frac{1}{G_{vh}}\tau_{xy} \tag{56}$$

$$\varepsilon_{s(yz)} = \frac{1}{G_{hv}}\tau_{yz} \tag{57}$$

$$\varepsilon_{s(zx)} = \frac{1}{G_{vh}}\tau_{zx} \tag{58}$$

where

ε_x^e = elastic strain in x-direction (horizontal)
ε_y^e = elastic strain in y-direction (vertical)
ε_z^e = elastic strain in z-direction (horizontal)
σ_x = stress in x-direction (horizontal)
σ_y = stress in y-direction (vertical)
σ_z = stress in z-direction (horizontal)
E_h = horizontal modulus of elasticity
E_v = vertical modulus of elasticity
ν_{vh} = Poisson's ratio (effect of horizontal force on vertical strain)
ν_{hh} = Poisson's ratio (effect of horizontal force on horizontal strain)
ν_{hv} = Poisson's ratio (effect of vertical force on horizontal strain)
$\varepsilon_{s(xy)}$ = shear strain in xy-plane
$\varepsilon_{s(yz)}$ = shear strain in yz-plane
$\varepsilon_{s(zx)}$ = shear strain in zx-plane
G_{vh} = shear modulus (effect of horizontal forces in vertical plane)
G_{hv} = shear modulus (effect of vertical forces in horizontal plane)
τ_{xy} = shear stress in xy-plane
τ_{yz} = shear stress in yz-plane
τ_{zx} = shear stress in zx-plane

Equations 53–58 can be written in matrix form (59)

$$\begin{bmatrix} \varepsilon_x^e \\ \varepsilon_y^e \\ \varepsilon_z^e \\ \varepsilon_{s(xy)} \\ \varepsilon_{s(yz)} \\ \varepsilon_{s(zx)} \end{bmatrix} = \begin{bmatrix} 1/E_h & -\nu_{vh}/E_v & -\nu_{hh}/E_h & O & O & O \\ -\nu_{hv}/E_h & 1/E_v & -\nu_{hv}/E_h & O & O & O \\ -\nu_{hh}/E_h & -\nu_{vh}/E_v & 1/E_h & O & O & O \\ O & O & O & 1/G_{vh} & O & O \\ O & O & O & O & 1/G_{hv} & O \\ O & O & O & O & O & 1/G_{vh} \end{bmatrix} \begin{bmatrix} \sigma_x \\ \sigma_y \\ \sigma_z \\ \varepsilon_{s(xy)} \\ \varepsilon_{s(yz)} \\ \varepsilon_{s(zx)} \end{bmatrix} \quad (59)$$

In equations (53)–(59), the strains due to compression are positive and those due to elongation negative. Similarly, the decrease in volume is positive.

The values of ν_{hv} and ν_{vh} are related to each other. In accordance with the law of the conservation of energy, ν_{vh} and ν_{hv} obey equation (60)

$$\frac{\nu_{hv}}{E_h} = \frac{\nu_{vh}}{E_v} \quad (60)$$

The shear modulus G is related to the corresponding modulus of elasticity E and Poisson's ratio ν as in equation (61)

$$G = \frac{E}{2(1+\nu)} \quad (61)$$

where

G = shear modulus
E = modulus of elasticity
ν = Poisson's ratio

Poisson's ratio can be determined from the measurements in triaxial tests or with the aid of the coefficient of earth pressure at rest, K_o, which is the ratio of the principal effective stresses. It obeys equation (62)

$$K_o = \frac{\sigma_3'}{\sigma_1'} = \frac{\sigma_3 - u}{\sigma_1 - u} \quad (62)$$

where

K_o = coefficient of earth pressure at rest
u = pore water pressure

For K_o in a normally consolidated state, i.e. K_{nc}, Jaky (1944) derived an empirical equation (63)

$$K_{nc} = (1 + \tfrac{2}{3}\sin\phi')\left(\frac{1-\sin\phi'}{1+\sin\phi'}\right) \quad (63)$$

where

K_{nc} = coefficient of earth pressure at rest in normally consolidated soil
ϕ' = effective friction angle

Jaky also proposed a simplified empirical formula (64)

$$K_{nc} = 0.9(1-\sin\phi') \quad (64)$$

This has since been widely used in the form (65)

$$K_{nc} = 1-\sin\phi' \quad (65)$$

Equation (65) is applicable when used with the effective friction angle of the critical state.

Several equations have been proposed for the relation of K_o to the over-consolidation ratio (*OCR*).

When determined during the unloading phase, K_o can be calculated from an empirical formula (66) (Wroth 1975). It applies to lightly over-consolidated soil (*OCR* up to 5).

$$K_o = OCR\,K_{nc} - \frac{\nu'}{1-\nu'}(OCR-1) \quad (66)$$

where

OCR = over-consolidation ratio
ν' = effective Poisson's ratio

OCR is obtained from equation (67)

$$OCR = \frac{\sigma'_{vc}}{\sigma'_v} \quad (67)$$

where

σ'_{vc} = maximum vertical effective stress = preconsolidation stress
σ'_v = vertical effective stress

If K_o and K_{nc} in equation (66) have been measured in the laboratory, v' can be derived from equation (68)

$$v' = \frac{OCR\,K_{nc} - K_o}{OCR\,K_{nc} - K_o + OCR - 1} \tag{68}$$

Instead of equation (66), an empirical relation between K_o and OCR is obtained from equation (69) (Parry 1982)

$$K_o = K_{nc}\,(OCR)^{\phi'} \tag{69}$$

where

ϕ' = angle of friction in terms of effective stress (in radians)

The preconsolidation stress, σ'_{vc}, can be determined with an oedometer or it can be estimated roughly from the empirical equation of the plasticity index and the unconfined shear strength (70) (Skempton 1957)

$$\frac{c_u}{\sigma'_{vc}} = 0.11 + 0.0037\,I_p \tag{70}$$

where

c_u = unconfined shear strength
I_p = plasticity index
σ'_{vc} = preconsolidation stress

3 Programs used in simulation

3.1 Choosing the models used in calculations

The clay foundation to be modelled consists of a dry-crust top layer underlain by a deep clay layer. The test embankment was built using dry-crust clay as embankment material. The section to be modelled contains both heavily over-consolidated and lightly over-consolidated clay layers and a heavily over-consolidated compacted embankment structure. The normally consolidated state must also be taken into consideration after loading. Consolidation of clay layers is essential in the Taasia case.

The programs chosen contain soil models for each of the consolidation states and different types of yield conditions.

3.2 The CRISP-90 program

3.2.1 Structure of the program and material models

The simulation of the test embankment on clay deposits was carried out with the CRISP-90 program, a finite element program including different soil models and capable of analysing coupled problems, too. The principles of the program were described by Britto and Gunn (1987).

This FEM-program permits the use of triangular or quadrilateral elements (2-dimensional calculation) or hexahedral elements (3-dimensional calculation). It calculates both displacement and pore water pressure. The changes in pore water pressure are calculated as a function of time from the general consolidation equation of Biot (1941).

The program comprises six different material models:

1 elastic, anisotropic/isotropic
2 elastic, changing linearly with depth
3 Modified Cam-Clay
4 Cam-Clay
5 elastic, perfectly plastic
6 Schofield model

The parameters used in the different models are explained in Table 1.

The CRISP-90 program restricts the use of models, and so the Modified Cam-Clay, Cam-Clay and Schofield models, which require information about the stress history of the material, cannot be employed in elements simulating construction.

Here the elastic, anisotropic/isotropic and elastic, perfectly plastic models were used for the dam structure, and the Modified Cam-Clay, elastic, perfectly plastic and Schofield models for the dry-crust layer and the underlying clay layers. In the elastic, perfectly plastic model, the Mohr-Coulomb failure criterion was used. For the dam structure, the elastic, anisotropic/isotropic model, the elastic, changing linearly with depth model and the elastic, perfectly plastic model could be applied. The elastic, changing linearly with depth model was not used because the dam structure was fairly homogeneous. In an earlier analysis (Pickles 1989)

Table 1. Material models available in CRISP 90 program (Britto and Gunn 1990).

NTY property	1	2	3	4	5	6
P(1)	E_h	E_o	κ	κ	E_o	κ
P(2)	E_v	y_0	λ	λ	ν	λ
P(3)	ν_{hh}	m	e_{cs}	e_{cs}	c_o	e_{cs}
P(4)	ν_{vh}	ν	M	M	ϕ	M
P(5)	G_{hv}	0	$Gorv'$	$Gorv'$	y_0	$Gorv'$
P(6)	0	0	0	0	J	0
p(7)**	← ——— 0 for drained, K_w for undrained, γ_w for consolidation ——— →					
P(8)	← ——————————— γ ——————————— →					
P(9)**	← ——— k_x for consolidation, 0 for drained or undrained ——————— →					
P(10)**	← — k_y for consolidation, 0 for drained or undrained ——————————— →					
P(11)	0	0	0	0	m_E	H
P(12)	0	0	0	0	m_c	S
P(13)						0
P(14)		not present for models 1 to 5				0
P(15)						k_{xt}
P(16)						k_{yt}

NTY - material property type
- 1 - elastic, isotropic/anisotropic
- 2 - elastic, linear variation with depth
- 3 - Modified Cam-Clay (MCC)
- 4 - Cam-Clay (CC)
- 5 - elastic, perfectly plastic (see parameter J below)
- 6 - The Scholfield soil model (SCH) (requires 16 properties)

** these material properties are dependent on the element *types.*

For the Schofield soil model material properties P(13) to P(16) are input in a second line.

6th property for model number 5:

J - yield criterion
- 1 - von Mises
- 2 - Tresca
- 3 - Drucker-Prager
- 4 - Mohr-Coulomb

In the above

γ	-	unit weight of soil
k_x, k_y	-	coefficients of permeability in x- and y-directions
γ_w	-	unit weight of water
k_w	-	bulk modulus of water
k_{xt}, k_{yt}	-	coefficients of permeability in tensile crack region
E_o	-	Young's modulus at y_o
m_E	-	rate of increase in Young's modulus with depth
H	-	slope of Hvorslev surface along constant volume section in p', q-space
S	-	slope of tensile crack region in p', q-space
m_c	-	rate of increase in shear strength with depth
c_o	-	cohesion at $y = y_o$
G	-	shear modulus
ν	-	Poisson's ratio

an elastic, perfectly plastic model with the Mohr-Coulomb yield criterion was found to represent embankment fill better than the other soil models available in CRISP. The elastic, anisotropic/isotropic model served as the basic model for the embankment because the embankment behaves in an elastic manner in the construction simulation stage.

For modelling of the dry crust layer, both the elastic and the critical state models were available. Of the critical state models, Modified Cam-Clay model and the Schofield model were chosen as two different approaches. The Modified Cam-Clay model comprises an even, nonlinear yield surface (Fig. 4b), and the Schofield model involves use of the Hvorslev failure criterion (Fig. 5). The Schofield model was used with an assigned value of isotropic consolidation stress to ensure that the test results and the model curve meet at the most important stress level.

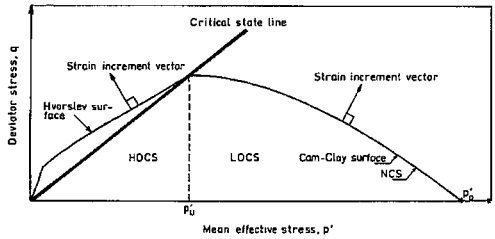

HOCS = heavily overconsolidated state
LOCS = lightly overconsolidated state
NCS = normally consolidated state

$$q=(M-H)p_u(p/p_u)+Hp'$$

Fig. 5. Schofield soil model (Britto and Gunn 1990). Division of stress region into subregions in p',q-coordinate system (Atkinson 1981). The model is included in CRISP-90.

In addition to the data on material behaviour, the CRISP-90 program is given known stresses, pore water pressures, displacements and tractions and their directions as initial and boundary conditions.

The software consists of a geometric program and a principal program (Britto and Gunn 1990). The geometric program generates the element mesh used in the calculations. The element type and the numbering and coordinates of the elements and their nodes are given as starting values.

The principal program with its numerous subprograms executes the calculation proper. The program, which is given data on materials and the boundary conditions as starting values, calculates stresses and strains in accordance with given periods. The construction is simulated as taking place in steps. The periods can be divided into subperiods.

3.2.2 Behaviour models for normally consolidated clay

The normally consolidated soft clay deposits were simulated with the Modified Cam-Clay and Schofield models.

The Modified Cam-Clay model applies the elliptical form of the yield curve, which is superior to the original Cam-Clay yield curve. The Hvorslev failure criterion applies the linear failure model to the over-consolidated state as explained in the next section. The original Cam-Clay model is used only for the part of the yield curve near the critical state and thus its influence will be small.

3.2.3 Behaviour models for over-consolidated clay

In the p',q-plane (Fig. 5) the over-consolidation state (i.e. the elastic state) in the Schofield model is limited by a yield curve on which the soil is normally consolidated; by the Hvorslev surface, where the soil is in a failure state; and by the tensile crack region.

The stress states of over-consolidated soils are usually divided into heavily and lightly over-consolidated regions in the p',q-plane, as shown in Fig. 5 (Atkinson 1981). The soil is said to be heavily over-consolidated for stress state in the p',q-plane is on the left-hand side of the critical state, and lightly over-consolidated on the right-hand side. The division corresponds to the division of soils into dry and wet stress-strain classes.

In the course of their history the over-consolidated soil layers have been under stresses higher than those currently prevailing. At stresses lower than the previous maximum stress (preconsolidation stress) these layers behave in accordance with the model of over-consolidated clay. At stresses exceeding the preconsolidation stress the soil behaves as normally consolidated.

Over-consolidated clays can be modelled with models made specifically for them or with the elastic and elastic/plastic models. In this study the Modified Cam-Clay model and the Schofield

model were also used in the calculation of deformations of over-consolidated dry crust.

The models developed for over-consolidated clays include the Schofield model (in CRISP-90) and the Roscoe–Hvorslev model. The former was developed from the original Cam-Clay model and the latter from the Modified Cam-Clay model (Houlsby et al. 1982, Britto and Gunn 1990). The clay in the models fails in accordance with Hvorslev's failure theory (Hvorslev 1937) (Fig. 5). The normally consolidated stress state is treated in the Schofield model in the same way as in the Cam-Clay model (Fig. 5), and in the Roscoe–Hvorslev model in the same way as in the Modified Cam-Clay model (Fig. 6).

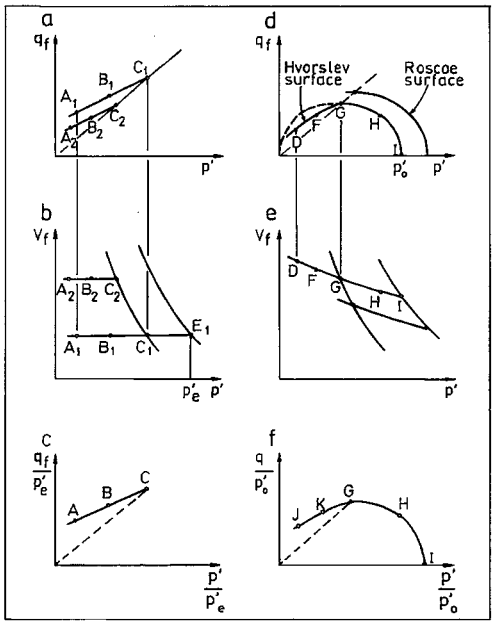

p' = mean effective stress
q = deviator stress at failure
V_f = specific volume at failure

Fig. 6. Determination of Hvorslev failure surface (Houlsby et al. 1982).

According to Hvorslev's failure theory (Hvorslev 1937), samples that fail at the same water content (water-saturated samples at the same specific volume) form a line in the p',q_f-plane in the over-consolidation region (Fig. 6a). ($q_f = q$ in the failure state). These lines end on the critical state line. Failure lines determined at different water contents (specific volumes) can be normalised by dividing the values of p' and q_f by the pressure obtained from the normal consolidation curve corresponding to the prevailing water content (specific volume) (Fig. 6b and c).

Hvorslev's surface and the stable state boundary surface of the Modified Cam-Clay model are combined in Fig. 6d and e. Laboratory data can be normalised by dividing the p′ and q-values by the isotropic preconsolidation pressure p'_o (Fig. 6f).

In the classical development of critical state models (Schofield and Wroth 1968, Roscoe and Burland 1968), elastic shear strains are assumed to be zero. As this assumption would result in division by zero in calculations of the finite element method based on displacement, the Modified Cam-Clay, Cam-Clay and Schofield models of the CRISP program utilize the properties with which the non-zero elastic shear strains are calculated. The elastic properties are given to the program as a single number, which the program recognizes owing to its value. If the value is less than 0.5 it is Poisson's ratio; higher numbers refer to the shear modulus. The elastic bulk modulus caused by the effective stresses is obtained from equation (71)

$$K' = \frac{E'}{3(1-2\nu')} = \frac{Vp'}{\kappa} \qquad (71)$$

where

K' = elastic bulk modulus (effective stresses)

The equation was obtained by differentiating the equation of the κ line [equation (25)].

Shear strain was calculated by giving Poisson's ratio ν' (effective Poisson's ratio) a constant value. The elastic shear modulus G then varied in the same way as did the elastic bulk modulus K'.

Addition of the extra elastic strains makes very little difference to the predictions of Cam-Clay models (Britto and Gunn 1987). The effect of the values of the effective Poisson's ratio is dealt with in Section 6.2.

In the elastic, perfectly plastic model with the Mohr-Coulomb failure criterion, the yield surface and the failure surface coincide. The failure surface is expressed by equation (72)

$$\sigma_1' - \sigma_3' = \sin\phi''(\sigma_1' + \sigma_3' + 2c'\cot\phi') \qquad (72)$$

where

ϕ' = angle of friction in terms of effective stresses (degrees)
c' = cohesion intercept in terms of effective stresses

This equation can be expressed in general form (72a) (Naylor 1978)

$$q = Mp' + N \tag{72a}$$

where

$$M = \frac{3\sin\phi}{\sqrt{3}\cos\theta - \sin\theta\sin\phi} \tag{72b}$$

$$N = \frac{3c\cos\phi}{\sqrt{3}\cos\theta - \sin\theta\sin\phi} \tag{72c}$$

θ = Lode angle
ϕ = angle of friction
c = cohesion

3.2.4 Consolidation model

Increases and decreases in pore water pressure in the soil are tied to the stress-strain calculation during the construction periods, but also to the consolidation calculation performed after construction with the aid of specific elements for the time after construction (Britto and Gunn 1987). All the details have been described by Britto and Gunn (1987 and 1990).

Changes in pore water pressure as a function of time are calculated by giving the distribution of the insitu pore pressures expressed as initial hydrostatic values for the geometric program. The head of the pore water pressure is then obtained from equation (73)

$$h = \frac{u}{\gamma_w} + z \tag{73}$$

where

h = head of pore water pressure
u = pore water pressure
γ_w = unit weight of water
z = height of point (from the reference plane)

The over-consolidation ratio was calculated by determining the preconsolidation pressure σ_{vc} in oedometer tests. For the dry crust it was also determined from equation (70).

In the elastic, perfectly plastic model, elastic strains are calculated isotropically ($E_h = E_v = E$). It is possible to allow for the linear variation in Young's modulus according to equation (74)

$$E = E_o + m_E(y_o - y) \tag{74}$$

where

E = Young's modulus in elevation y
E_o = Young's modulus in elevation y_o
m_E = rate of increase in Young's modulus with depth

Poisson's ratio ν' is constant in the elastic, perfectly plastic model.

The variation in the pressure head between the points results in water flow, i.e., seepage or consolidation. In the CRISP program, the portion of pore water pressure that exceeds the initial value is called absolute excess pore water pressure. It is defined by equation (75)

$$\bar{u} = h\gamma_w \tag{75}$$

where

$\bar{u}$ = excess pore water pressure

Consolidation equations

The consolidation equations used in CRISP-90 follow the theory developed by Biot (1941).

The movement of water in the soil is assumed to obey Darcy's law [equations (76) and (77)]

$$v_x = -k_x \frac{\delta h}{\delta x} = -\frac{k_x}{\gamma_w}\frac{\delta \bar{u}}{\delta x} \tag{76}$$

$$v_y = -k_y \frac{\delta h}{\delta y} = -\frac{k_y}{\gamma_w}\frac{\delta \bar{u}}{\delta y} \tag{77}$$

where

v_x = flow rate in x-direction
v_y = flow rate in y-direcion
k_x = hydraulic conductivity in x-direction
k_y = hydraulic conductivity in y-direction

In addition to Darcy's law, condition (78) (equation of continuity) is valid

$$\frac{\delta v_x}{\delta x}+\frac{\delta v_y}{\delta y}=\frac{\delta(\varepsilon_v)}{\delta t} \tag{78}$$

In the initial data the stresses are given as effective stresses σ_x' and σ_y' In the computation, the program makes use of parameters derived from the effective stresses.

Methods used in solving the equations

The continuity and compatibility of the stresses are solved in the program (Britto and Gunn 1987) with the method of virtual work [equations (79) and (80)]

$$\frac{\delta \sigma_x}{\delta x}+\frac{\delta \tau_{xy}}{\delta y}=\omega_x \tag{79}$$

$$\frac{\delta \tau_{xy}}{\delta x}+\frac{\delta \sigma_y}{\delta y}=\omega_y \tag{80}$$

where

ω_x = body force in x-direction
ω_y = body force in y-direction

Together with the constitutive equations of stresses and strains, equations (59) can be developed into a matrix of equations for the finite element method with the aid of Galerkin's weighted residual method (Britto and Gunn 1987). Use is also made of the Green's theorem (Zienkiewicz and Taylor 1989). As a result, stresses and pore water pressures with the corresponding displacements are obtained for given periods.

3.3 The Z-soil program

3.3.1 Structure of the program and material models

The simulation of the test embankment on a clay foundation was also made with the Z-soil program (Zace Services Ltd 1993), which uses quadrilateral elements generated automatically. Triangular elements are dealt with as quadrilateral elements in such a manner that in triangular elements the third and fourth nodes are identical. First the section included in the calculations is divided into macroelements, which together form a coarse mesh. The macroelements can then be divided by a split common to all elements or by dividing each macroelement separately. The program comprises following material and analysis models:

Material models
1 Linear elastic
2 Drucker-Prager
3 Drucker-Prager-cap
Analysis models
4 Biot's
5 Creep

Here, consolidation with the generalized Darcy's law and the Drucker-Prager Cap model for plasticity was used. Associative flow rules were applied. The program also allows for the use of non-associative flow rules.

The consolidation calculation is based principally on the theories explained in Section 3.2.4.

All the data to be collected for the Z-soil calculation are given in Table 2. The model used in the calculations combines a Drucker-Prager criterion with an ellipsoidal cap closure similar to the 'wet part' on the Modified Cam-Clay ellipse (Zace Services Ltd 1993).

The yield locus for the Drucker-Prager Cap model in the Z-soil program is shown in Fig. 7.

3.3.2 Behaviour models for normally consolidated and over-consolidated clays

The failure surface in the over-consolidated stage is modelled with the Drucker-Prager criterion. The failure line is defined by equation (81)

$$f(\sigma)=a_\phi I_1+\sqrt{J_2}-k=0 \tag{81}$$

where a_ϕ and k are material parameters. a_ϕ and k can be calculated from the Mohr-Coulomb parameters c' and ϕ'. In the triaxial condition (axial compression) with adjustment to external Mohr-Coulomb edges, equations (82) and (83) are applied

$$a_\phi=(2\sin\phi')/\sqrt{3}(3-\sin\phi') \tag{82}$$

$$k=(6c'\cos\phi')/\sqrt{3}(3-\sin\phi') \tag{83}$$

In Fig. 7, a_ϕ and k are shown through the parameters M_f and p_T'. The interrelations are given in equations (84) and (85)

$$M_f=3\sqrt{3}a_\phi \tag{84}$$

$$p_T'=k/3a_\phi \tag{85}$$

In the adjustment to internal Mohr-Coulomb edges, the parameters a_ϕ and k are given by equa-

Table 2. Material data in Z-soil calculation (Zace Services Ltd 1993).

Material property	Parameter	Symbol	Dimension
Elasticity	Unit weight	γ	$(kN\,m^{-3})$
	Young's modulus	E	$(kN\,m^{-2})$
	Poisson's ratio	ν	( )
Plasticity	Cohesion	c'	$(kN\,m^{-2})$
	Friction angle	ϕ'	(^{0})
Extended plasticity	Non assosiated angle	ψ	(^{0})
	DP adjusted[1)]		( )
Cap	Initial void ratio	e_0	( )
	Compression index	λ	$(kN\,m^{-2})$
	Preconssolidation pressure	p_0'	$(kN\,m^{-2})$
Consolidation	Initial void ratio	e_0	( )
	Fluid bulk modulus	K_w	$(kN\,m^{-2})$
	Permeability	k_x	$(m\,s^{-1})$
		k_y	$(m\,s^{-1})$
	Unit weight of water	γ_w	$(kN\,m^{-3})$
	Angle of orthotrophy	Θ_f	(^{0})

[1)] DP adjusts the Drucker-Prager coefficient to the Mohr-Coulomb criterion

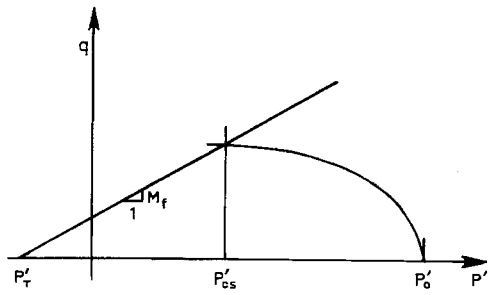

– Drucker-Prager criterion:

$$F=a_\phi I_1+\sqrt{J_2}-k=0$$

Cap

$$E=3J_2+M^2(p'-p_0')(p'+p_T')=q^2+$$
$$M^2(p'-p_0')(p'+p_T')$$

Fig. 7. Determination of yield surface in Z-soil program cap model (Zace Services Ltd 1993).

tions (86) and (87)

$$a_\phi=(2\sin\phi')/\sqrt{3}(3+\sin\phi') \quad (86)$$

$$k=(6c'\cos\phi')/\sqrt{3}(3+\sin\phi') \quad (87)$$

Yielding in the normally consolidated state is defined by equation (88)

$$q^2+M_f^2(p'-p_o')(p'+p_T')=0 \quad (88)$$

where

p_T' = the intersection of the Drucker-Prager line and the p'-axis in the p',q-plane.

Equation (88) is similar to equation (42). The difference is that the ellipse of equation (42) has a horizontal length p_o' whereas the ellipse of equation (88) has a horizontal length $p_o'+p_T'$.

In the plane strain condition with an assumption of associated flow, the relations are as in equations (89) and (90)

$$a_\phi=\tan\phi'/\sqrt{9+12\tan^2\phi'} \quad (89)$$

$$k=3c'/\sqrt{9+12\tan^2\phi'} \quad (90)$$

The flow rule defines the direction of plastic flow (equation 91)

$$d\varepsilon^p=d\lambda P \quad (91)$$

where

$d\lambda$ = positive scalar defining the amplitude of plastic flow. $d\lambda$ is calculated by iteration.

P = direction of plastic flow

For associative plasticity, the direction of flow P coincides with that of normal Q to the yield surface (91) (equation 92)

$$Q = P = df / d\sigma \tag{92}$$

For the Drucker-Prager criterion, equation (93) applies

$$Q_{ij} = \frac{1}{2\sqrt{J_2}} s_{ij} - a_\phi \, \delta_{ij} \tag{93}$$

where

δ_{ij} = Kronecker delta ($\delta_{ij} = 1$ if $i = j$; $\delta_{ij} = 0$ if $i \neq j$)

s_{ij} = deviatoric stress tensor

The model used is comparable to the Roscoe-Hvorslev model and the Schofield model (CRISP-90). The Drucker-Prager model has no strain softening effects.

In addition to elastic-plastic and consolidation settlements many investigators have demonstrated the phenomenon known as creep effect, or secondary consolidation (Bjerrum 1967, Singh and Mitchell 1968, Borja 1984). It was not considered here because of the relatively short time during which settlements were monitored.

4 The Taasia earth dam and test embankment

4.1 Soils in the study area

The location of the proposed earth dam at Taasia and a map of the dam area are shown in Fig. 1. The longitudinal section of the dam is given in Appendix 1 and the cross-section in Appendix 2. The boundaries between the soil layers are based on field and laboratory tests. The index properties of the soil layers are listed in Table 3.

Deep clay deposits are located in the right-hand portion of the proposed dam (Appendix 1), being at their deepest at the right abutment. As the bedrock is close to the surface at the left abutment, it was proposed that the dam would rest on bedrock there. In the cross-sectional direction of the dam (Appendix 2), the soil layers are of fairly constant thickness throughout the dam area. The cross-section selected represents the key site in the design.

The majority of the soil samples analysed in the laboratory were taken from two areas (Fig. 1), one under the downstream loading berm and the other under the upstream berm of the proposed dam.

The test embankment, which was constructed in the upstream area in 1980 (Fig. 1 and Appendix 2), is shown on the map in Fig. 8, as a longitudinal section in Fig. 9 and as a cross-section in Fig. 10. The soil profile under the test embankment is shown in Fig. 11. The test embankment was constructed using dry-crust clay from an adjacent site. The critical state models were tested by comparing the computaional data with the values of test embankment settlement measured over a 15-year period (1980–1995).

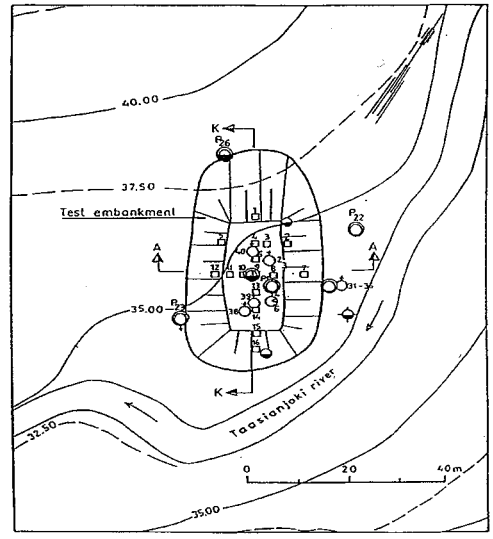

Fig. 8. Map of Taasia test embankment and location of test points. Sections are as Figs. 9 and 10.

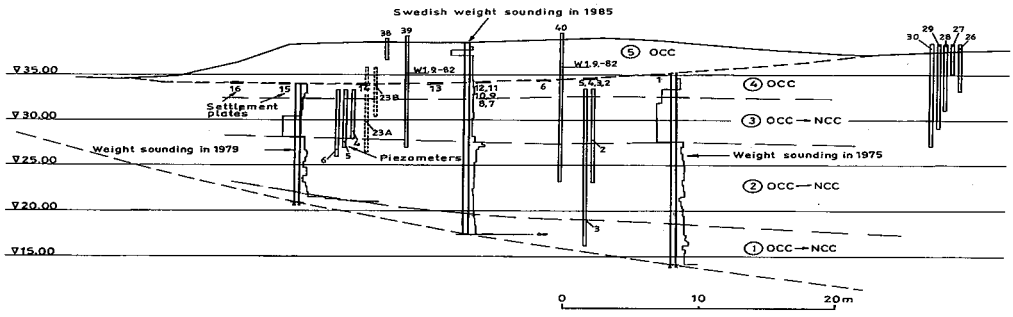

①–⑤ = Soil layers
NCC = Normally consolidated clay
OCC = Over-consolidated clay

Fig. 9. Longitudinal section K-K of Taasia test embankment (Fig. 8).

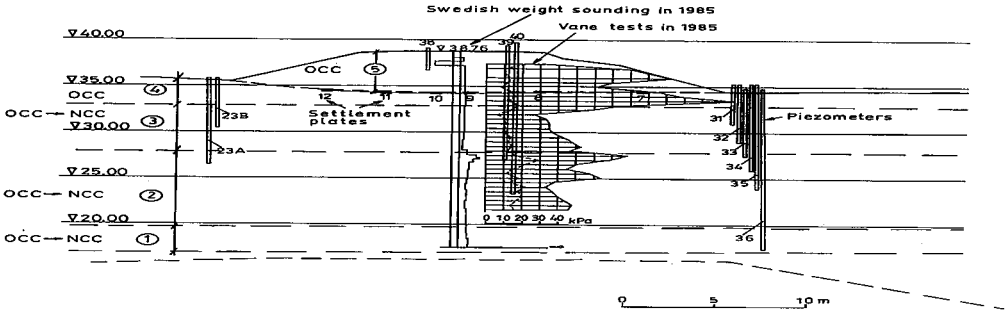

①–⑤ = Soil layers
NCC = Normally consolidated clay
OCC = Over-consolidated clay

Fig. 10. Cross-section A–A of Taasia test embankment (Fig. 8).

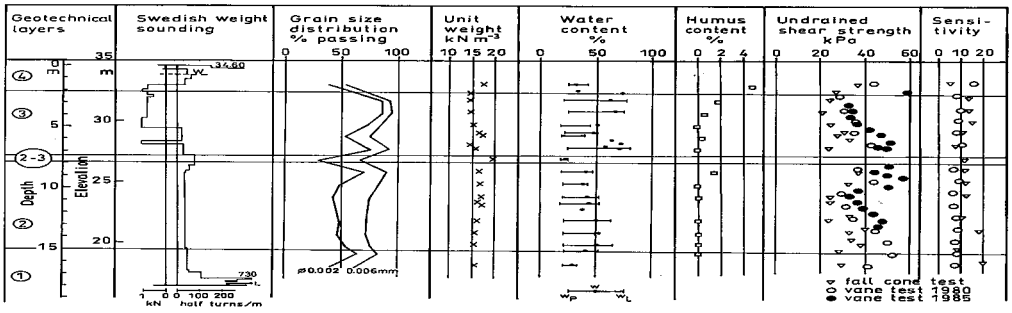

Fig. 11. Site investigation profile. Foundation of Taasia test embankment. Point 1.

Table 3. Taasia earth dam. Index properties of foundation soil. All tests.

Layer N = number of samples depth from ground surface m	Clay content %	Humus content %	Unit weight kNm^{-3}	Water content %	Liquid limit %	Plastic limit %	Shear strength, fall-cone test kPa	Sensitivity, fall-cone test	Shear strength, vane test kPa	Sensitivity, vane test
4	25.5–61.0	0.8–5.1	15.5–21.0	17.8–78	36.8–74	17.8–50	37.4–240	6–12.2	35.1–55.5	4–16
N = 100	34.5[m)]	2.3[m)]	18.3[m)]	33.6[m)]	58.8[m)]	32.2[m)]	149.9[m)]	9.0[m)]	45.0[m)]	7.0m)
<2.2	11.9[d)]	1.9[d)]	1.7[d)]	9.4[d)]	17.4[d)]	15.0[d)]	94.2[d)]	2.7[d)]	7.0[d)]	4.4[d)]
	N = 8	N = 4	N = 36	N = 81	N = 4	N = 4	N = 4	N = 4	N = 6	N = 6
3	29.4–95.0	0–46	14.3–18.4	35–106	39.5–114	20.4–81	9.8–48	3.4–20	18.6–42.7	1.9–32.2
N = 370	72.3[m)]	1.4[m)]	15.6[m)]	75.6[m)]	86.1[m)]	58.1[m)]	27.4[m)]	13.5[m)]	31.2[m)]	10.0[m)]
2.2–7.5	19.1[d)]	1.1[d)]	1.0[d)]	18.0[d)]	23.4[d)]	19.4[d)]	5.1[d)]	3.6[d)]	7.1[d)]	6.8[d)]
	N=19	N = 19	N = 133	N = 265	N = 20	N = 20	N = 75	N = 20	N = 15	N = 15
2–3	31	1.4	19.7	27–28	30	8	17–94.1	12	–	–
N = 8	N = 1	N = 1	N = 1	27.8[m)]	N = 1	N = 1	47.0[m)]	N = 1		
7.5–7.8				0.4[d)]			41.3[d)]			
				N = 5			N = 3			
2	12.7–89	0–25	14.4–19.0	28.8–96	32.5–115	12.4–84	23–44	9–28	29.5–50.1	5–13
N = 220	57.3[m)]	0.5[m)]	16.3[m)]	60.5[m)]	72.2[m)]	47.1[m)]	31.3[m)]	16.3[m)]	39.4[m)]	8.0[m)]
7.8–15	17.8[d)]	0.7[d)]	1.0[d)]	13.9[d)]	20.6[d)]	18.2[d)]	5.0[d)]	4.2[d)]	6.2[d)]	2.2[d)]
	N = 23	N = 23	N = 62	N = 162	N = 24	N = 24	N = 32	N = 23	N = 23	N = 22
1	40–65	–	15.9–19.2	32–56	32–75	11–49	27.8–34.8	9.0–30.3	33.4–52.6	5.0–9.5
N = 23	50[m)]	N = 3	17.7[m)]	39.6[m)]	47.9[m)]	25.8[m)]	31.2[m)]	18.6[m)]	42.0[m)]	7.0[m)]
>15	14[d)]		1.2[d)]	6.2[d)]	23.6[d)]	20.4[d)]	3.1[d)]	9.0[d)]	7.9[d)]	2.1[d)]
	N = 3		N = 5	N = 17	N = 3	N = 3	N = 4	N = 4	N = 4	N = 4

m) = mean value
d) = standard deviation

4.2 Geological origin and index properties of the soil layers

Geology of the construction site

The geological origin of the clay deposit was established at Geological Survey of Finland by submitting the soil samples from the downstream study area to pollen analyses at 2-m intervals from depths of 1.0 to 16.7 m.

The bulk of the sedimentary sequence (16.7–3.0 m) is very poor in pollen. Arboreal pollen (AP) is Betula-dominant and contains redeposited pollen (e.g. Corylus and Alnus). Non-arboreal pollen (NAP) is mainly composed of Cyperanceae, Graminaceae, Artemisia and Chenopodiacea.

The pollen assemblage is interpreted as younger Dryas or early Preboreal (Rankama 1964), a stage that corresponds to the Baltic Ice Lake and Yoldia Sea in the evolution of the Baltic Sea. At a depth of 2–3 m, there is a distinct gap in the pollen succession. The upper part (samples from depths of 1.0 m and 2.0 m) is dated to either the late Subboreal or the late Subatlantic climatic interval; both intervals belong to the late postglacial stage of the Baltic Sea.

The mineral compositions of the Taasia clay samples as established at Geological Survey of Finland are listed in Table 4 in order of estimated abundances. As the slides representing the whole sample showed only quartz, plagioclase and potassium feldspar with some indications of mica, chlorite or kaolin, concentrate was made from the fine fraction, which was then studied on a slide oriented by precipitation.

The structure of the foundation layers was also studied with the aid of split samples (Kallio 1980, Pitkänen 1982). These samples were taken from the downstream study area. In the study of Kallio, the samples were taken from two adjacent points to form a continuous core. Shown in Fig. 12 are the cores photographed four days after splitting. The samples were later restudied when fully dry. Under the dry crust, the profiles studied usually have varved clay to a depth of 3–4 m. This is underlain by homogeneous clay down to a depth of 5–6 m, after which varved clay appears again. The thickness of the varves varies, and there are layers of homogeneous clay in the varved clay.

Index properties

The location of the soil layers in the foundation of the test embankment is shown in Figs. 9 and 10 and in the area of the whole proposed earth dam in Appendices 1 and 2. The soil profile under the test embankment is shown in Fig. 11.

The index properties of the soil in the dam foundation are given in Table 3.

Table 4. Mineral composition of Taasia clay. Downstream study area (area 2 in Fig. 1). Ground surface at 35.00 m.

Sample depth from ground surface m	Mineral composition in estimated declining order of abundance
1.1–1.2	Quartz, plagioclase, potassium feldspar, kaolinite, chlorite and possibly minor montmorillonite.
2.3–2.4	Quartz, plagioclase, potassium feldspar, kaolinite, illite, chlorite and hornblende
4.4–4.5	Muscovite, chlorite, plagioclase, quartz, potassium feldspar and hornblende.
8.4–8.5	Moscovite, kaolinite, quartz, plagioclase, chlorite, potassium feldspar and hornblende
14.25–14.35	Muscovite, kaolinite, plagioclase, quartz, chlorite, potassium feldspar and hornblende

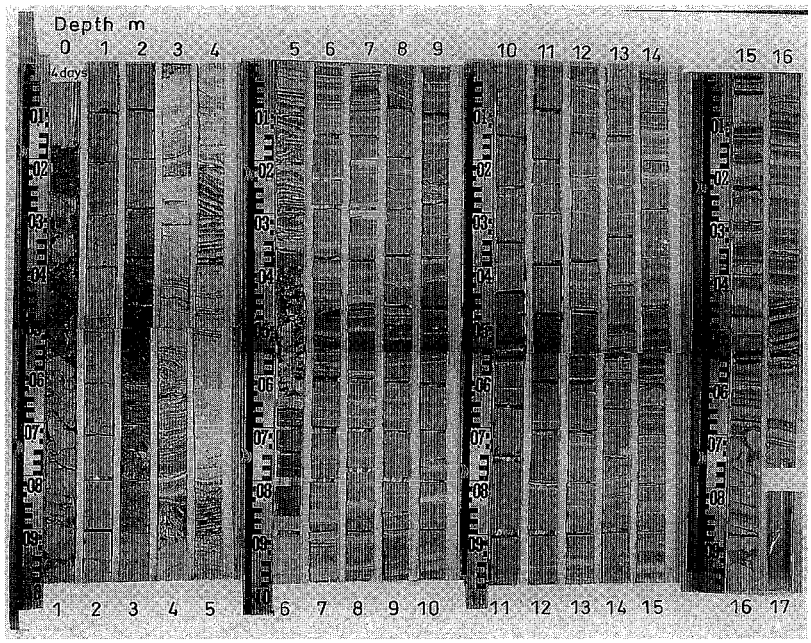

Fig. 12. Taasia earth dam. Area 2 (Fig. 1). Split core from depth of 0–16.75 m, four days after splitting. (Photo by T. Eronen)

Table 5. Taasia test embankment. Hydraulic conductivity data on Taasia test embankment foundation recorded on August 23–26, 1983. Location of tubes shown in Figs. 8–10.

Tube no.	Elevation of sensor m	Hydraulic conductivity m s^{-1}
38	36.62	$10^{-9.85}$
27	35.08	$10^{-9.71}$
26	33.15	$10^{-9.48}$
28	31.05	$10^{-9.49}$
31	30.98	$10^{-9.28}$
23B	30.46	$10^{-9.14}$
29	29.09	$10^{-9.53}$
32	28.99	$10^{-9.30}$
33	27.48	$10^{-9.47}$
30	27.10	$10^{-9.34}$
39	27.02	$10^{-9.40}$
23A	26.49	$10^{-9.34}$
34	25.96	$10^{-9.03}$
35	23.96	$10^{-9.21}$
40	23.37	$10^{-9.45}$
I	18.10	$10^{-7.51}$
36	17.45	$10^{-9.15}$

Hydraulic conductivity

The insitu hydraulic conductivity of the soil layers was determined with the aid of piezometers installed at various depths for measuring pore water pressure. The results are given in Table 5. The measurements were made by letting a 1.0-m-high water column seep into the soil with a view to finding layers of higher permeability in the clay deposit. No clearly permeable interlayers were, however, discovered (Loukola 1985).

Hydraulic conductivity was calculated from equation (94) (Cedergren 1967)

$$k=\frac{r^2}{2L(t_2-t_1)}\ln\left(\frac{L}{R}\right)\ln\left(\frac{h_1}{h_2}\right) \qquad (94)$$

where

k = hydraulic conductivity (ms^{-1})
R = radius of sensor tip (m)
r = radius of tube attached to sensor (m)
L = length of sensor (m)
t_1 = time (s)
t_2 = time (s)
h_1 = water level in tube at time t_1 (m)
h_2 = water level in tube at time t_2 (m)

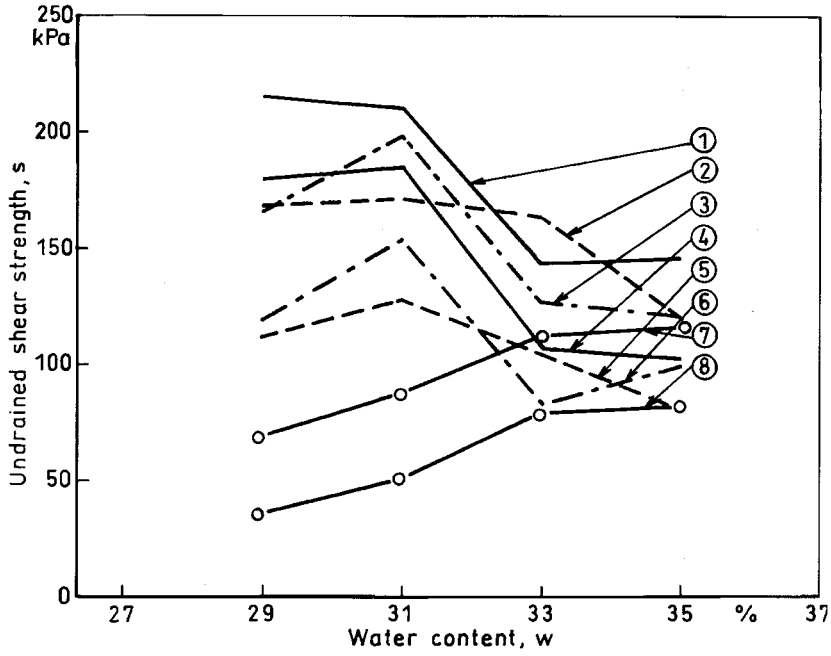

1. Fall cone test, 6 compaction passes, m
2. Fall cone test, 4 compaction passes, m
3. Fall cone test, 2 compaction passes, m
4. Fall cone test, 6 compaction passes, m-d
5. Fall cone test, 4 compaction passes, m-d
6. Fall cone test, 2 compaction passes, m-d
7. Vane test, 6 compaction passes, m
8. Vane test, 6 compaction passes, m-d

m = mean value
d = standard deviation

Fig. 13. Taasia test embankment. Undrained shear strength as function of water content. Tests during construction.

The value calculated from equation (94) refers mainly to the horizontal hydraulic conductivity in layered earth, which is higher than vertical hydraulic conductivity. The values given by the test are rather rough owing to errors caused by breakage of the soil structure.

As the layers of different grain sizes are horizontal in the varved clay, the ratio of horizontal hydraulic conductivity to vertical hydraulic conductivity for the clay layers is taken as 10 in the calculation. This also takes into account the variation in hydraulic conductivities in each layer to be calculated. The effect of the ratio of horizontal hydraulic conductivity to vertical hydraulic conductivity is determined in the sensitivity analysis in Chapter 6.

Undrained shear strength

The shear strength values measured in situ with vane tests and in the laboratory with fall-cone tests are included in Table 3 and Fig. 11. Unconfined compression tests were not made because of the difficulty of taking large enough undisturbed samples. The test data on the test embankment foundation and on samples taken from that foundation are plotted in Fig. 13.

Geotechnical layers for calculations

For the finite-element calculation, the geotechnical layers in the formation were numbered from the bottom upwards.

The deepest layer (1) is drained by the underlying, more permeable layers. Calculated from all test data, its average water content is 39.6%. Under the test embankment the corresponding value is 46.6%. In the whole area the water content is between the plastic and liquid limits. The values of undrained shear strength are fairly low, with an av-

erage of 31.2 kPa when measured with the fall-cone test, and 42.0 kPa when measured with the vane test (1980). The values under the test embankment are 29 kPa and 47 kPa, respectively. The difference in shear strength between layer 1 and the next layer (2) is quite small.

Layers 2 and 3 are of lightly over-consolidated clay, with average water contents of 60.5% and 75.6%, respectively, as calculated from all test data. Under the test embankment, the average water content values of the layers are 58.6% and 72.8%, respectively. These values are usually about 10% lower than the liquid limit and only seldom exceed it. The undrained shear strength values in both layers are quite low, the average being between 27.4 kPa and 39.4 kPa (1980) (Table 3). The data from under the test embankment are similar (Fig. 11).

A thin, drier layer with an undrained shear strength higher than that of layers 2 and 3 was encountered at the test points at depths of 7.5–7.8 m. Under the test embankment, the value of undrained shear strength measured with the fall-cone test was up to 94 kPa; the value could not be measured with the vane test. As the layer is very thin it was not considered as a separate geotechnical layer in calculations.

The dry-crust layer (4) is of heavily over-consolidated clay, with an average water content (33.6%) between the plastic and liquid limits. The layer is appropriate for cut-off material for the dam. More index test data and undrained shear strength data on the compacted dry-crust clay are given in Section 4.3.

Five years after construction of the dam the undrained shear strength was assessed with a vane test. Some increase in values was noted (Fig. 11).

4.3 Construction and monitoring of the test embankment

A test embankment about 4.5 m high was constructed between August 18 and September 9, 1980, at the site of the proposed dam (Figs 8–10). The test embankment was built of dry-crust clay extracted from a depth of 0.4–1.5 m in a nearby slope.

Before the start of the construction, a humus layer about 0.4 m thick was removed from the embankment site and the clay extract site. Sixteen settlement plates were installed under the embankment, and six pore pressure sensors were placed at various depths in the foundation soil. Six more sensors were later installed (in 1985).

The material for the test embankment was transported and compacted with a 22-ton crawler tractor. The test observations were recorded after two, four and six passes. During each pass the crawler of the tractor passed over each point once.

Table 6 lists the values of index properties as determined from the Taasia test embankment material. Fig. 13 shows the results of vane tests and fall-cone tests made after different compaction passes as a function of the water content.

The material of the test embankment is fine-grained clay, with a liquid limit of 61% and a plastic limit of 26%. The water content usually varied between 26% and 35%, extreme values being 20% and 60%. Except in the dryer samples, the water

Table 6. Index properties of Taasia test embankment material

Unit weight kN m^{-2}	Water content %	Clay content %	Liquid limit %	Plastic limit %	Plasticity index %
17.92	33.5	68.4	61	26	35
N = 80	N = 80	N = 9	N = 3	N = 3	N = 3
d = 0.82					

N = number of samples
d = standard deviation

content was between the plastic and liquid limits.

The average unconfined compression strength as determined by fall-cone tests was between 120 and 215 kPa, with a standard deviation of about 50 kPa, depending on the water content. The increase in compaction passes increased the average by about 40 kPa and somewhat reduced the standard deviation (Fig. 13). The increase was not clear for all water contents.

Vane tests were usually made after six compaction passes. The average shear strength fluctuated between 70 and 113 kPa, inreasing with the increase in water content. The standard deviation fluctuated between 33 and 36 kPa, being about half of the minimum of the average. According to the vane test results, the optimum water content for compaction is 33–35%.

The test embankment was monitored for about 15 years. Table 7 and Fig. 14 show the results of the settlement plate measurements and Fig. 15 gives the data on pore water pressure. The structure and foundation of the test embankment were studied with sounding in 1979 and 1985. The results are given in Figs. 9 and 10.

4.4 Stress and strain properties

4.4.1 Methods used for stress and strain tests

The undrained shear strength of the deep clay layers and dry-crust clay was determined in situ with vane tests and in the laboratory with fall-cone tests (Loukola 1985). The results of the vane tests are depicted in Figs. 10, 11 and 13 and Table 3, and those of the fall-cone tests in Figs. 11 and 13 and Table 3. Tests to determine the other strength and deformation parameters of the deep clay layers were performed with conventional equipment. The triaxial tests were made with an apparatus in which axial deformation takes place at a more or less constant rate. The settlement tests were undertaken with an oedometer in which the load was applied incrementally, and each increment lasting as long as the settlement continued (within the accuracy of measurements). Some samples had been taken horizontally, and in them compression could be applied horizontally.

The dry-crust clay was studied in a similar fashion but also with stress-controlled triaxial equipment.

The triaxial tests and settlement tests were con-

Table 7. Settlement of settlement plates

Plate no.	Level of plates 29.8.80 m	Settlements at different times m												
		9.9.80	9.10.80	5.2.81	15.4.81	8.7.81	10.9.81	19.1.82	5.5.82	11.5.85	week 26 1988	week 43 1990	week 47 1993	week 32 1995
3	34.65	0.085	0.095	0.105	0.110	0.115			0.123	0.131	0.141	0.150	0.153	0.154
4	34.73	0.070	0.085				0.089	0.095	0.096	0.105	0.107	0.118	0.120	0.121
6	34.53	0.105	0.120	0.130	0.137	0.145	0.151	0.158	0.160	0.174	0.180	0.190	0.191	0.192
8	34.45	0.105	0.125	0.150	0.160	0.165	0.173	0.180	0.182	0.192	0.200		0.213	0.214
9	34.33	0.105	0.130	0.140	0.145	0.155	0.168	0.174	0.178	0.192	0.201	0.213	0.215	0.216
10	34.24	0.090	0.110	0.120	0.125	0.135	0.146	0.152	0.156	0.172	0.180	0.188	0.186	0.187
11	34.34	0.070	0.075	0.085	0.095	0.104	0.105	0.105	0.114	0.122	0.132	0.138	0.138	0.138
13	34.15	0.095	0.120	0.140	0.150	0.161	0.170	0.175	0.179	0.193	0.206	0.218	0.220	0.221
14	34.05	0.110	0.125	0.145	0.150	0.167	0.175	0.180	0.186	0.193	0.202	0.217	0.218	0.218
	*)	0.093	0.109	0.127	0.134	0.143	0.147	0.152	0.153	0.164	0.172	0.179	0.184	0.185

*) Average of settlements of different plates

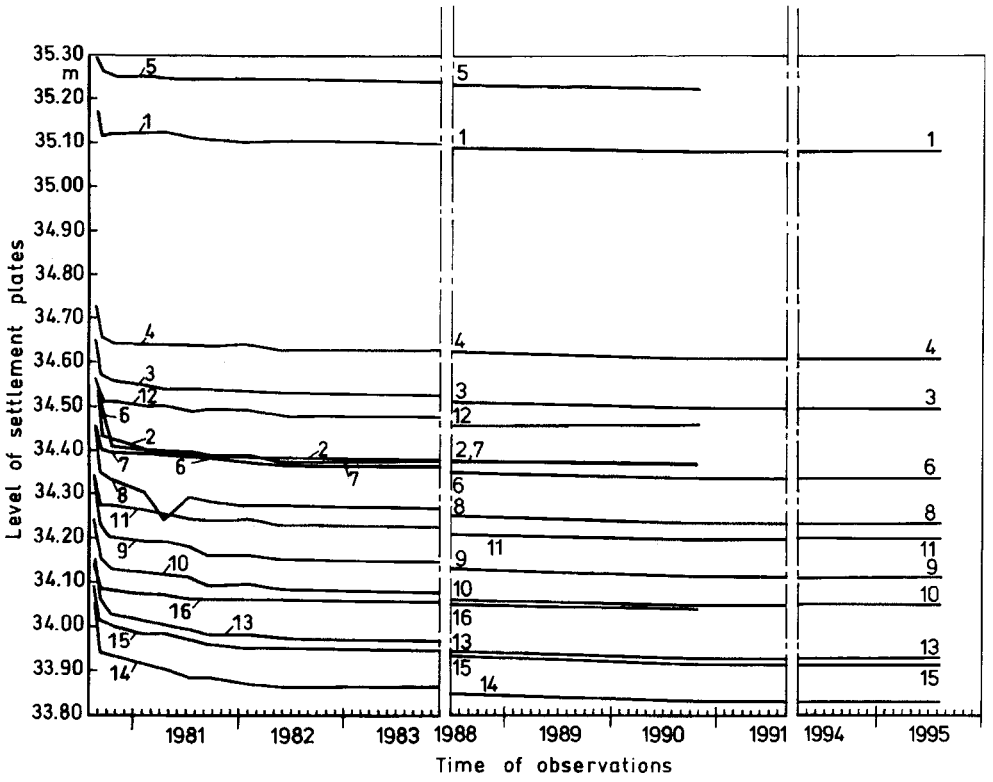

Fig. 14. Taasia test embankment. Settlement of settlement plates in 1980–1995. Location of plates shown in Figs. 8 and 9.

ducted at the laboratory of Soil Mechanics and Foundation Engineering of Helsinki University of Technology and at the Soil laboratory of the National Board of Waters. The technique used in the triaxial tests was mainly developed in the USA (Lambe 1954, Young and Townsend 1980) and in the UK (Bishop and Henkel 1964, Bishop and Wesley 1975). The technique applied to the settlement tests was developed in Norway (Janbu et al. 1964).

The triaxial compression tests of the layers under the dry crust were made both isotropically and anisotropically as either consolidated undrained tests or consolidated drained tests. In the anisotropic tests, the ratio of principal stresses after consolidation, σ_3/σ_1, was given values of 0.8 and 0.6. The isotropic consolidation tests were made with the triaxial apparatus to determine the deformation parameters. In addition, consolidation tests were made with the oedometer. Both apparatuses were used to determine the effects of the first loading and of load reduction and reloading. Tests on the samples of clay layers under the dry crust are described in Section 4.4.2.

Except for the undrained shear strength, the strength and deformation parameters of the dry-crust clay were determined with a conventional and a stress-controlled triaxial test apparatus and an oedometer. The dry-crust clay was studied on samples from the test embankment and from the dry-crust layer. The tests, whether consolidated undrained or consolidated drained, were performed isotropically and anisotropically. In the anisotropic tests, the ratio of principal stresses after consolidation, σ_3/σ_1, was given values of 0.8 and 0.6. The stress-controlled apparatus was also used for K_o tests in which the cross-section of the sample was kept constant during compression. The consolidation tests with the triaxial apparatus and oedometer were made in the same way as for the layers under the dry crust. The tests on the dry-crust clay are described in Section 4.4.3.

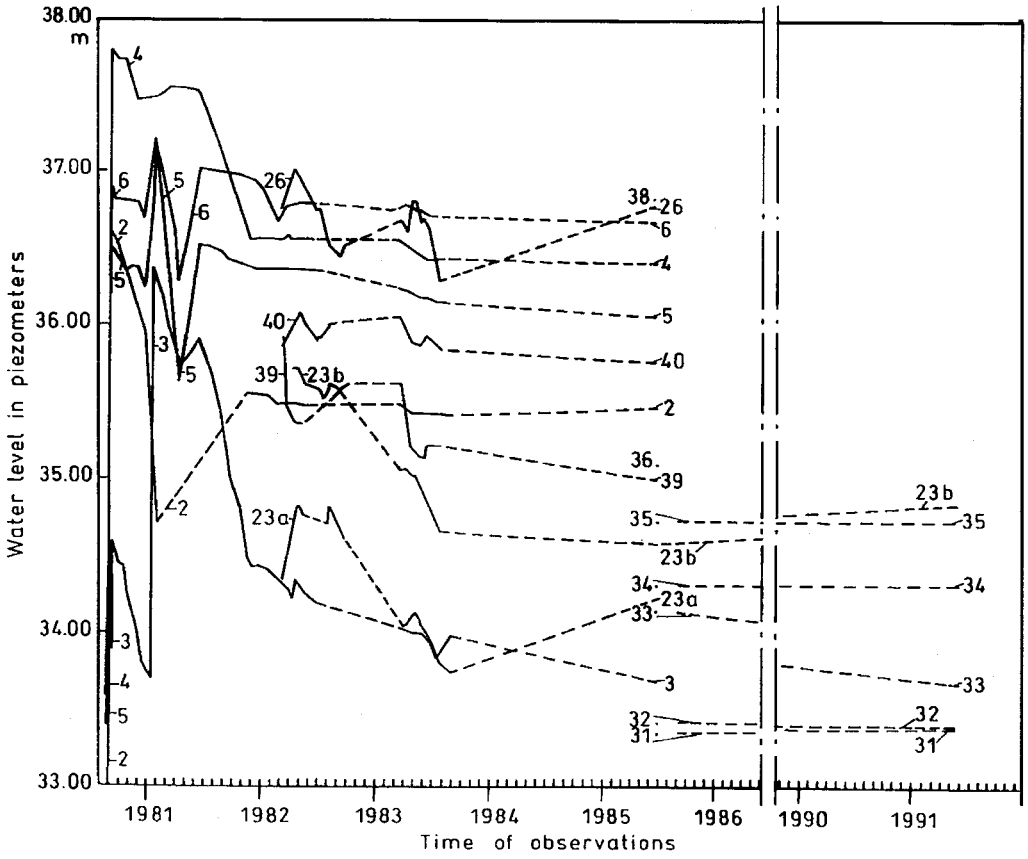

Fig. 15. Taasia test embankment. Pore water pressure in 1980–1991. Location of sensors shown in Figs. 8 and 9.

4.4.2 Studies on clay layers under the dry crust

Triaxial tests

The first triaxial tests on the samples from the deep clay layers were made at Helsinki University of Technology in 1979 and 1980, using a triaxial apparatus manufactured by Geonor A/S (Lojander 1980, Casagrande 1980). The samples were of two sizes, the smaller ones 3.6 cm in diameter and 8.0 cm high, and the bigger ones 5.0 cm in diameter and 10.0 cm high. The tests were made as consolidated, undrained tests at a rate of shear of 1–2% h^{-1}. As the rate of shear is relatively fast, care must be taken in developing the parameters for the calculations.

According to the oedometer data on these samples (Lojander 1980), the preconsolidation stress of the layer is 90 kPa. In Appendix 3 the results of the tests on samples taken from the soft clay layer are shown as ε_1,q and ε_1,u diagrams. In Fig. 16 the test results are shown as p',q diagrams. In Fig. 17 the test results have been normalised by dividing the stresses of the normally consolidated sample by the isotropic cell pressure, and the stresses of the over-consolidation samples by the preconsolidation stress, σ_{vc}' = 90 kPa. As the normal compression stress values obtained with the isotropic consolidation tests were similar to the preconsolidation stresses obtained with the oedometers, the procedure described was used. Assuming that the normally consolidated sample approaches the critical state after failure, a value of 1.2 is obtained for parameter M. Provided that the heavily over-consolidated (in the sense of stress regions in Fig. 5) samples fail on Hvorslev's line,

the slope of Hvorslev's line gets the value 0.74. The H value was taken as the average of two measurements. More confidence for the H value will be given by tests to be described later. The increase in pore pressure was so great that the mean effective stress decreased in normally consolidated and slightly over-consolidated samples.

Triaxial drained shear tests were made at the

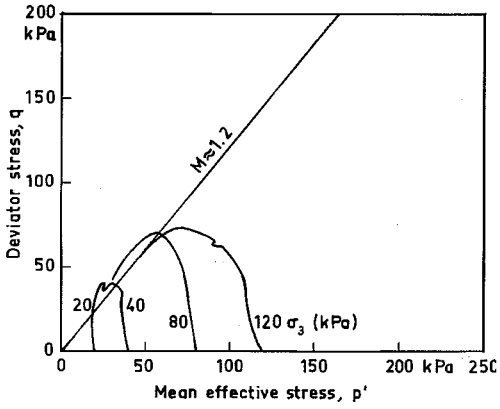

Fig. 16. Foundation of Taasia test embankment. Layer 3. Sample set 1. w = 84–92%. Triaxial CIUC test. Sampling depth 2.47–2.96 m. σ'_{vc} = 90 kPa.

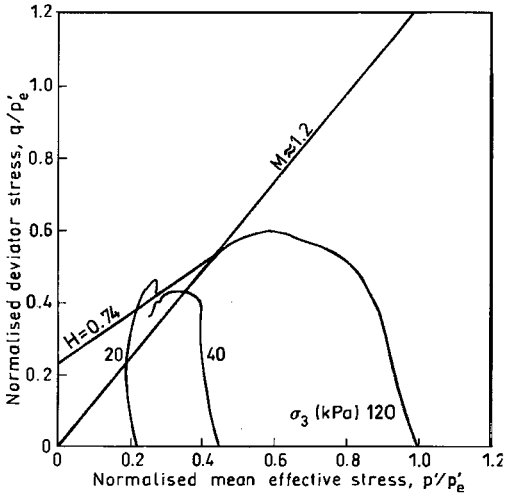

Fig. 17. Foundation of Taasia test embankment. Layer 3. Sample set 1. w = 84–92%. Triaxial CIUC test normalised by cell pressure (normally consolidated samples) or preconsolidation stress (over-consolidated samples). Sampling depth 2.47–2.96 m. σ'_{vc} = 90 kPa.

National Board of Waters in 1986 and 1987 on samples taken from a depth of 3.0–3.5 m in the ground under the test embankment. The samples were 7.50 cm high and 3.76 cm in diameter. The shear rate (ε_1 / t) was about 1.2% d^{-1}. The samples were consolidated anisotropically by applying the horizontal and vertical stresses in ratios of 0.6 or 0.8. The samples were also consolidated isotropically. In one of these tests shearing continued until failure of the sample. The tests were carried out with a conventional triaxial apparatus. In addition to stresses and deformations, low pore water pressure was measured and taken into account in the calculation of results.

The results of the tests are shown in Appendix 4 and Figs. 18 and 19. Three samples were tested as initially over-consolidated, the others as normally consolidated. The tests generally continued until 10–13% axial deformation; the isotropically consolidated test was continued to 16% axial deformation. The shear strain continued to 8–13%. The water content of the samples ranged from 60 to 79%, which is slightly under the liquid limit of the soil layer. According to the critical state theory, the increment in the volume change of a soil sample disappears once the sample reaches the critical state. In these tests, the critical state does not seem to be reached, even at 16% axial deformation. In all tests the $d\varepsilon_v$ to $d\varepsilon_s$ ratio decreased to about half of the initial values (initially, the increments in volume change and shear strain were of the same order of magnitude, on average), as the critical state was not properly reached. As the ratio of the deviator stress to the volumetric stress (q / p') increased simultaneously from 0.5 to 0.7–0.8, the most probable value for M is 1.0. In Fig. 20 the test data on the initially over-consolidated samples have been normalised with the equivalent stress taken from the normal consolidation line in a combination of the results of the consolidation tests of undisturbed samples at the same V-value. The states of the samples have been changed from the over-consolidated state to the normally consolidated state. Fig. 20 also gives 1.0 for the M-value.

Triaxial drained shear tests on over-consolidated samples were made at Helsinki University of Technology in 1991. The samples tested had been consolidated at an isotropic pressure of 60 kPa. The shear (Fig. 21) gives an M-value of 1.05, which is a little larger than that previously obtained. Repeated shearing tests on an over-consolidated sample have been reported by Lojander

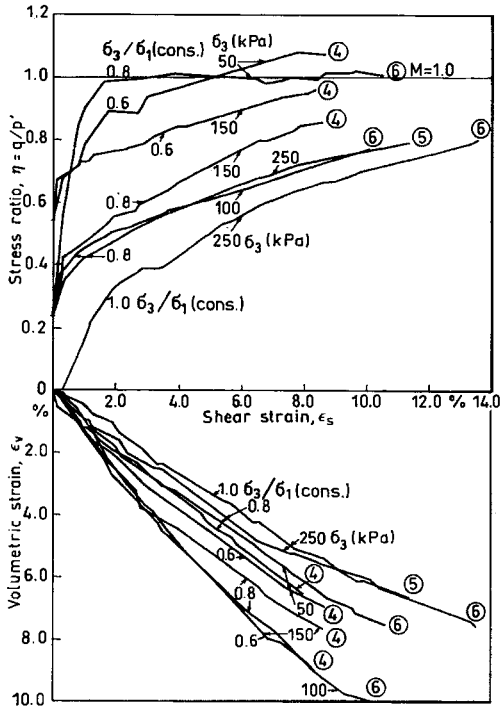

Fig. 18. Foundation of Taasia test embankment. Layer 3. Sample sets 4, 5 and 6. Triaxial CADC test. Samples from level 31.75 m. w = 60-79%. σ'_{vc} = 85 kPa. ε_1 / t = 1.2 % d^{-1}.

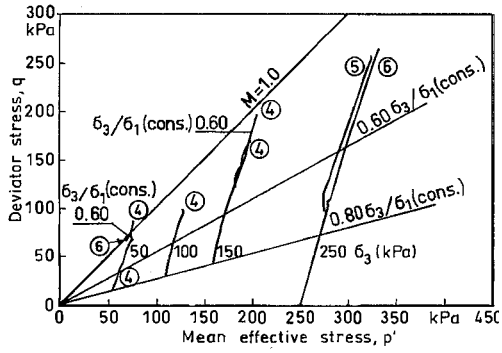

Fig. 19. Foundation of Taasia test embankment. Layer 3. Sample sets 4, 5 and 6. w = 60–79%. Triaxial CADC test. σ'_{vc} = 85 kPa.

(1993) (Fig. 22). He got 0.70 for the H-value (Fig. 22), which corresponds to the earlier result (Fig. 17).

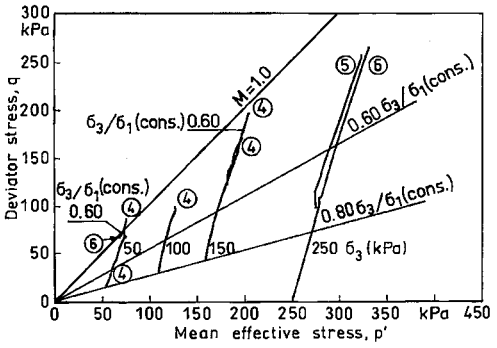

Fig. 20. Foundation of Taasia test embankment. Layer 3. Sample sets 4 and 6. w = 60–79%. Triaxial CADC test normalised by equivalent stress of isotropic normal compression line (Fig. 33). $\sigma_{vc}{}'$ = 85 kPa. Only initially over-consolidated tests shown.

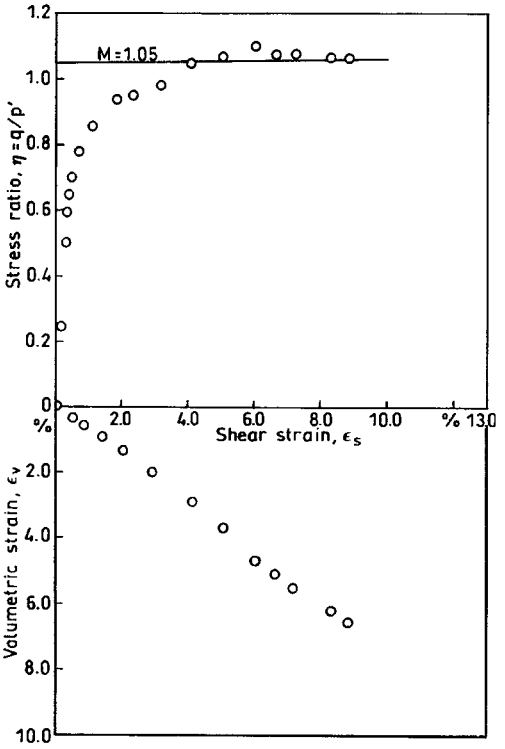

Fig. 21. Foundation of Taasia test embankment. Layer 3. Triaxial CICD. σ_3 =30 kPa. Samples near test embankment from level 31.90 m. w = 90%, σ'_{vc} = 60 kPa, ε_1 / t = 0.3%d^{-1}.

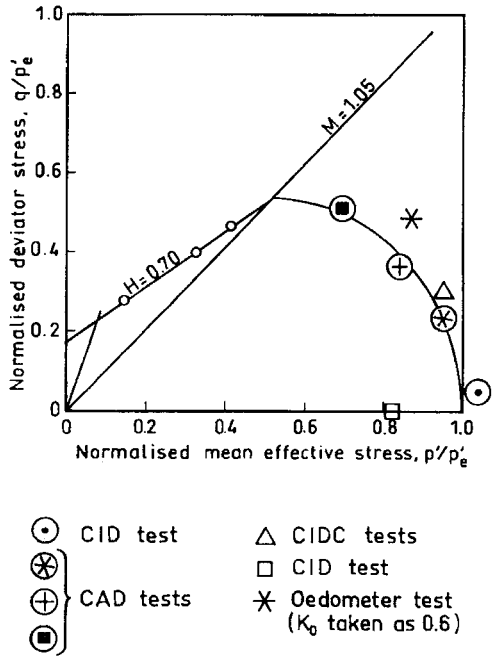

Fig. 22. Foundation of Taasia test embankment (Lojander et al. 1993). Layer 3. Triaxial CIDC. Samples near test embankment from 31.90 m level. Consolidation with different stress ratios and repeated shearing. $\varepsilon_1/t=0.3\%d^{-1}$. Stresses normalised with equivalent pressure of normal consolidation line.

Consolidation tests

The parameters of the critical state models, λ and κ were determined from the isotropic triaxial consolidation tests. The same parameters were also determined from the oedometer tests. The values of λ and κ for the deepest layers were calculated from the tested values with the aid of the index properties as will be explained later.

The isotropic consolidation tests were performed with a conventional triaxial apparatus on samples taken from the foundation of the test embankment at the 31.50–32.00 m level. The samples were 7.5 cm high and 3.8 cm in diameter. The following load series were applied: 12.5 kPa, 25 kPa, 50 kPa, 100 kPa, 200 kPa, 25 kPa, 6.25 kPa, 0 kPa, 12.5 kPa, 50 kPa, 100 kPa, 200 kPa and 250 kPa. Each loading step lasted at least 24 hours. The first test gave λ = 0.81 and κ = 0.02 and the second test λ = 1.01 and κ = 0.04 for the values of the critical state parameters. The κ-value of the first test was taken from the first loading, as the swell and repeated load test gave a value, κ = 0, that differed from the values of the other tests. Thus it cannot be correct (Table 8).

The samples from the deep clay layer were also submitted to oedometer tests. The average values of the critical state parameters calculated from the tests were λ = 0.77 and κ = 0.045 (Table 8).

For determination of the complete settlement lines in the critical state model, the parameters V_λ or e_o, which define the positions of the lines, are needed in addition to the parameters λ and κ, which define the slopes of the lines. The parameters V_λ, corresponding to normal consolidation, are in the range 6.0-8.0. V_λ-values have been taken into account in combining the test results.

The results of the drained triaxial test (Figs 18-20) are shown in the $\ln p', V$-coordinate system in Fig. 23. According to the critial state theory, the drained tests should end on the line parallel to the normal consolidation line. The vertical distance between the lines of isotropic consolidation and critical state in the Cam-Clay model is λ - κ as shown by equation (32), and in the Modified Cam-Clay model ($\lambda - \kappa$) ln 2 according to equation (43). When the points describing the critical state

Table 8. Parameters of critical state models λ and κ and preconsolidation pressure p_o'/p'_{K_o} for clay layer under dry crust

Type of testing	λ	κ	p_o'/p'_{K_o} kPa
Isotropic consolidation in triaxial apparatus	0.91	0.02	82
Oedometer test	0.77	0.045	65

were joined, $\lambda = 0.44$ was obtained as the slope of the critical state line.

As the critical state was not attained in the drained tests the lines are not parallel, and the results do not obey equations (32) and (43).

The values of p_o (isotropic test) and p'_{K_o} (one-dimensional test) determined from the tests were 82 kPa and 65 kPa, respectively (Table 8). The p'_{K_o} was calculated using the K_o-value 0.6. At the time of the experiment, 0.6 was assumed to be the most probable value for K_o for normally consolidated clay. In the finite element calculations the preconsolidation stresses of the earlier tests (Lojander 1980, Casagrande 1980) were applied.

4.4.3 Studies on dry-crust clay

The dry-crust clay with samples taken from the test embankment during and after its construction was studied at the National Board of Waters. The samples from the embankment had a water content of 30–42%.

Undisturbed dry-crust samples were studied at Helsinki University of Technology (Lojander 1980, Casagrande 1980). Their water content varied in the range 34–50%.

The embankment samples were studied with undrained and drained triaxial tests. K_o-tests and oedometer tests were also performed. The undrained triaxial tests were made in a conventional apparatus. The drained test was made in a conventional and a stress-controlled apparatus. The latter has a triaxial cell in which the water pressure (cell pressure) is generated around the sample with the aid of a compensating device; the ends of the sample are submitted to axial load with another compensating device. Back pressure can also be applied to the sample by directing water pressure to the upper end of the sample with the aid of a special compensating device. The pore water pressure inside the sample is measured with a gauge. A similar apparatus is used to measure the cell pressure. Axial load is measured with an electronic unit provided with a pressure sensor. Axial deformation is measured with a strain gauge. In the drained test, the pore pressure dissipated against the back pressure. In the K_o-tests, the perimeter of the sample is kept constant with the aid of a strain gauge. The equipment was developed in UK (Bishop and Wesley 1975).

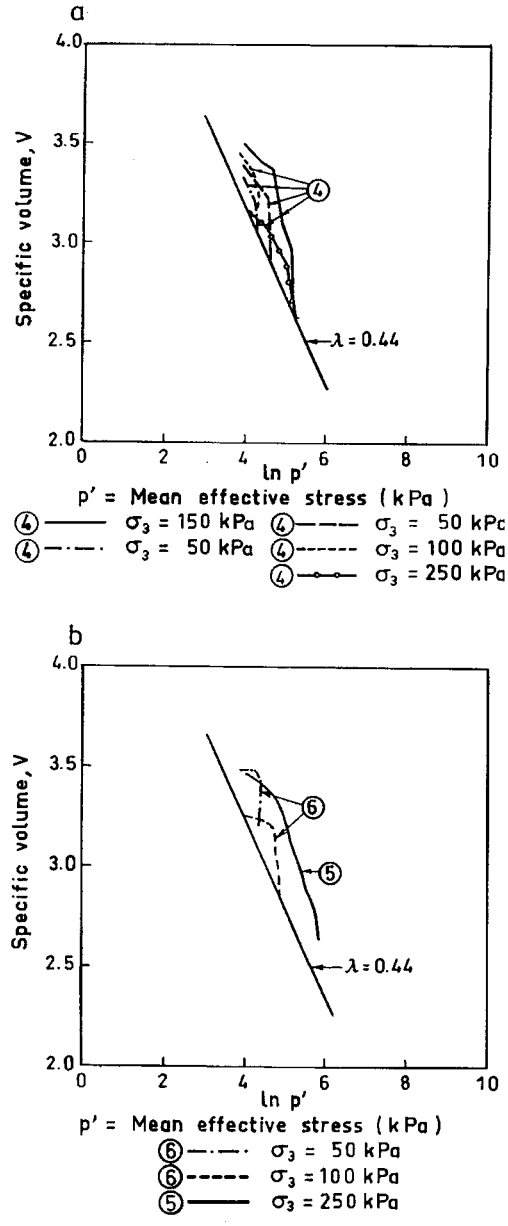

Fig. 23. Taasia test embankment foundation. Layer 3. Sample sets 4, 5 and 6. Triaxial CADC test. Samples from 31.50–32.00 m level.

Samples from the test embankment

Figs. 24–26 give the results of the drained triaxial tests on samples from the finished test embank-

ment. Shearing of the samples was non-linear. Fig. 27 gives the oedometer results for the same samples. The samples were heavily over-consolidated, as their water content was 33–42%. According to the oedometer tests, the preconsolidation pressure was about 700 kPa. The $\varepsilon_s, \varepsilon_v$ curves indicate that the samples had reached the critical state. After the yield the volumes of the samples remained constant. At the end of the yield the q/p' – ratio was, however, declining and could presumably have reached the lower constant value of M = 1.1. The tests were stopped at about 11% deformation. The q/p' – ratio at the yield is 1.2 and the corresponding friction angle $\phi_{cs}' = 30.0^\circ$. If the q/p' – ratio changes to 1.1 as shear continues, it corresponds to the friction angle $\phi_{cs}' = 27.7^\circ$. In Fig. 25 the test results have been normalised with the normal consolidation line drawn with the combined results of deep clay layers and the dry-crust clay. Assuming that 1.1 is the most probable value of M, the slope of Hvorslev's line is $H \approx 1.0$. The errors due to the test technique are discussed in Section 6.3.

Fig. 28 shows the results of drained tests made with a stress- controlled apparatus and plotted in the p', q – coordinate system. The samples were taken during construction of the test embankment after six compaction passes. The water content of the samples was 30–35%. These samples, too, were submitted to oedometer tests. Oedometer tests gave the slope (κ – value) of the test in the $\ln(p'), V$ – plane an average value of 0.03. In the triaxial tests the samples were consolidated anisotropically using $\sigma_3 / \sigma_2 = 0.8$, which was considered to be the most probable value during the tests. In the tests, attention was paid to the formation of the shear plane. According to the test data, shear took place when the stress ratio was above the critical state. Assuming M = 1.1 in the normally consolidated state and the preconsolidation stress σ'_{vc} = 700 kPa, the slope of Hvorslev's line gets the value H = 0.82. In this case the test data conform more closely to Hvorslev's theory than do the results of the drained tests on the samples from the finished embankment, even though the conditions were similar. The deformation rate in this set of tests was 4% d^{-1}, whereas in the drained test on embankment samples it was 1.1% d^{-1} (Figs 24-26).

Undrained triaxial tests were made with a conventional apparatus on samples taken while the

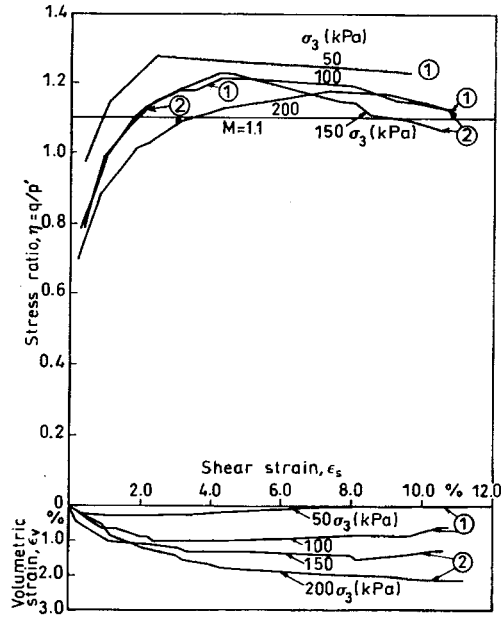

Fig. 24. Samples from Taasia test embankment. Sample sets 1 and 2. Triaxial CADC test. σ'_{vc} = 700 kPa. w = 33–42% $\sigma_3 / \sigma_1 = 0.8$.

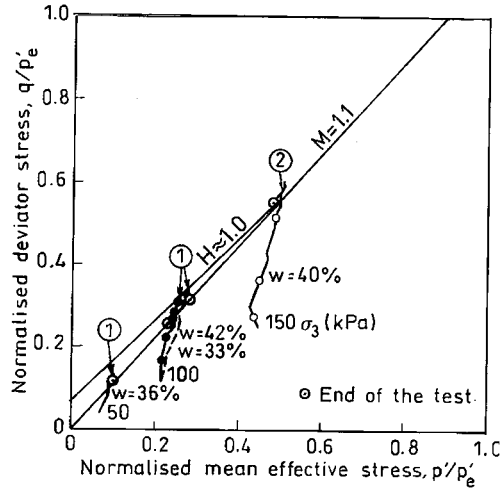

Fig. 25. Taasia test embankment. Sample sets 1 and 2. Triaxial CADC test normalised by equivalent stress from combined isotropic normal compression line (Fig. 34). σ'_{vc} = 700 kPa. w = 33–42%.

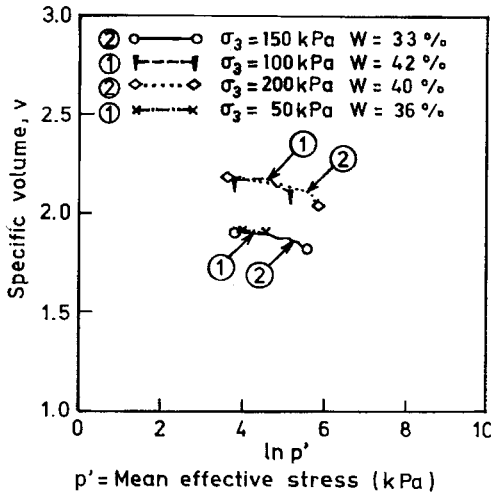

Fig. 26. Samples from Taasia test embankment. Sample sets 1 and 2. Triaxial CADC test. σ'_{vc} = 700 kPa. w = 33–42%.

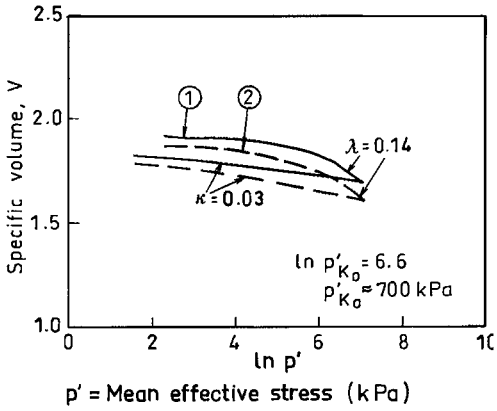

Fig. 27. Samples from Taasia test embankment. Sample sets 1 and 2. An oedometer test. w = 33–42%.

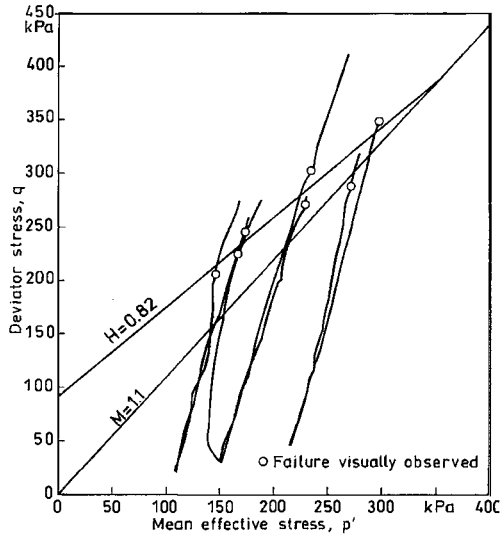

Fig. 28. Taasia test embankment. Sample set 3. Layer compacted six times before sampling. Stress-controlled triaxial CADC test. w = 30–35%.

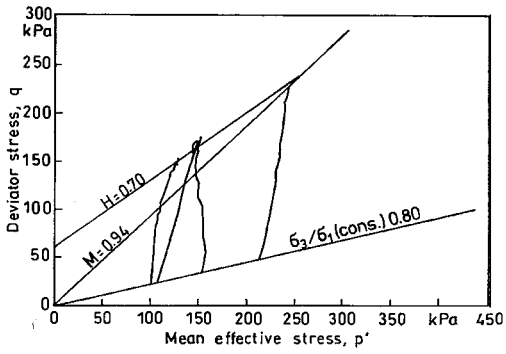

Fig. 29. Taasia test embankment. Sample set 4. Layer compacted twice before sampling. Triaxial CAUC test. w = 30–34%. Back pressure used in consolidation.

test embankment was being built (Fig. 29). These samples were taken from the test embankment after two compaction passes. The water content varied in the range 30–34%. The shears behaved in accordance with Hvorslev's theory. The test series gave 0.94 as the value of the parameter M, whereas the most probable value from the drained tests was 1.1. The test series gave H = 0.70 for the slope of Hvorslev's line.

Undisturbed samples from the dry crust

The dry-crust clay was also studied with undisturbed samples in undrained tests using conventional triaxial equipment. The deformation rate was 1% d^{-1}. The samples, which measured 3.6 cm x 8.0 cm, had a water content of 35–39%. The results of the tests are shown in Fig. 30. The shearing in the tests exhibited a distinct maximum strength. M is about 1.2–1.4 as estimated from

the ε_3,q/p'-curves. The shear took place at q,p'-values of 1.7–2.1. The results indicate that failure clearly takes place above the critical state. The test results correspond to those obtained in stress-controlled tests on material from the finished test embankment, in which the maximum shear stresses were substantially above the critical state. As the tests were conducted at the same water content and specific volume, no normalisation was made. In the case of undisturbed dry crust, ageing may have changed the yield envelope.

Dry-crust clay was also studied on undisturbed samples with the aid of an oedometer, the water content of the samples being 38–50%. The results of the oedometer tests are shown in Fig. 31. Various tests gave 40, 90 and 446 kPa as preconsolidation values of p' for the K_o normal compression stress. A K_o-value of 0.67 was used in the calculations. The great scatter in values is due to the difference in water contents, to the difficulty of shaping the samples and to the desiccation cracks in the samples. The preconsolidation pressure of the dry crust calculated from Skempton's equation (70) was 196 kPa.

Determination of the coefficient of earth pressure at rest; samples from the test embankment

Tests to determine the coefficient of earth pressure at rest, K_o, were made by gradually increasing the cell pressure and the axial pressure and keeping the cross-sectional area of the sample constant. The procedure used for determining K_o has been described by Davis and Poulos (1963). The perimeter of the sample was monitored with a strain gauge. Shown in Fig. 32 are the results of two tests, the first without consolidation during the increase in stresses and the second with overnight consolidation. The samples were taken from the test embankment after six compaction passes. The calculations were based on effective stresses.

The more reliable result, K_o = 0.67, was obtained from the test in which samples were consolidated during the test. The result of the second test did not differ markedly from that of the first, except that the pore pressure was distributed more heterogeneously in the sample and was thus less reliable.

Different values were obtained for the preconsolidation pressure σ_{vc}'. As the slope in the σ_1', σ_3' diagram changes at the maximum effective pressure, σ_1' = 370 kPa, it represents the point of change from the over-consolidated state to the normal consolidated state. According to the test, K_o gets a value of 0.56 in the normal consolidated state.

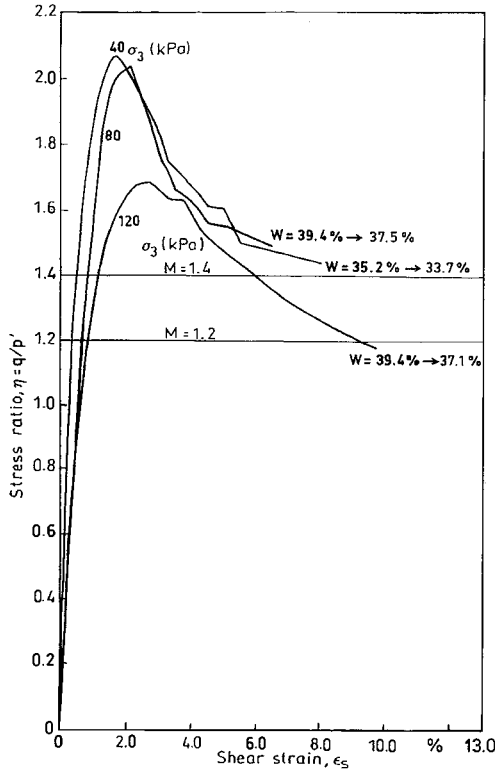

Fig. 30. Taasia earth dam. Undisturbed dry crust (layer 4). Area 2 (Fig. 1). Triaxial CIUC test. w = 35–39%.

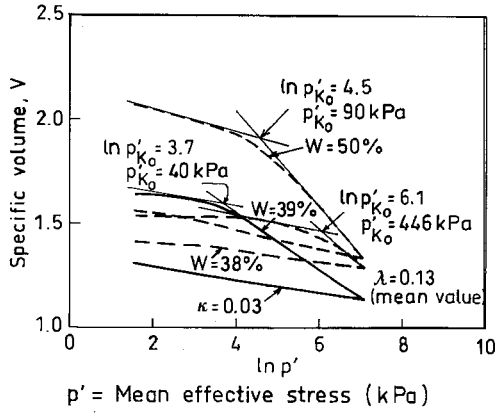

Fig. 31. Taasia earth dam. Undisturbed dry crust (layer 4). Area 2 (Fig. 1). Sample set 1. An oedometer test. w = 38–50%.

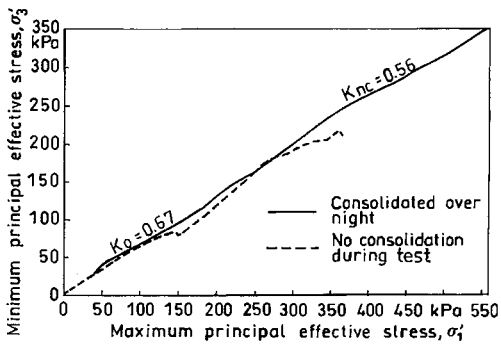

Fig. 32. Taasia test embankment. Sample set 3. Determination of coefficient of earth pressure at rest, K'_o in triaxial test. Sample taken from test embankment after six compaction passes. w = 34%. σ'_{vc} = 370 kPa.

4.4.4 Determination of critical state parameters with index tests

Sections 4.4.2 and 4.4.3 dealt with the laboratory tests used to determine the parameters of the deep clay layers and dry-crust clay on the basis of the critical state theory.

Critical state parameters can also be estimated from index properties. As a rule, the critical state parameters are determined in several ways, and the results are compared with each other to ensure reliable design values. The determination of critical state parameters from index properties has been studied by Wroth and Wood (Wroth and Wood 1978, Wood 1983, 1984, 1985, Wroth 1984).

The critical state constant of plastic clays λ can be determined from plasticity properties. Wood (1983) has derived equation (95) for the relationship between the constant λ and the plasticity index I_p.

$$\lambda = (I_p G_s) / \ln R \tag{95}$$

where

I_p = plasticity index

$$G_s = \frac{\gamma_s}{\gamma_w} \tag{96}$$

G_s = specific gravity of soil grains
γ_s = unit weight of soil particles
γ_w = unit weight of water

$$R = \frac{c_P}{c_L} \tag{97}$$

where
c_P = shear strength at plastic limit
c_L = shear strength at liquid limit

According to Wroth and Wood (1978), R = 100 can be used for many clays.

The index tests gave lower λ-values than did the oedometer and triaxial tests. The values obtained from the index properties can only be used to determine the λ-ratios of different layers. The tests showed that the value (100) of the constant R (equation 97) is too high for the clay studied.

4.4.5 Combined results of consolidation and drained shear tests

The results of different consolidation tests are combined in Fig. 33. The values plotted are averages of each test group. The results were used in normalisation as explained in Sections 4.4.2 and 4.4.3.

As the dry crust clay and the underlying deep clay layers are similar in origin, the results, too, are

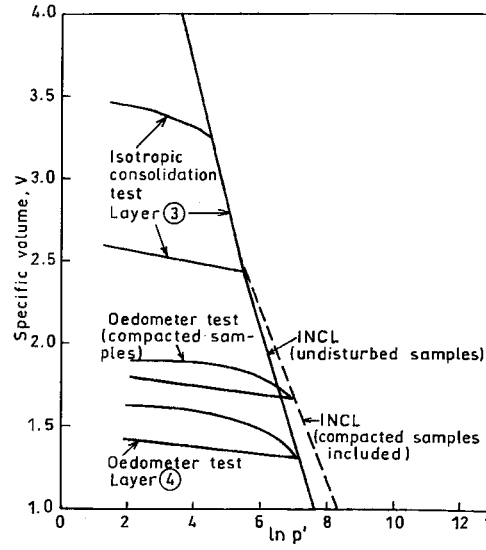

p' = Mean effective stress (kPa)
INCL = Isotropic normal consolidation line

Fig. 33. Foundation of Taasia earth dam. Combined results of consolidation tests of undisturbed samples.

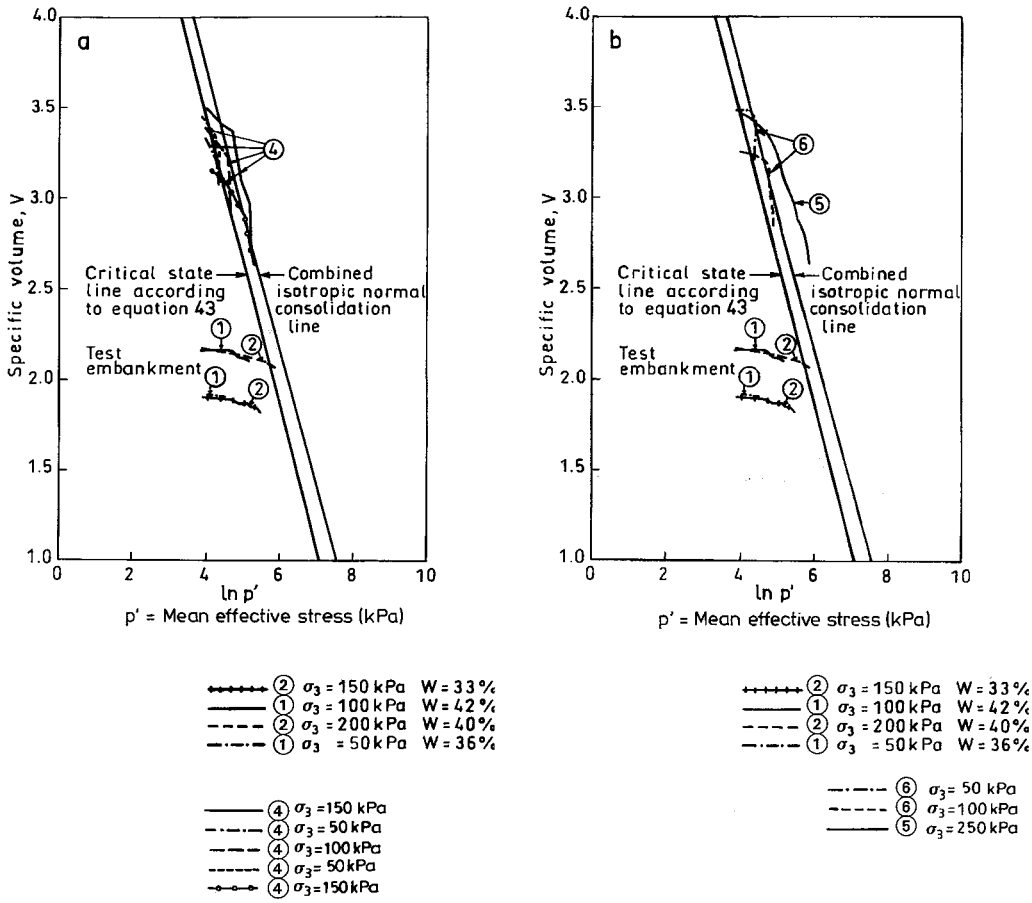

Fig. 34. Taasia earth dam. Combination of results of drained shear tests.

fairly similar. At pressures similar to the preconsolidation pressures of the dry-crust clay, the normal consolidation line varied, depending on the type of test. The undisturbed samples yielded at lower values than in the tests on compacted samples or samples from the test embankment. Laboratory and site compaction both made the dry-crust clay stiffer than the original dry-crust layer. Moreover, as the undisturbed dry-crust clay samples gave a high failure strength, the compacted samples did not behave exactly like the dry-crust clay layer.

The drained shear test data are combined in Fig. 34, which plots the critical-state line calculated from equation (43) and the isotropic normal consolidation line. It is seen that the stress-strain states in the tests were approaching the critical state.

4.4.6 Model suitable for the over-consolidated Taasia clay

Typical results for the different kinds of triaxial tests made on Taasia clay in this project are shown in the p',q-coordinate system in Fig. 35. Tests on clay layers under dry crust show that the tangent of the slope of the straight line drawn according to the experiments is about 0.8. The q-value with zero p'-value is 20 kPa. As a similar line is drawn from the test results of over-consolidated specimens, the average tangent of the slope is about 1.0. The q-value with a zero p'-value for undisturbed dry-crust samples is of the order of 50 kPa.

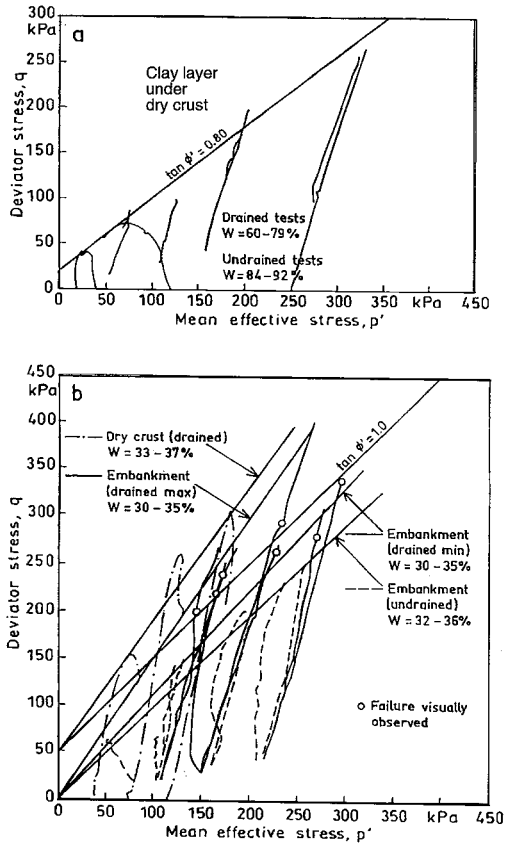

Fig. 35. Typical results of triaxial tests plotted in p', q-plane.

According to the experiments, Taasia clay gives higher ϕ'-values in the over-consolidated state than in the normally consolidated state. The q-value with zero p'-value (corresponding to cohesion) is also higher in the over-consolidated state.

As discussed by Jamiolkowski et al. (1991), there is much doubt about the shear strength parameters of over-consolidated clays when compared with the same clays as normally consolidated. It is usually assumed that the peak value of the friction angle (ϕ') of an over-consolidated soil is equal to or slightly lower than that of normally consolidated soil. With the exception of normally consolidated and lightly over-consolidated soils, the cohesion c' is not zero, resulting in a function of the clay mineralogy and OCR.

This assumption implies that, in both normally consolidated and over-consolidated clays, the failure envelope is linear. However, laboratory experiments (Mesri and Abdel-Ghaffar 1993) indicate that the failure envelope of naturally over-consolidated stiff, aged and boulder clays is non-linear. Mesri and Abdel-Ghaffar report a variation of ϕ' and c' as a function of OCR for London clay.

The common assumption that the friction angle ϕ' is the same for a clay in the over-consolidated and normally consolidated states applies only to lightly over-consolidated clays. A more difficult problem arises with the design value of the cohesion c'. In the case of Taasia clay, laboratory tests were made when it was in the normally consolidated state and the over-consolidated state. Over-consolidated samples were taken from the natural layers and from the test embankment.

The results for Taasia clay support earlier findings (Burland 1990, Leroueil and Vaughan 1990) that intact clays yield and fail with greater deviator stresses than do the corresponding destructured clays.

As the model with Hvorslev's surface and the modified Cam-Clay model were the best critical state models available in the CRISP-90 program, they were used in such a manner that the parameters represented conditions in the pressure range of the test embankment foundation. As will be seen, both models can be used in the Taasia case.

Calculations were also made with the Z-soil program, where the cap similar to the Modified Cam-Clay yield surface and the Drucker-Prager model are combined. This model can also be used in the Taasia case.

In respect of strain characteristics, the CRISP-90 program is theoretically suitable for Taasia clay, as can be seen from Fig. 34.

5 Simulation calculations for settlement of the Taasia test embankment

5.1 Sections and parameters used in calculations with the CRISP-90 program

The cross-section of the test embankment used in the calculations is shown in Fig. 36. As the properties of the embankment and its foundation are symmetric about the mid-line of the embankment, only half of the embankment is treated in this context. Also shown in Fig. 36 are the element mesh

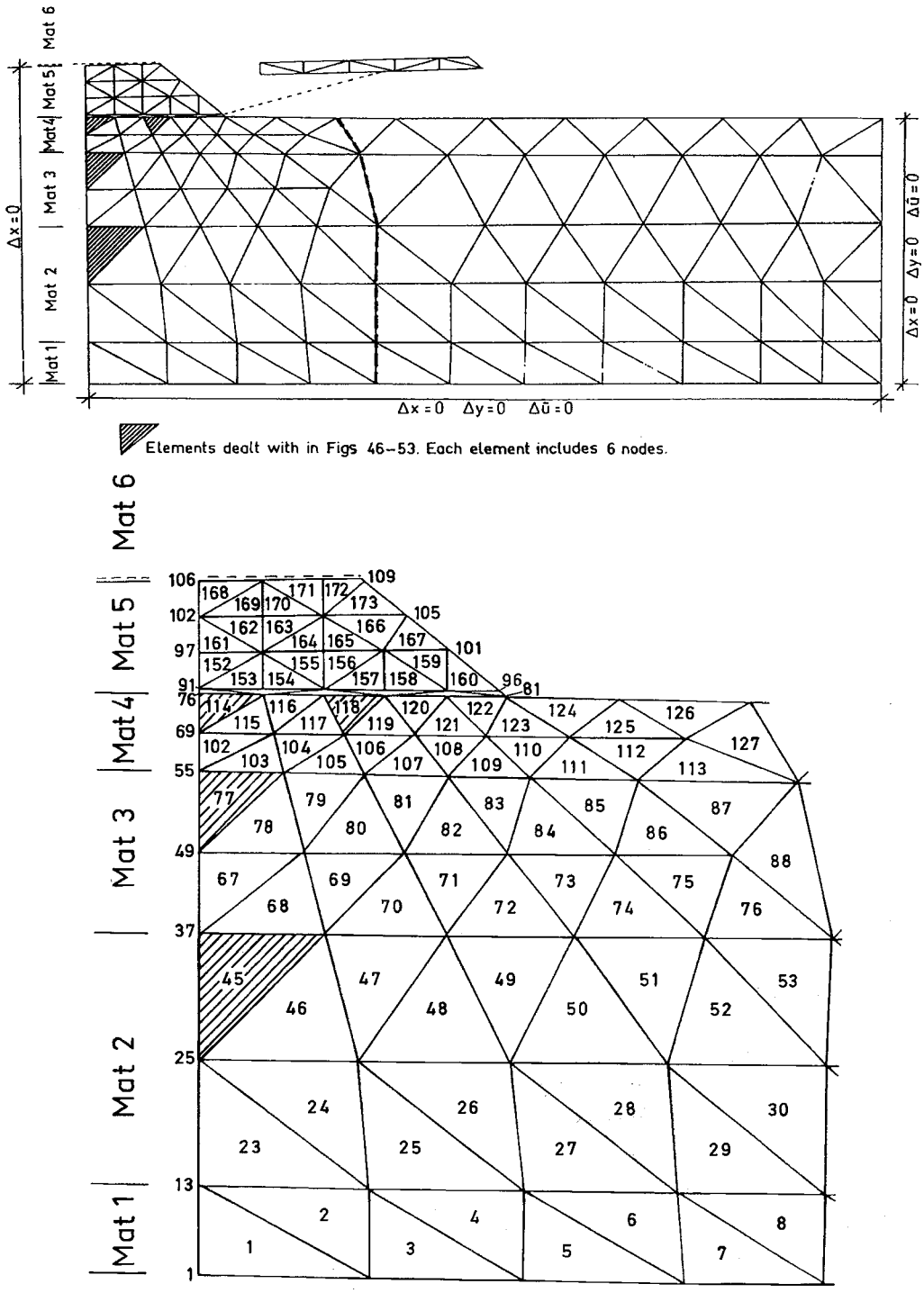

Fig. 36. Calculation cross-section of test embankment with element mesh for CRISP 90 program. Parameters used in calculation are listed in Table 9.

and boundary conditions. Calculation were made with triangular elements. Each element included 6 nodes. In the calculation illustrated with figures the results of the Modified Cam-Clay model and the Schofield model were compared with each other and with the measured settlement and pore water pressure data. The parameters used in the calculation are listed in Table 9. The calculation was mainly based on the most probable values of the parameters determined in the laboratory and on the hydraulic conductivity values determined in situ. The horizontal hydraulic conductivity was taken as ten times the vertical owing to the layered structure of the clay and the variation in hydraulic conductivities in each calculation layer. Because of the behaviour of the test embankment, the parameter κ was assigned a value 0.02, which is somewhat lower than the value, 0.03, often measured in the laboratory. In calculations, the hydraulic conductivity of the test embankment and the dry crust was assumed to be higher than that measured, as the embankment and dry crust are not water-saturated and thus absorb water at the initial stage. Moreover, the conditions prevailing during the construction of the test embankment support the assumption that the pore water pressures that developed in the dry crust were lower than the additional load.

The p_o'-values for the Schofield model were applied in such a manner that the yield curves of the Schofield model and the Modified Cam-Clay model meet at the critical state line. It is important that the yield curves follow the soil behaviour in this area. The laboratory results supported the Modified Cam-Clay-type yield curve. In addition to the modelling described above, various calculations were made using the elastic, perfectly plastic model with the Mohr-Coulomb yield criterion (Table 10). The results of the calculations are given in Section 5.2, and are compared with the measured data on the test embankment in Section 6.1. The effect of the different parameters on the calculated settlement is discussed in Section 6.2.

The construction of the test embankment was simulated in a 17-day undertaking divided into 22 increments. The consolidation following construction was divided into 38 increments: the first year ends at increment 38, the tenth year at increment 50 and the hundredth year at increment 60. The calculations described in detail were performed with the elastic isotropic model for the test embankment and with the Modified Cam-Clay model or Schofield model for the foundation. Comparison of the calculated and measured settlements and pore water pressures with each other permitted conclusions to be drawn about the appropriateness of the parameters chosen.

Identical results were obtained when the elastic, perfectly plastic model with the Mohr-Coulomb yield criterion replaced the elastic isotropic model as test embankment material.

5.2 Calculation results with the CRISP-90 program

The principal stresses, pore water pressure and displacements prevailing at different periods were printed out as were the changes in settlement and pore water pressure at some nodal points as a function of time. Also printed out were a list of elements approaching the critical state and the values of the mean effective stress, deviator stress and shear strain of some elements as a function of time.

Fig. 37 shows the increment of the maximum principal stress caused by the test embankment immediately after construction. Depicted in Fig. 38 is the excess pore water pressure at the same time, and in Fig. 39 the increment of minimum principal stress. Figs. 40–42 give the distribution of the stress increments one year after construction, and Figs. 43–45 ten years after construction. Figs. 46–49 exhibit settlement and excess pore water pressure as a function of time at different nodal points.

Figs. 50–53 illustrate the development of stresses and shear strain at the centre of three elements under the mid-line of the embankment and one element halfway to the side of the test embankment. Fig. 54 gives a list of elements that approach the critical state at different times.

Figs. 55–57 present charts of the displacement at the end of construction, one year after construction and ten years after construction, respectively. Fig. 58 presents the directions of maximum principal stresses at the end of construction.

As described in Section 5.1, various calculations were made using the elastic perfectly plastic model with the Mohr-Coulomb yield criterion (Table 10). When only the test embankment was modelled as elastic perfectly plastic material, the results were identical to those shown. However, when the dry-crust clay was also modelled with the elastic, perfectly plastic model a very low value was obtained for post-construction settlement.

Table 9. Initial parameters of simulation calculation (layers in Fig. 36)

Material layer	E_h kPa	E_v kPa	ν_{hh}	ν_{vh}	G_{hv} kPa	γ $kN\,m^{-3}$	k_x $m\,s^{-1}$	k_y $m\,s^{-1}$	K_o	
6	3,000	3,000	0.35	0.35	2,000	0	$5x10^{-9}$	$5x10^{-9}$	0.67	
5	3,000	3,000	0.35	0.35	2,000	18	$5x10^{-9}$	$5x10^{-9}$	0.67	
	κ	λ	e_{cs}	M	ν'	γ $kN\,m^{-3}$	k_x $m\,s^{-1}$	k_y $m\,s^{-1}$	K_o	H
4	0.02	0.30	2.65	1.2	0.40	18	$5x10^{-9}$	$5x10^{-9}$	0.67	0.68
3	0.02	0.60	4.25	1.0	0.35	15	$5x10^{-10}$	$5x10^{-11}$	0.6	0.68
2	0.02	0.50	3.80	1.0	0.35	17	$5x10^{-10}$	$5x10^{-11}$	0.6	0.68
1	0.02	0.30	3.15	1.0	0.35	17	$5x10^{-10}$	$5x10^{-11}$	0.6	0.68

	p_o' Modified Cam Clay model	p_o' Schofield model	k (cracking zone) = $1x10^{-8}$ $m\,s^{-1}$
in dry crust	200 kPa	272 kPa	
under dry crust	90 kPa	122 kPa	
at level 28.5 m	105 kPa	143 kPa	
at level 26.5 m	115 kPa	156 kPa	
at level 16.5 m	200 kPa	272 kPa	

Table 10. Parameters of calculation with model 5 (an elastic, perfectly plastic model with Mohr-Coulomb failure criterion)

Material layer	E_o *kPa*	ν	c_o *kPa*	ϕ' °	y_o	J	γ_w *kN m*$^{-3}$	γ *kN m*$^{-3}$	k_x *ms*$^{-1}$	k_y *ms*$^{-1}$	m_E	m_c
6	2,000 -5,000	0.35	0	30	0	4	10	0	$5x10^{-9}$	$5x10^{-9}$	0	0
5	2,000 -5,000	0.35	0	30	0	4	10	18	$5x10^{-9}$	$5x10^{-9}$	0	0
4	2,000 -5,000	0.35	0	30	0	4	10	18	$5x10^{-9}$	$5x10^{-9}$	0	0
3	4,000	0.25	0	25	0	4	10	15	$5x10^{-9}$	$5x10^{-10}$	0	0
2	4,000	0.25	0	25	0	4	10	17	$5x10^{-9}$	$5x10^{-10}$	0	0
1	4,000	0.25	0	25	0	4	10	17	$5x10^{-9}$	$5x10^{-10}$	0	0

J = 4 Mohr-Coulomb failure criterion

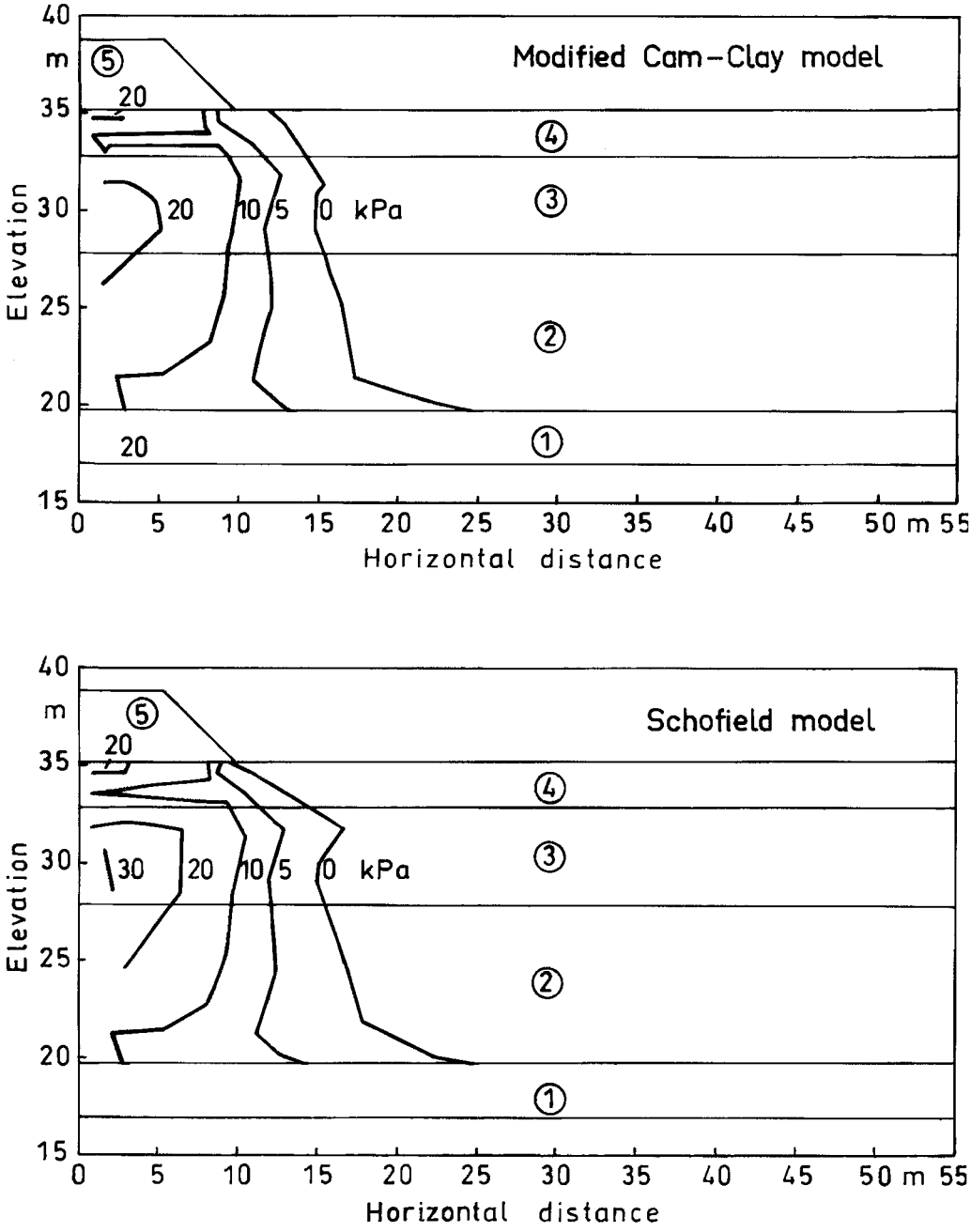

Fig. 37. Increase in maximum principal stress, $\Delta\ \sigma_3'$, at end of construction.

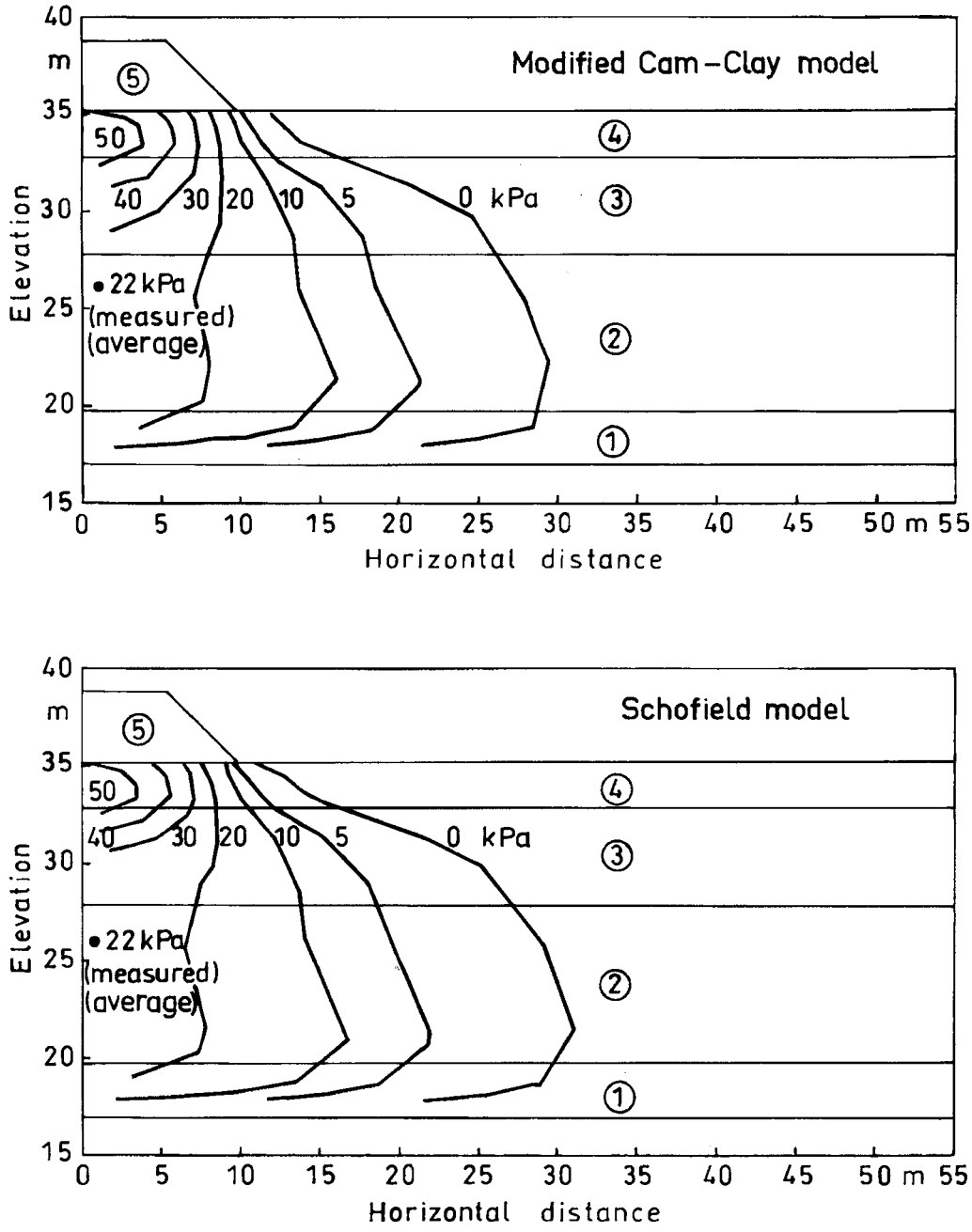

Fig. 38. Excess pore water pressure, Δu, at end of construction.

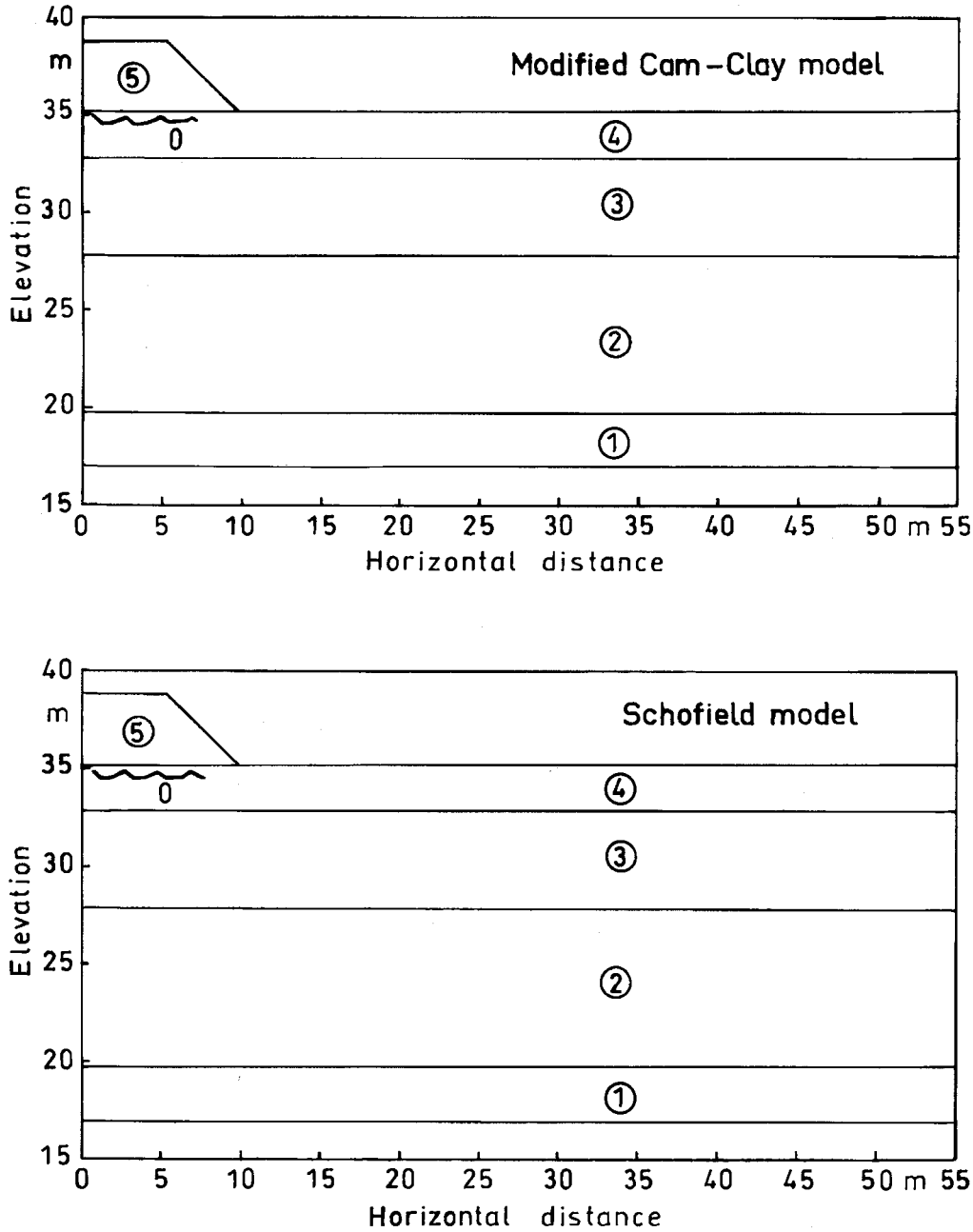

Fig. 39. Increase in minimum principal stress, $\Delta\ \sigma_3'$, at end of construction.

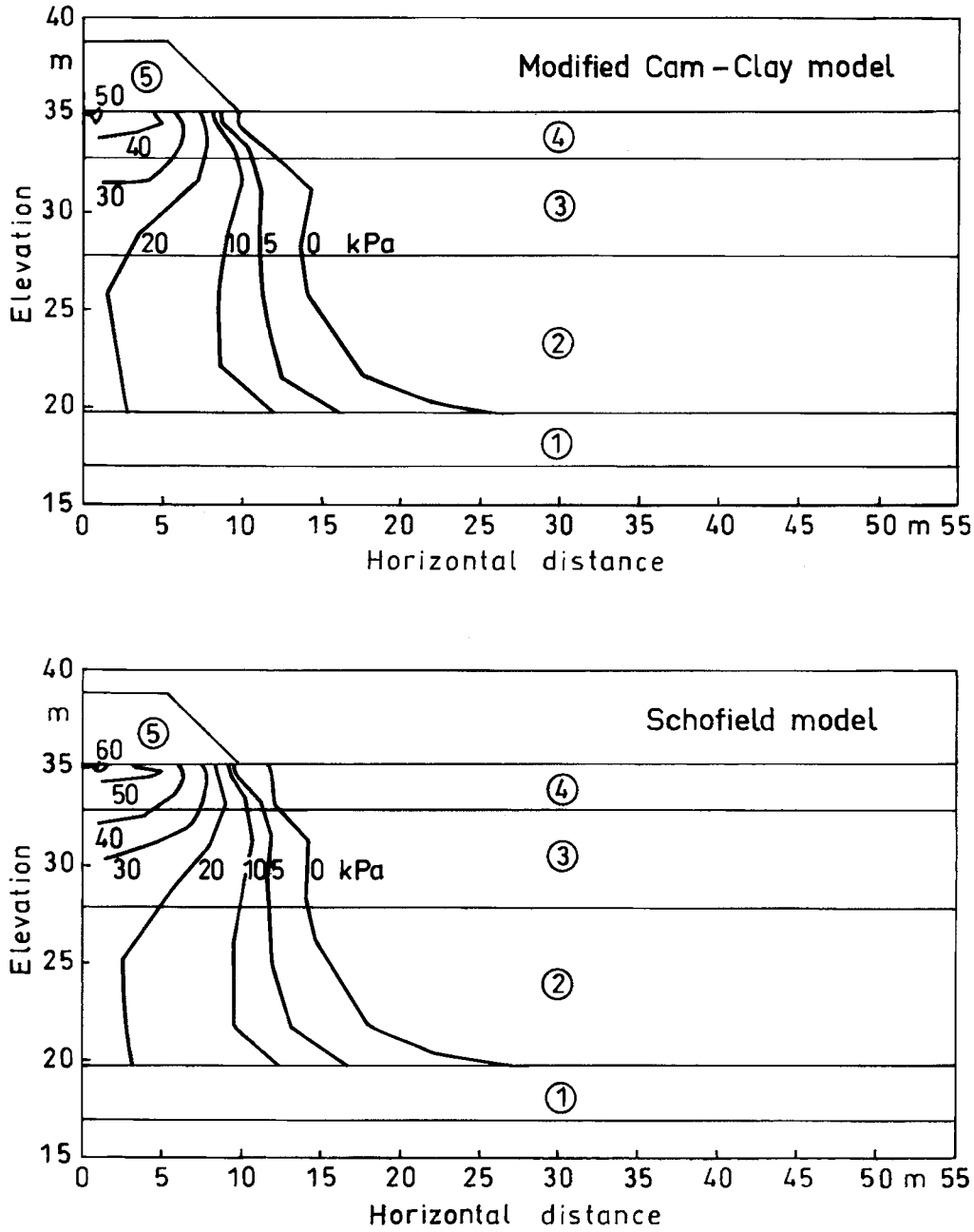

Fig. 40. Increase in maximum principal stress, $\Delta\ \sigma_1'$, one year after construction.

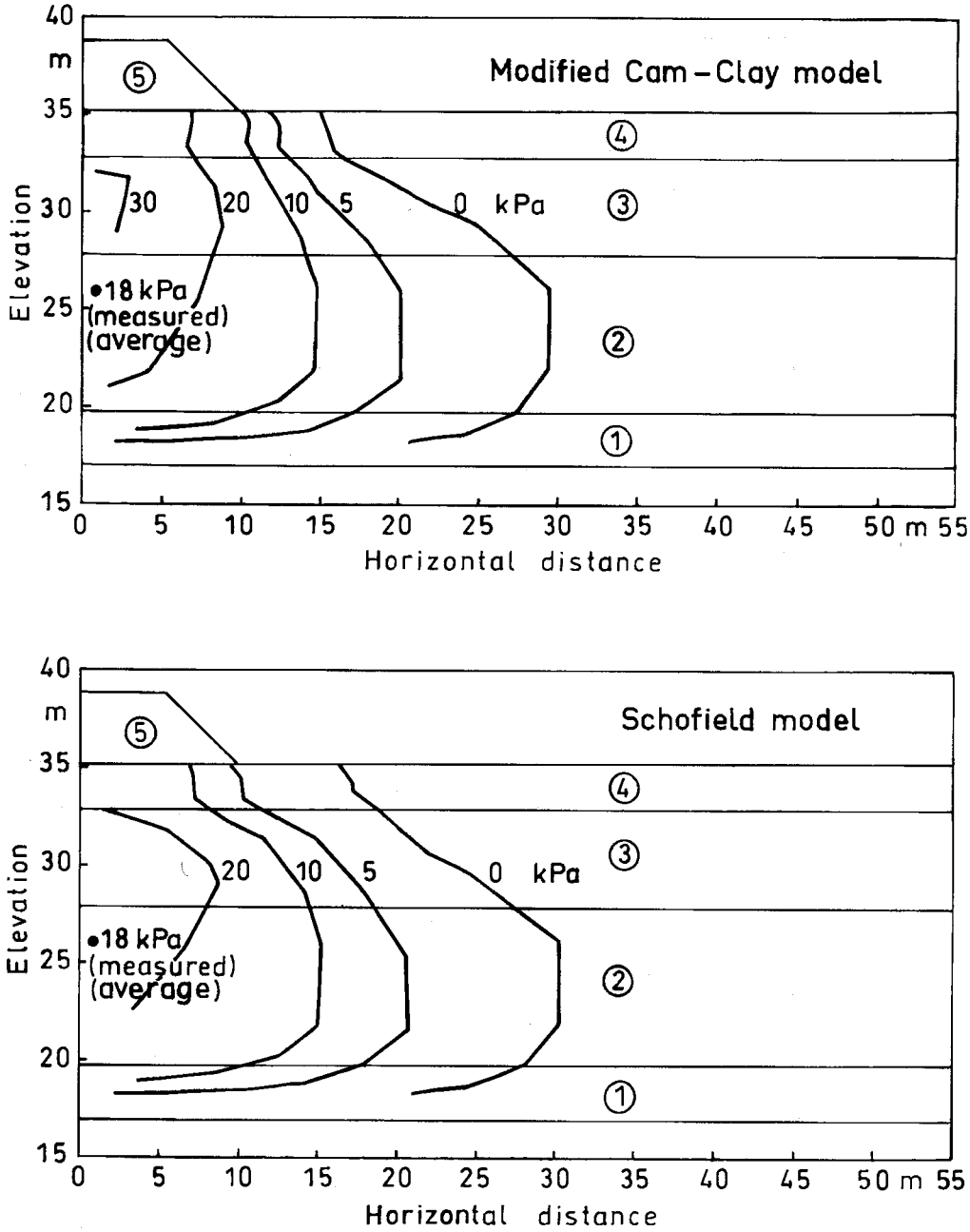

Fig. 41. Excess pore water pressure, Δu, one year after construction.

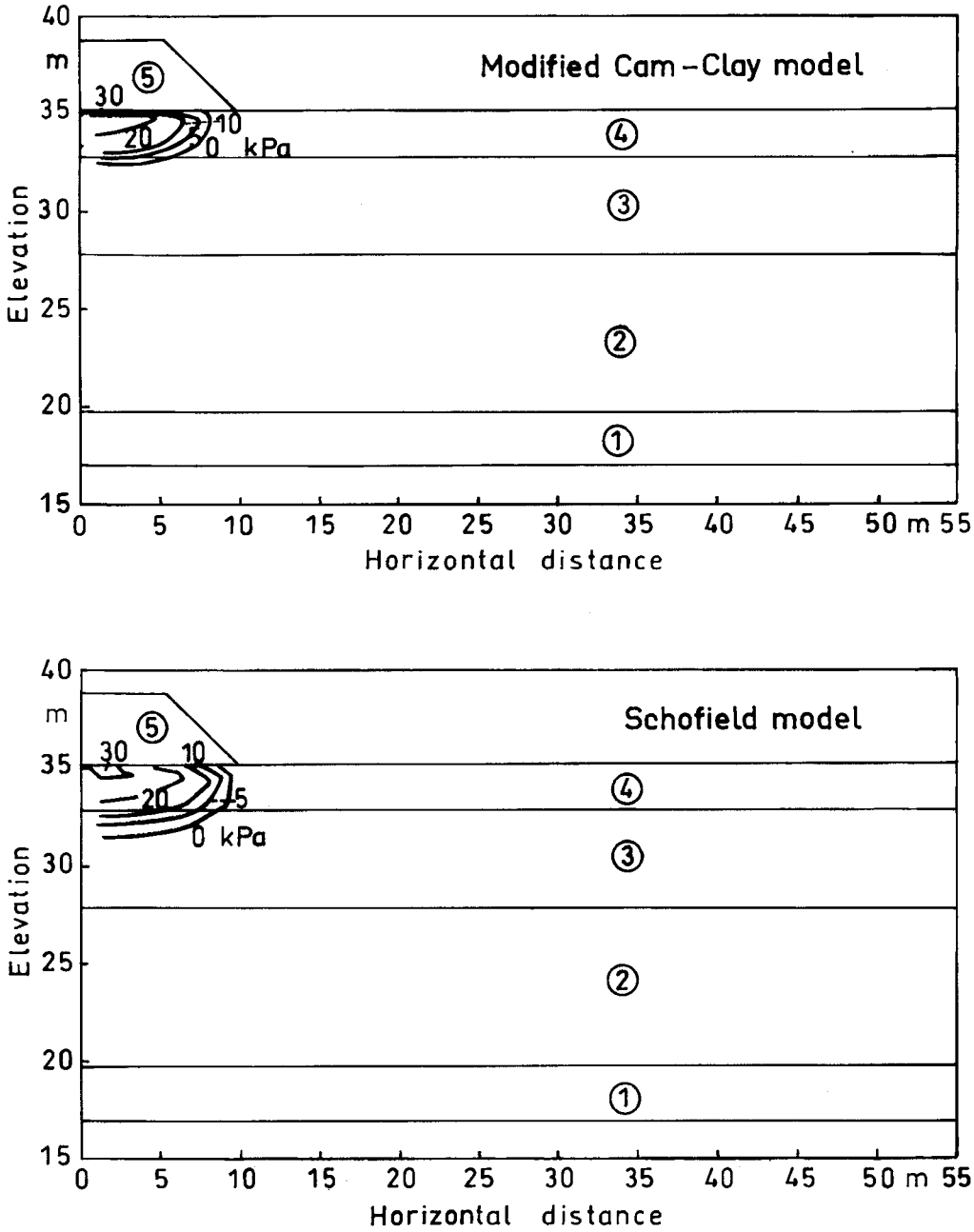

Fig. 42. Increase in minimum principal stress, $\Delta\ \sigma'_3$, one year after construction.

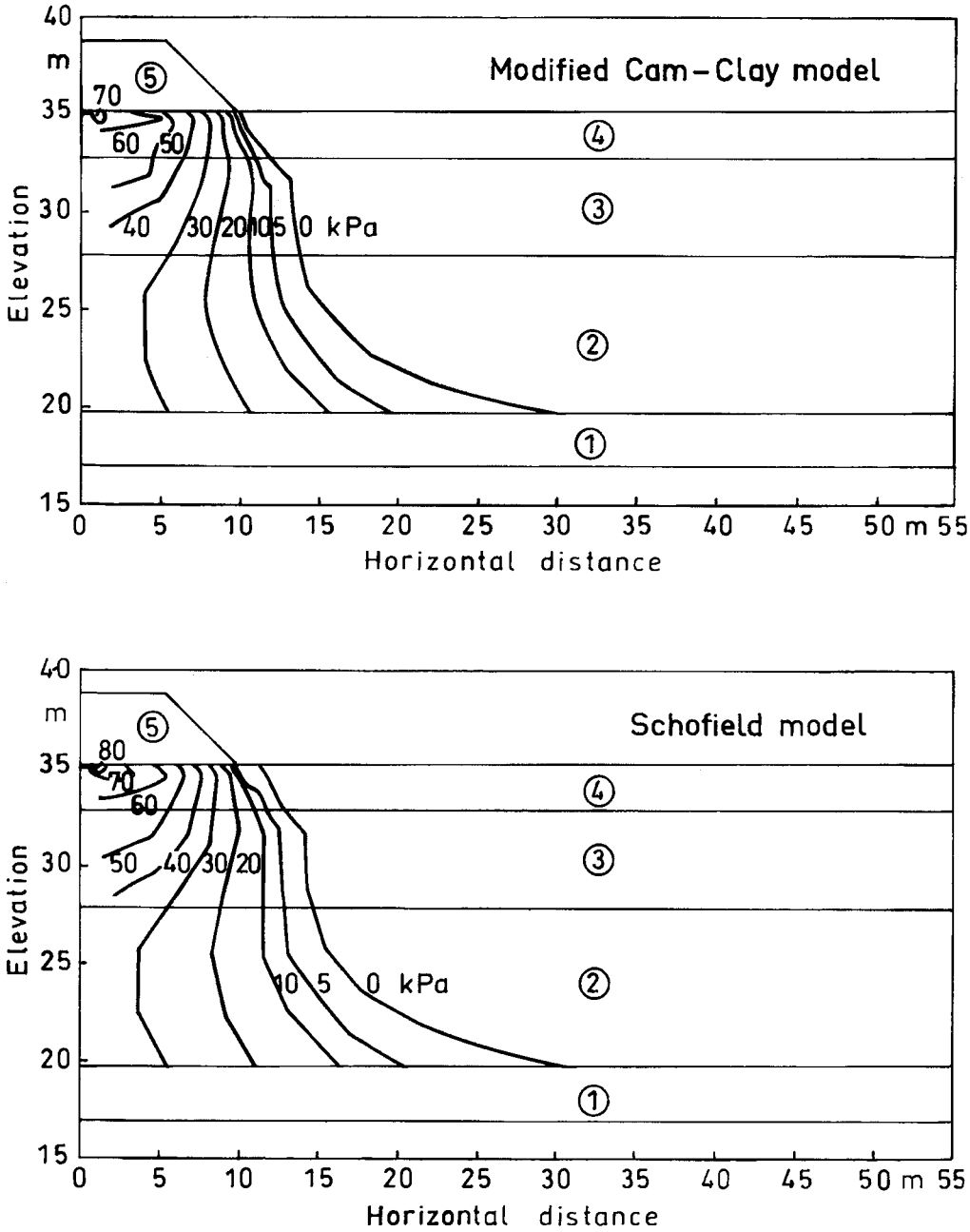

Fig. 43. Increase in maximum principal stress, $\Delta\ \sigma_1'$, 10 years after construction.

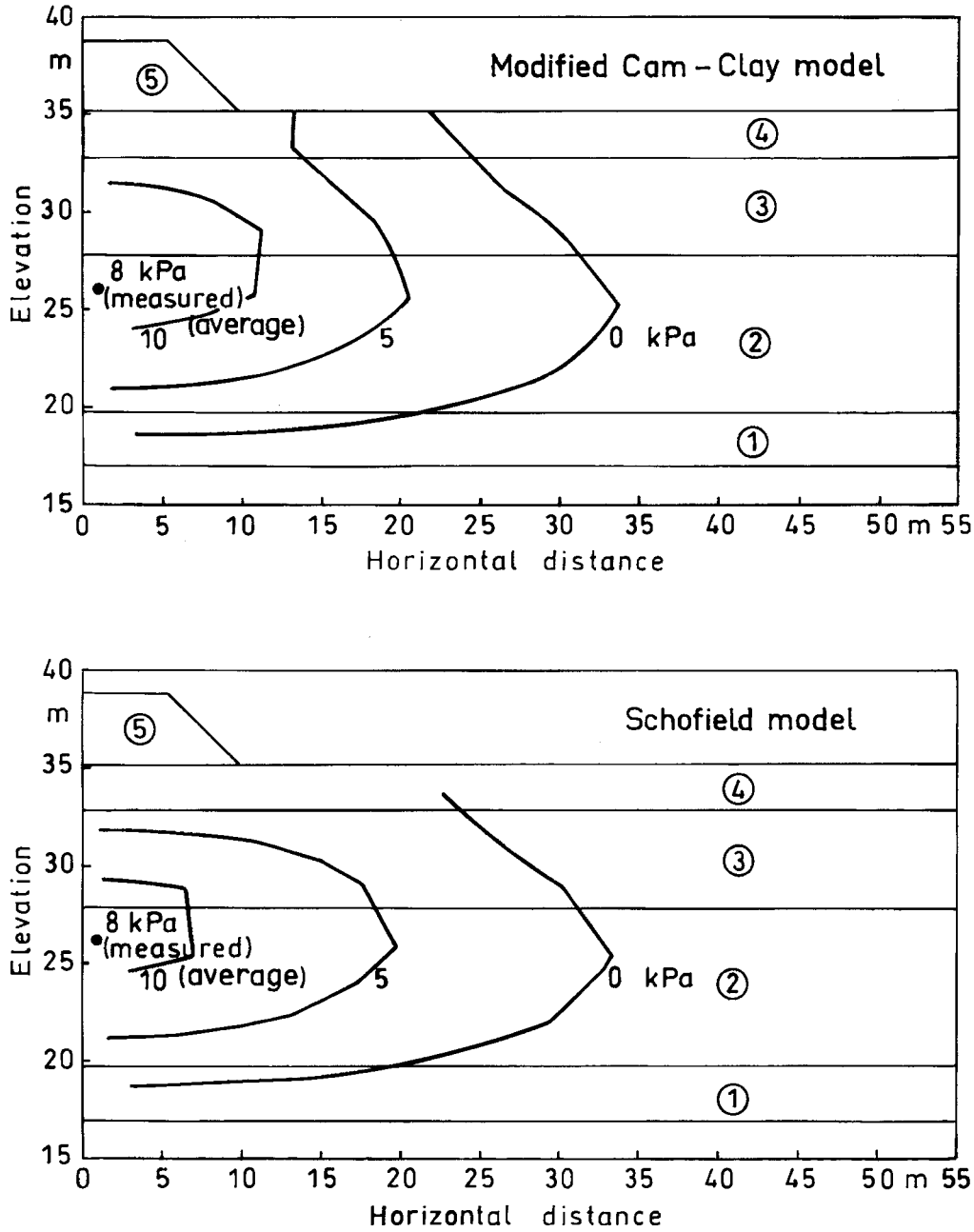

Fig. 44. Excess pore water pressure, Δu, 10 years after construction.

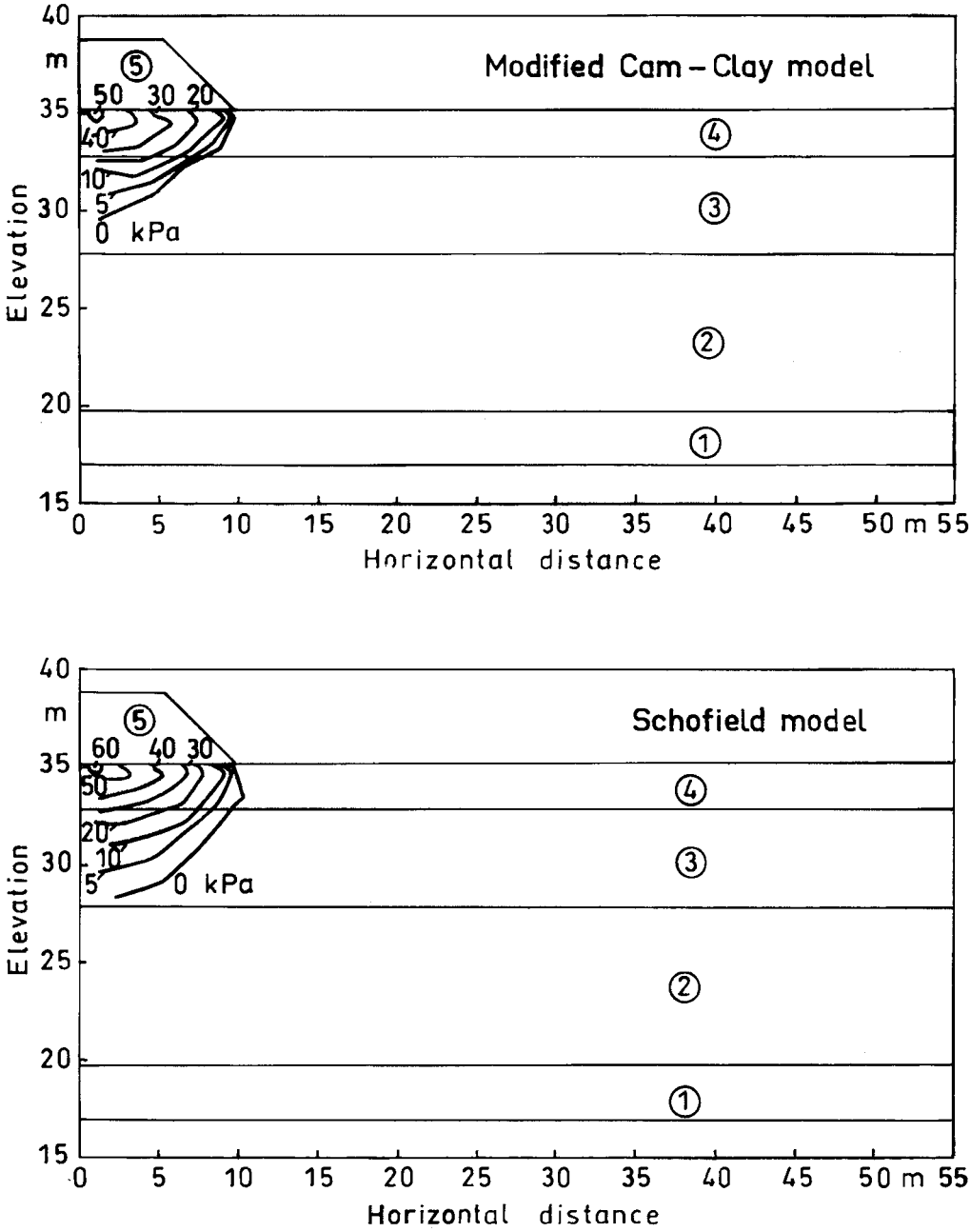

Fig. 45. Increase in minimum principal stress, $\Delta\ \sigma_3'$, 10 years after construction.

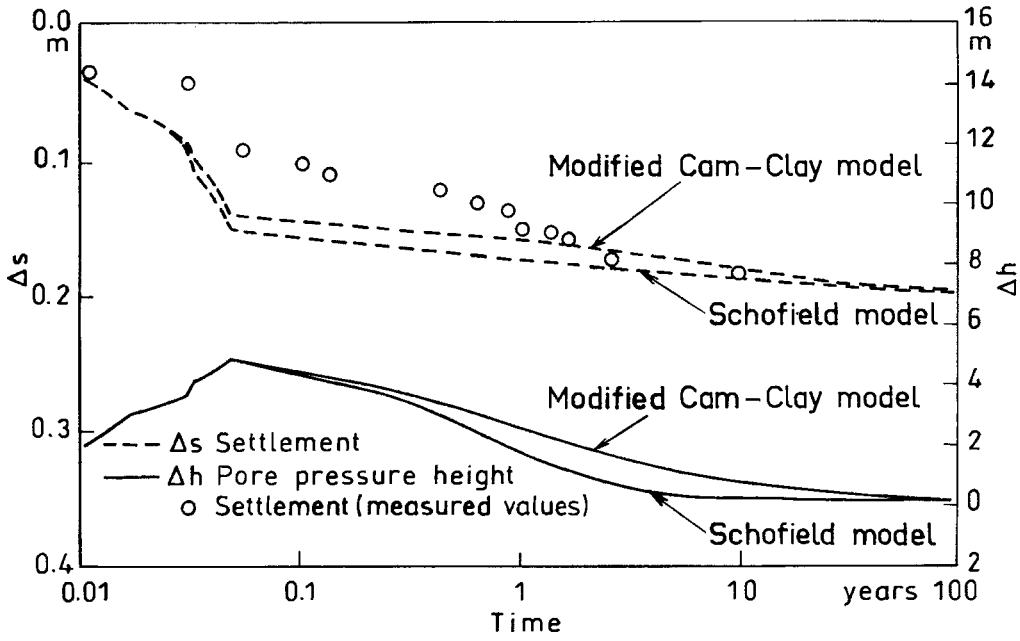

Fig. 46. Settlement and excess pore water pressure at nodal point 76 (ground surface) (Fig. 36).

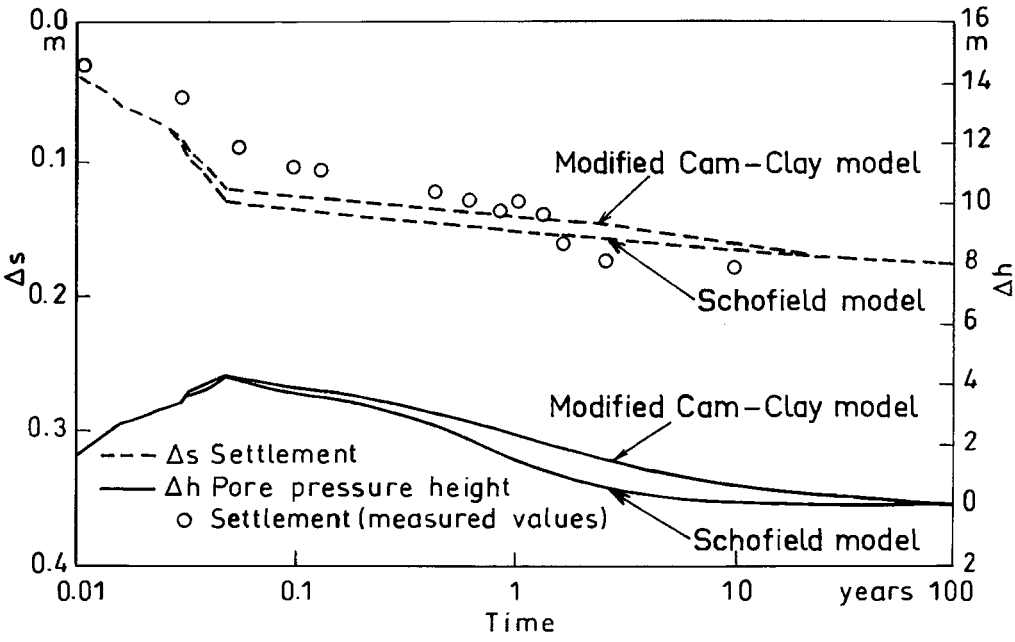

Fig. 47. Settlement and excess pore water pressure at nodal point 78 (ground surface) (Fig. 36).

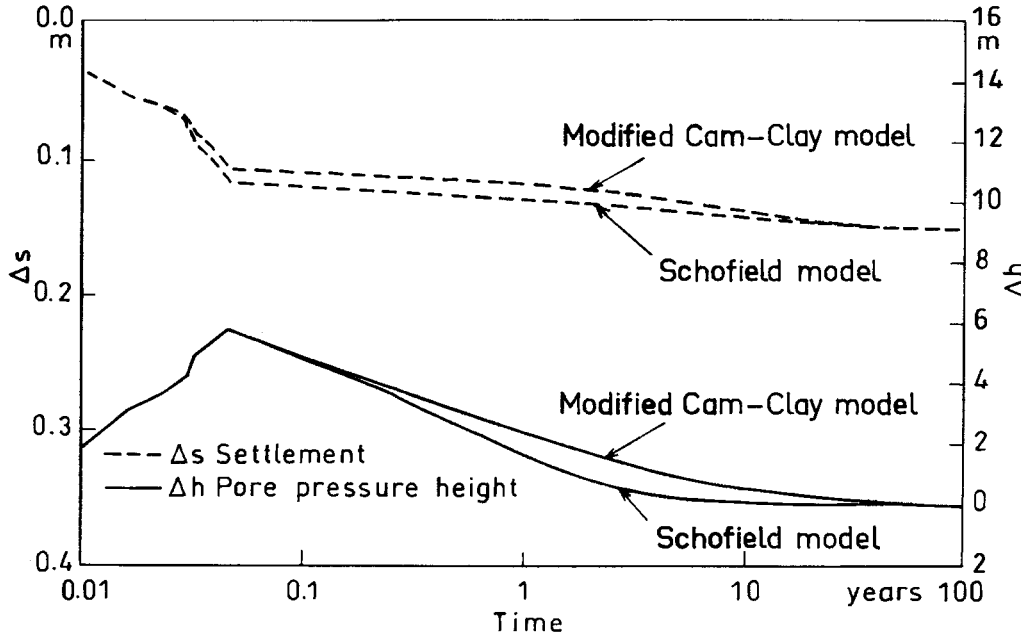

Fig. 48. Settlement and excess pore water pressure at nodal point 69 (dry crust) (Fig. 36).

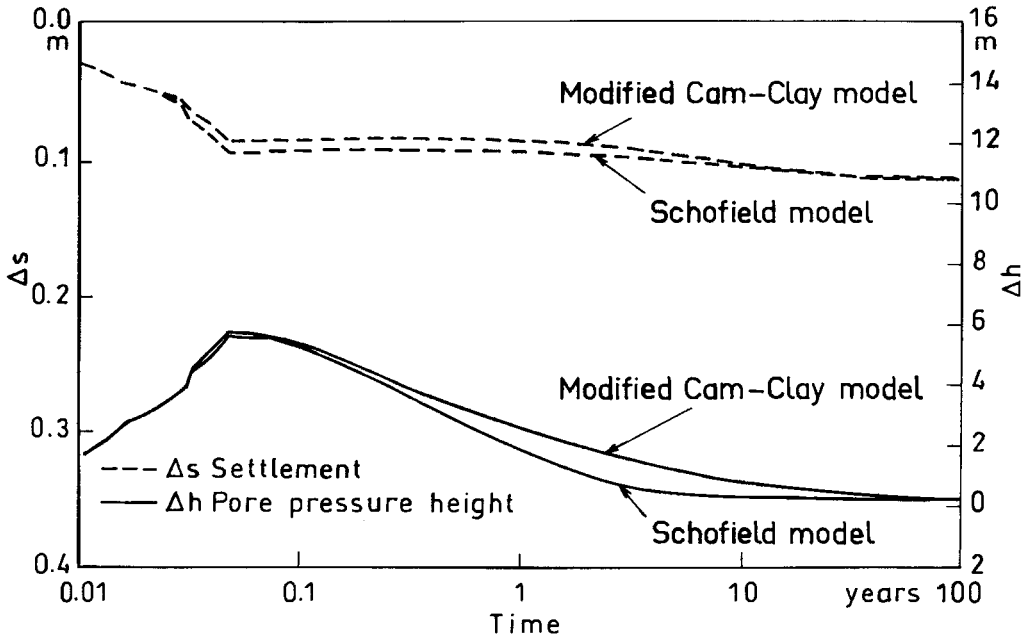

Fig. 49. Settlement and excess pore water pressure at nodal point 55 (lower surface of dry crust) (Fig. 36).

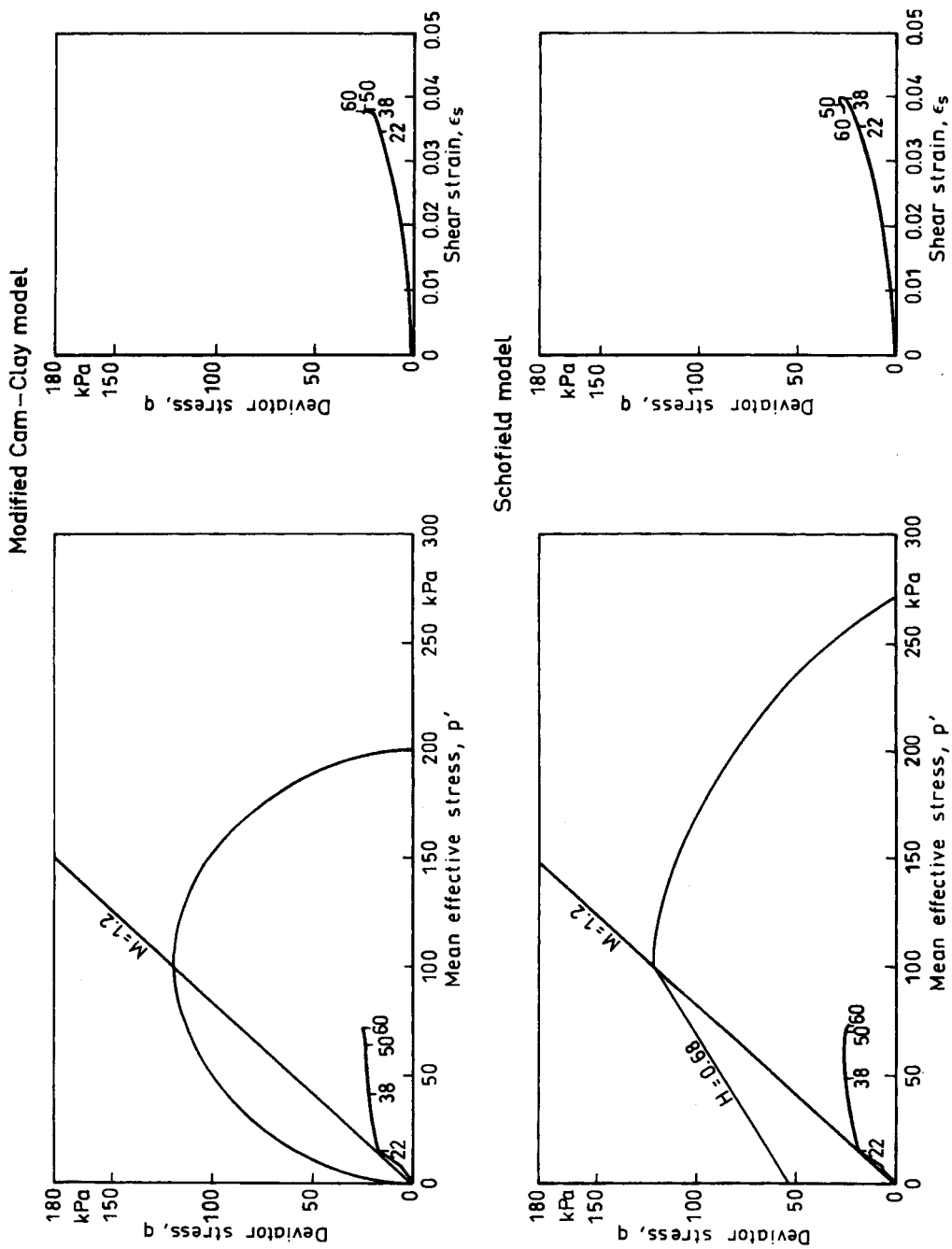

Fig. 50. Development of stresses and shear strain at centre of element 114 (at level of settlement plates) (Fig. 36).
Time increments: 22, at end of construction; 38, one year after construction; 50, 10 years after construction; 60, 100 years after construction.

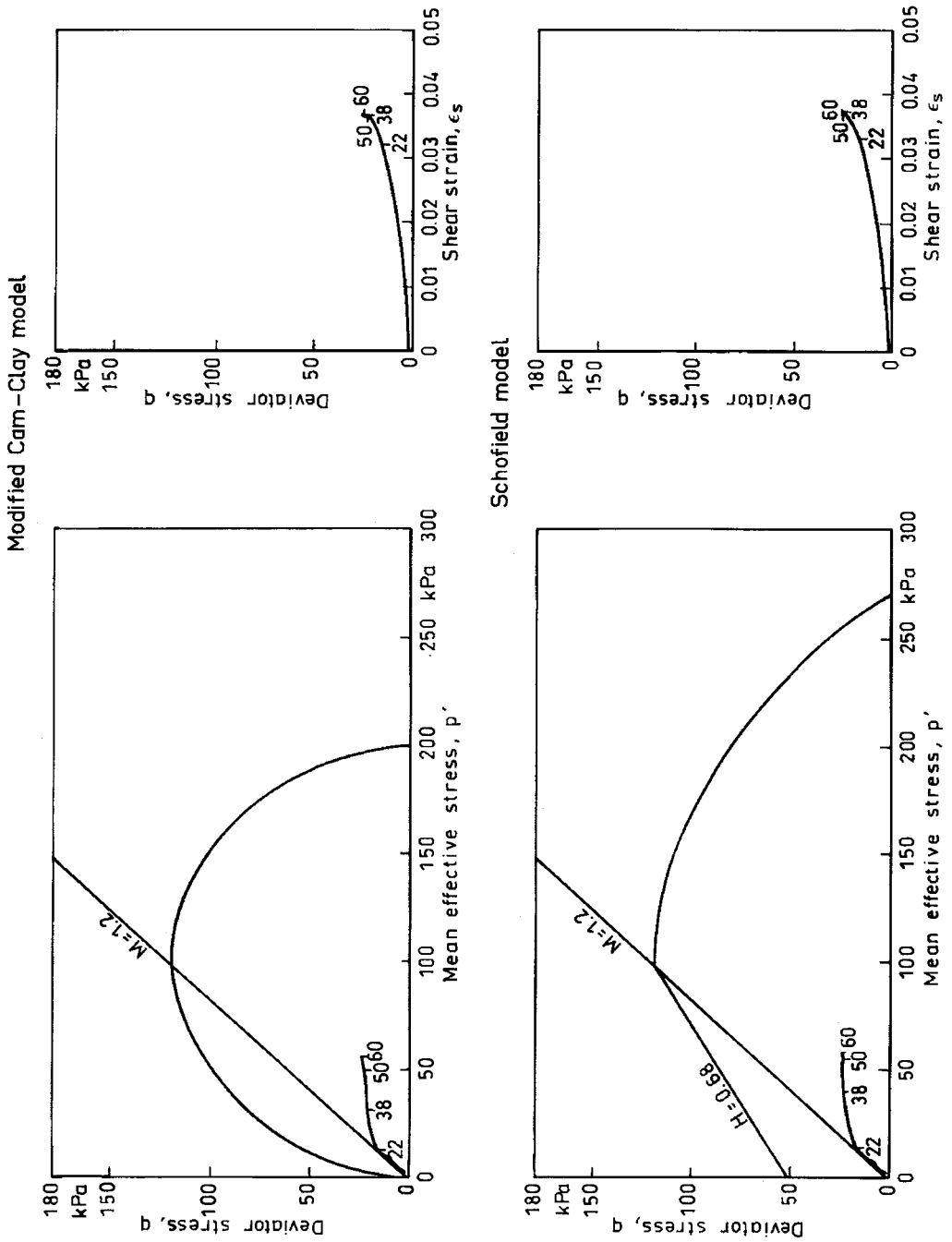

Fig. 51. Development of stresses and shear strain at centre of element 118 (at level of settlement plates) (Fig. 36).
Time increments: 22, at end of construction; 38, one year after construction; 50, 10 years after construction; 60, 100 years after construction.

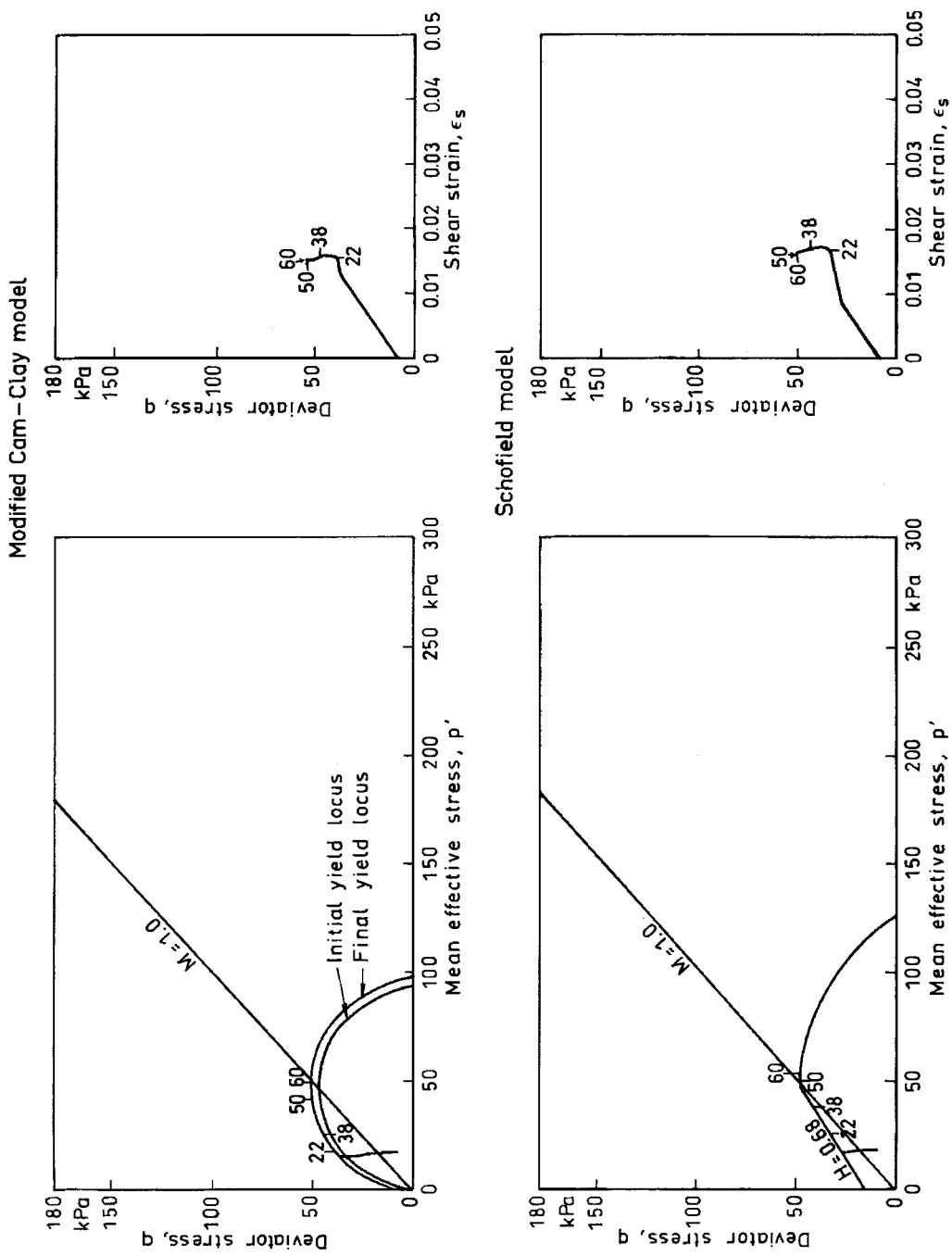

Fig. 52. Development of stresses and shear strain at centre of element 77 (under dry crust) (Fig. 36). Time increments: 22, at end of construction; 38, one year after construction; 50, 10 years after construction; 60, 100 years after construction.

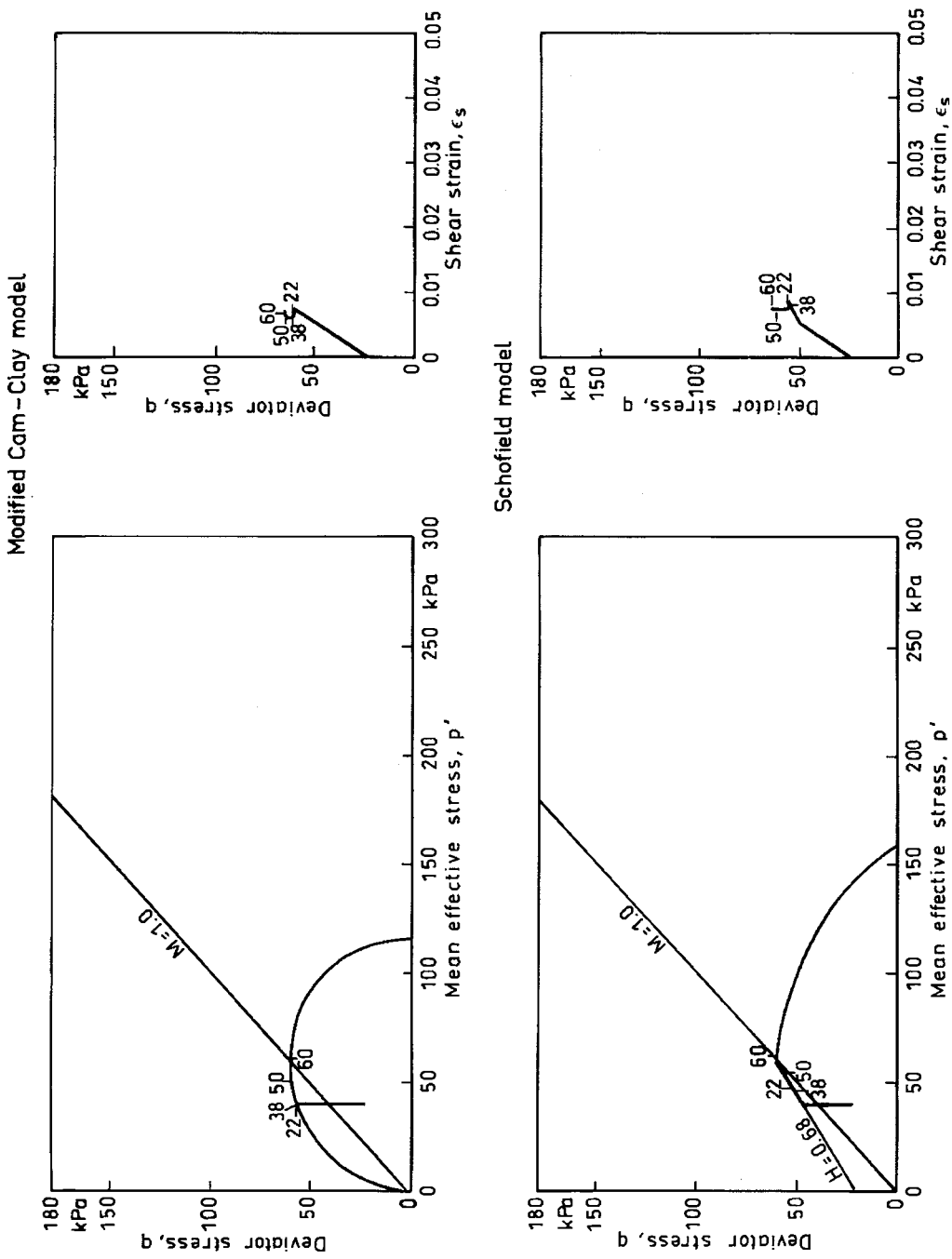

Fig. 53. Development of stresses and shear strain at centre of element 45 (layer 2) (Fig. 36).
Time increments: 22, at end of construction; 38, one year after construction; 50, 10 years after construction; 60, 100 years after construction.

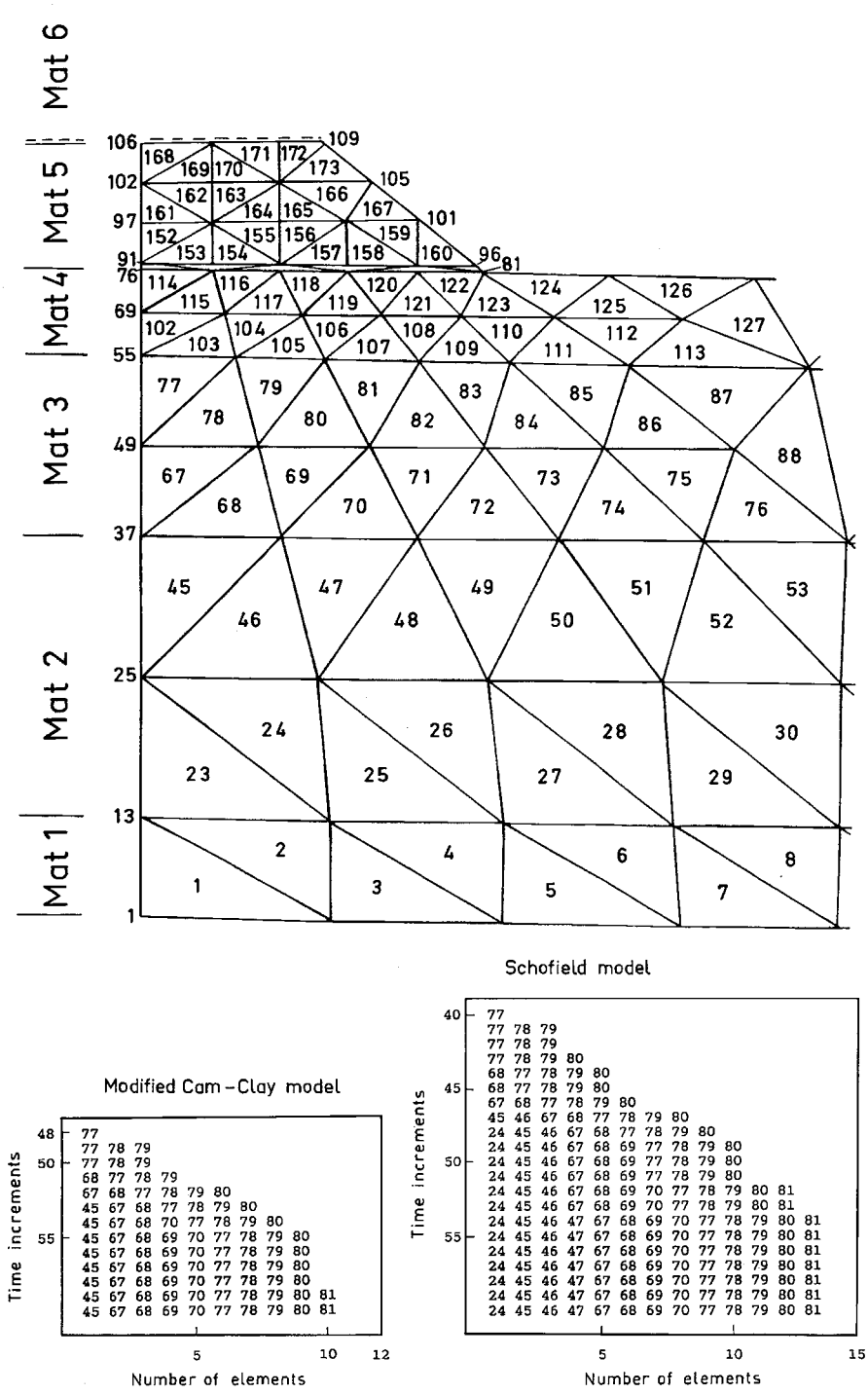

Fig. 54. Elements approaching critical state at different times.
Time increments: 22, at end of construction; 38, one year after construction; 50, 10 years after construction; 60, 100 years after construction.

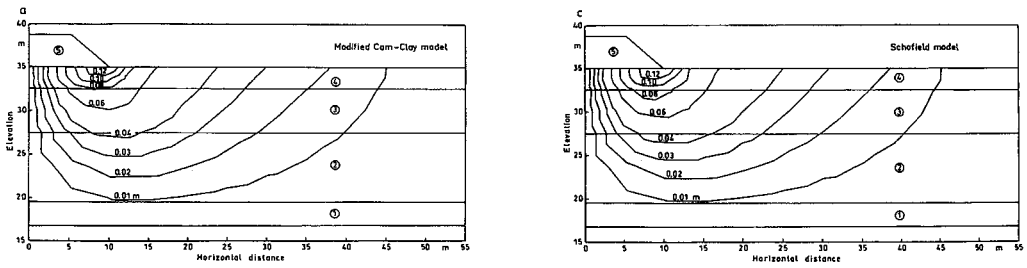

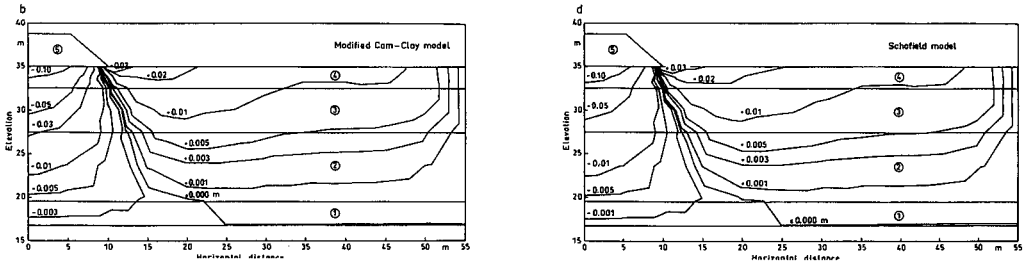

Fig. 55. Displacement at end of construction.

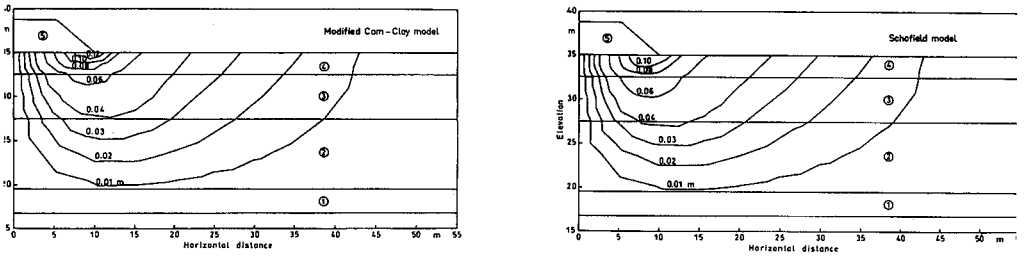

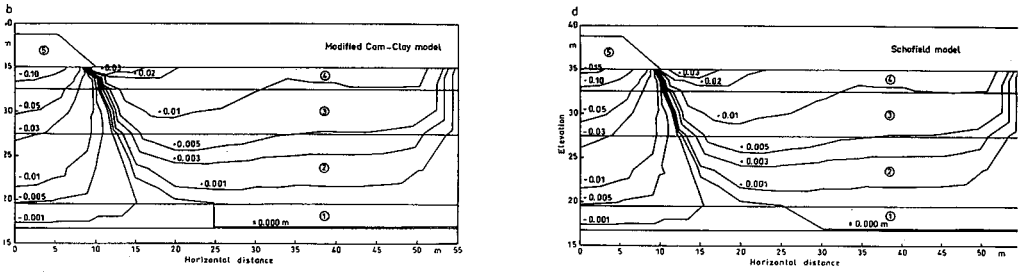

Fig. 56. Displacement one year after construction.

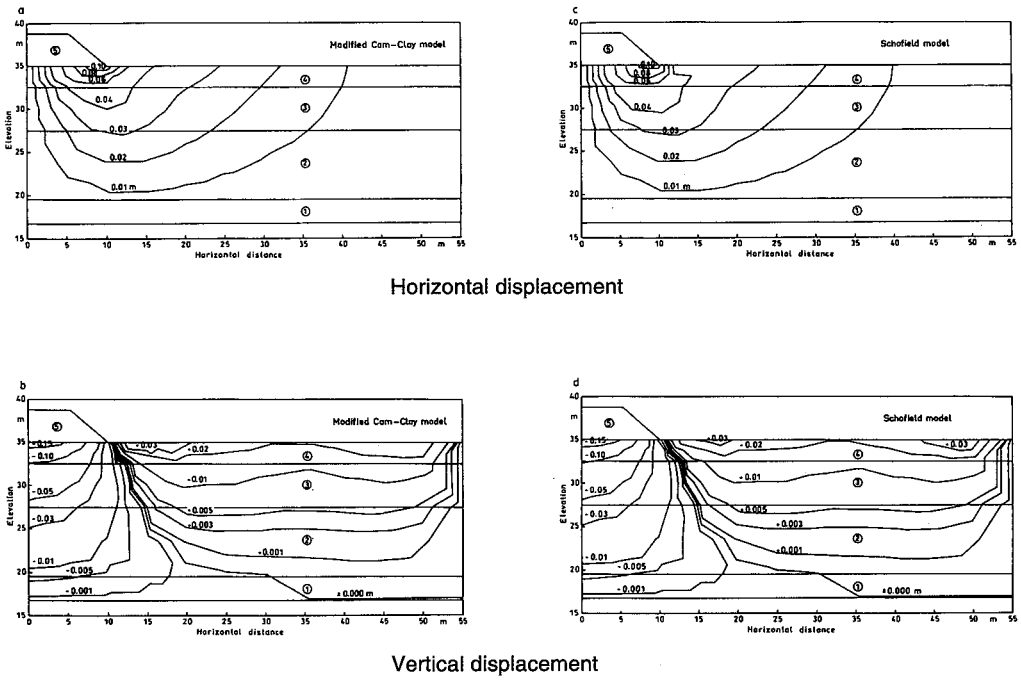

Fig. 57. Displacement 10 years after construction.

Pore pressure build-up in the deep clay layer was similar to that given by the original modelling. When all the cross-sections were included as elastic perfectly plastic material no reliable results were obtained at reasonable values of the parameters; the pore pressure values in particular were extremely low.

A sensitivity analysis was made using plane strain (Table 11) and axi-symmetric (Table 12) calculations. In the axi-symmetric calculations, the diameter of the test embankment was determined with the aid of the masses in the embankment. Slightly different data sets were used in the sensitivity analysis because different sets seemed to be the most probable ones at different stages of the project.

The values of the parameter κ varied in the range 0.02–0.04, depending on the tests. The same range of values was used in the calculations. The design values of the parameter λ were selected on the basis of triaxial consolidation and oedometer tests. Index properties were used to deduce the λ-values for different layers.

The values of the parameter e_{cs} correspond to the λ- and e_o-values obtained from the tests.

The values of the stress ratio M at critical state for the deep clay layers were derived from triaxial tests conducted on normally consolidated samples by accepting the most common values. The tests of over-consolidated samples gave higher values, which were taken into account in the value of M of the dry-crust layer.

The Poisson ratio ν' can be determined from the K_o-test made in the laboratory with equation (68), according to which $\nu' = 0.35$. As determined with equation (62), the ν'-value for the dry crust-crust clay is 0.40. The additional calculations used the value $\nu' = 0.2$ for the layers below the dry crust derived from the triaxial drained compression tests and $\nu' = 0.30$ for the dry crust.

The values of unit weights, γ, were determined from the investigation of the test embankment and its foundation (Fig. 11 and Table 6).

The coefficients of hydraulic conductivity, k_x and k_y, were obtained from field tests. The horizontal hydraulic conductivity k_x was taken as ten times the vertical hydraulic conductivity k_y due to the layered structure of the clay layers and the variation in hydraulic conductivities in each calculation layer. In the calculations, the hydraulic con-

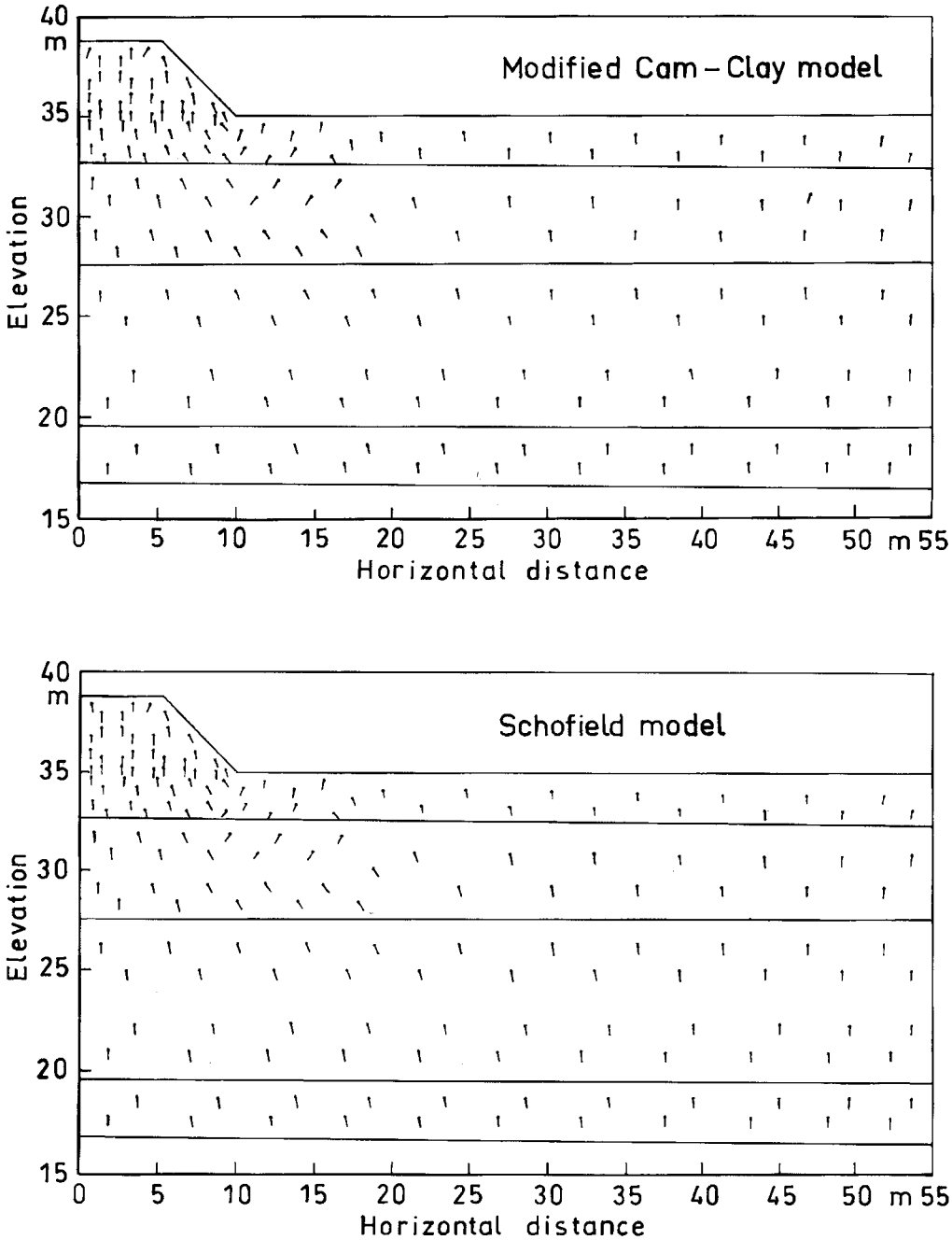

Fig. 58. Directions (outward from points) of maximum principal stresses at end of construction. Stresses given in Figs. 37 and 39.

Table 11. Sensitivity analysis. Data and calculated settlement of test embankment under centre line of embankment. Plane strain. The embankment is simulated with elastic model and the foundation with Modified Cam Clay or Schofield model.

	Data (as in Table 9 unless given separately Dimensions as in Table 9)	Settlement (cm) 10 years after construction Modified Cam Clay	Schofield model
1	All data as in Table 9	18.3	19.0
2	As in Table 9 but M = 0.9 for deep clay and 1.1 for dry crust	18.8	19.2
3	As in Table 9 but ν' = 0.25 for deep clay and 0.35 for dry crust	13.2	
4	As in Table 9 but ν' = 0.2 for deep clay and 0.3 for dry crust	11.4	
5	As in Table but κ = 0.03 and ν' = 0.25 for deep clay and 0.3 for dry crust		20.0
6	κ = 0.02; λ = 0.3 (layer 1), 0.5 (2), 0.6 (3), 0.14 (4); e_{cs} = 4.00 (1), 5.20 (2), 5.50 (3), 1.10 (4); M = 1.0 for deep clay and 1.2 for dry crust; ν' = 0.35; k_x = k_y = 5x10^{-10} for deep clay and 5x10^{-9} for dry crust and test embankment; p_o' as in Table 10 for Modified Cam Clay model; K_o as in Table 9; H = 0.45 for deep clay and 0.85 for dry crust	18.5	22.0
7	As in 6 but ν' = 0.2 for deep clay and 0.35 for dry crust and k_x = k_y = 2.8x10^{-8} for dry crust and test embankment	16.5	17.0
8	As in 6 but p_o' = 1.3 x p_o' in Table 10	19.0	19.0
9	As in 6 but λ = 0.5 (layer 1), 0.7 (2), 0.8 (3) and M = 0.9 for deep clay and 1.1 for dry crust; K_o as in 8	21.0	21.5
10	As in 6 but e_{cs} = 3.5 (layer 1), 4.7 (2), 5.0 (3) and M = 0.9 for deep clay and 1.0 for dry crust; K_o as in 8	20.0	20.4
		Total settlement Modified Cam Clay	Settlement during construction Modified Cam Clay
11	κ = 0.03; λ = 0.5 (layer 1), 0.7 (2), 0.8 (3), 0.07 (4); e_{cs} = 4.00 (1), 5.20 (2), 5.50 (3), 1.10 (4); M = 0.9 for deep clay and 1.15 for dry crust; ν' = 0.35; k_x = 5x10^{-10} for deep clay and 25x10^{-8} for dry crust; k_y = 5x10^{-11} for deep clay and 5x10^{-8} for dry crust; K_o = 0.67	22	19
12	As in 11 but κ = 0.02	15	
13	As in 11 but κ = 0.04	29	
14	As in 11 but λ = 0.6 (layer 1), 0.8 (2), 0.9 (3), 0.08 (4)	24	
15	As in 11 but λ = 0.4 (layer 1), 0.6 (2), 0.7 (3), 0.06 (4)	20	
16	As in 11 but M = 1.0 for deep clay and 1.25 for dry crust	21	
17	As in 11 but M = 1.1 for deep clay and 1.35 for dry crust	20	
18	As in 11 but M = 0.85 for deep clay and 1.1 for dry crust	23	
19	As in 11 but e_{cs} = 5.00 (layer 1), 6.20 (2), 6.50 (3)	20	
20	As in 11 but e_{cs} = 3.00 (layer 1), 4.20 (2), 4.50 (3)	23	
21	As in 11 but k_x = 25x10^{-7} for dry crust and k_y = 5x10^{-7} for dry crust		21
22	As in 11 but k_x = 5x10^{-8} for dry crust and k_y = 1x10^{-8} for dry crust		17
23	As in 11 but k_x = 50x10^{-8} for dry crust and k_y = 10x10^{-8} for dry crust		19
24	As in 11 but ν' = 0.3	18	
25	As in 11 but ν' = 0.4	28	
26	As in 11 but K_o = 0.7	21	
27	As in 11 but K_o = 0.6	23	

deep clay = layers 1-3; dry crust = layer 4 (Fig. 36)

Table 12. Sensitivity analysis. Axi-symmetric calculation. Data and calculated settlement of test embankment simulated with elastic model and foundation with Modified Cam Clay or Schofield model.

	Data (as in Table 9 unless given separately Dimensions as in Table 9)	Settlement (cm)	
		10 years after construction	
		Modified Cam Clay	Schofield model
1	$\kappa = 0.02$; $\lambda = 0.4$ (layer 1), 0.6 (2), 0.7 (3), 0.14 (4), $e_{cs} = 4.00$ (1), 5.20 (2), 5.50 (3), 1.10 (4); $M = 1.0$ for deep clay and 1.2 for dry crust; $\nu' = 0.35$ for deep clay 0,4 for dry crust; $H = 0.68$ for deep clay and 0.85 for dry crust; p_o' = as in Table 10 for Modified Cam Clay model	19.0	25.3
2	As in 1 but $\lambda = 0.3$ (layer 1), 0.5 (2), 0.6 (3), 0.3 (4); $e_{cs} = 3.15$ (1), 4.60 (2), 4.25 (3), 2.25 (4)	18.8	
		Total settlement Modified Cam Clay	
3	$\kappa = 0.03$; $\lambda = 0.5$ (layer 1), 0.7 (2), 0.8 (3), 0.07 (4); $e_{cs} = 4.00$ (1), 5.20 (2), 5.50 (3), 1.10 (4); $M = 0.9$ for deep clay and 1.15 for dry crust; $\nu' = 0.35$; $k_x = 5\text{x}10^{-10}$ for deep clay and $25\text{x}10^{-8}$ for dry crust; $k_y = 5\text{x}10^{-11}$ for deep clay and $5\text{x}10^{-8}$ for dry crust; $K_o = 0.67$	23	
4	As in 3 but $\kappa = 0.02$	16	
5	As in 3 but $\kappa = 0.04$	32	
6	As in 3 but $K_o = 0.6$	24	
7	As in 3 but $K_o = 0.7$	23	

deep clay = layers 1–3; dry crust = layer 4 (Fig. 36)

ductivity of the dry-crust clay was assigned values higher than those measured, as mentioned before.

The coefficients of elasticity of the dry-crust clay, E_h and E_v, were determined with drained triaxial tests.

The shear modulus G_{hv} was derived from the other elastic parameters, E and ν'.

A value determined in the laboratory, 0.67, was used for the coefficient of earth pressure at rest, K_o, of the dry-crust clay and 0.6 for that of the clay layers under the dry crust. The value for the dry-crust clay, 0,67, is quite low compared with earlier results. The effect of possible errors is discussed in Section 6.3.

The isotropic preconsolidation stress p_o' was obtained from the results of the oedometer and triaxial tests. The dry-crust layer was given as p_o' = 200 kPa. As the laboratory tests had shown that the yield locus corresponds to the Modified Cam-Clay equation, the isotropic preconsolidation stress for the Schofield model was assigned a value that made the initial yield locus curves meet at the critical state line (Table 9).

The effect of variations in different parameters, the element mesh and the time increment on the results was calculated. The results are explained in Section 6.2.

5.3 Parameters used in calculations with the Z-soil program

The parameters used in calculations with the Z-soil program are given in Table 13. The calculations were made by assuming plane strain conditions. The parameters were similar to those used in calculations with the CRISP-90 program. For the elastic calculations, only the E-value was given for the stress-strain relation, not the κ-value as in the CRISP-90 program. The Mohr-Coulomb parameters c' and ϕ' correspond to the parameter M and the Hvorslev surface in the CRISP-90 program. The time steps were the same as in the CRISP calculations. The element-mesh for Z-soil calculation is shown in Fig. 59.

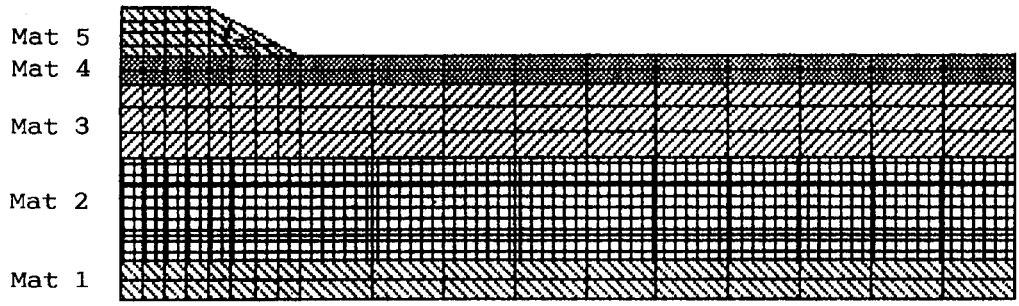

Fig. 59. Calculation cross-section of test embankment with element mesh for Z-soil program. Parameters used in calculation are listed in Table 13.

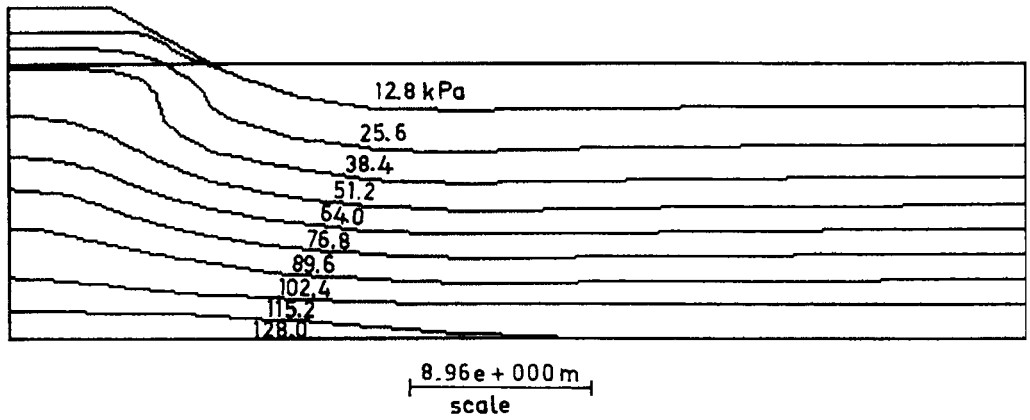

Fig. 60. Maximum effective principal stress $(\sigma_o + \Delta\sigma_1)$ contours immediately after construction. Z-soil.

5.4 Calculation results with the Z-soil program

The principal stresses, pore water pressure and displacements at different times were printed out as in the CRISP calculations. Fig. 60 gives the maximum effective principal stress contours caused by the embankment immediately after construction. Depicted in Fig. 61 is the excess pore water pressure at the same time and in Fig. 62 the minimum effective principal stress. Figs. 63–65 show the distribution of the stresses one year after construction, and Figs. 66–68 ten years after construction. Fig. 69 exhibits settlement as a function of time, and Fig. 70 the displacements ten years after construction. Fig. 71 illustrates the development of stresses under the centre of the test embankment in the first element under the dry crust and in the uppermost element of the material 2 layer.

Table 13. Initial parameters used in calculation with Z-soil program.

Layer no. 1					
Elasticity	Unit weight	γ	(kN m^{-3}) = 17		
	Young's modulus	E	(kN m^{-2}) = 4,000	Poisson's ratio	ν ( ) = 0,35
Plasticity	Cohesion	c'	(kN m^{-2}) = 8	Friction angle	ϕ' (°) = 20
Extended plasticity	Non assosiated angle	Ψ	( ) = 20	DP adjusted	( ) 1A[1]
Cap	In void ratio	e_o	( ) = 2.35		
	Compression index	λ	(kN m^{-2}) = 0.30	Preconsolidation pressure	p_o' (kN m^{-2}) = 187
Consolidation	initial void ratio	e_o	( ) = 2.35	Fluid bulk modified	K_w (kN m^{-2}) 2 x 10^5
	Permeability	k_x	(m s^{-1}) = 5x10^{-10}		k_y (m s^{-1}) = 5x10^{-11}
	Fluid weight	γ_w	(kN m^{-3}) 10	Angle of orthotrophy	Θ_f (°) 0
Layer no. 2					
Elasticity	γ = 17		E = 4,000		ν = 0.35
Plasticity	c' = 8		ϕ' = 20		
Extended plasticity	Ψ = 20		DP adjusted 1A[1]		
Cap	e_o = 2.40				p_o' = 144
	λ = 0.50				
Consolidation	e_o = 2.40		K_w = 2 x 10^5		Θ_f = 0
	k_x = 5x10^{-10}		k_y = 5x10^{-11}		
Layer no. 3					
Elasticity	γ = 15		E = 3,000		ν = 0.35
Plasticity	c' = 8		ϕ' = 20		
Extended plasticity	Ψ = 20		DP adjusted 1A[1]		
Cap	e_o = 2.45				p_o' = 100
	λ = 0.60				
Consolidation	e_o = 2.45		K_w = 2 x 10^5		Θ_f = 0
	k_x = 5x10^{-10}		k_y = 5x10^{-11}		
Layer no. 4					
Elasticity	γ = 18		E = 2,000		ν = 0.40
Plasticity	c' = 18		ϕ' = 20		
Extesded plasticity	Ψ = 25		DP adjusted 1A[1]		
Cap	e_o = 0.50				p_o' = 200
	λ = 0.30				
Consolidation	e_o = 0.50		K_w = 2 x 10^5		Θ_f = 0
	k_x = 5x10^{-9}		k_y = 5x10^{-9}		
Layer no. 5					
Elasticity	γ = 18		E = 4,000		ν = 0.40
Plasticity	c' = 18		ϕ' = 25		
Extended plasticity	Ψ = 25		DP adjusted 2A[1]		
Cap	e_o = 0.80				p_o' = 200
	λ = 0.30				
Consolidation	e_o = 0.80		K_w = 2 x 10^5		Θ_f = 0
	k_x = 5x10^{-9}		k_y = 5x10^{-9}		

1) 1A: adjust to external Mohr-Coulomb edges with associative plastic potential
2A: adjust to internal Mohr-Coulomb edges with associative plastic potential

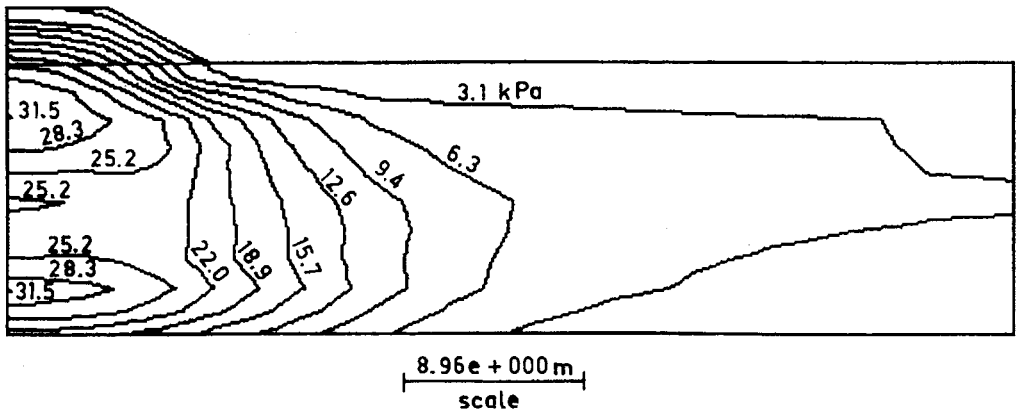

Fig. 61. Excess pore water pressure immediately after construction. Z-soil.

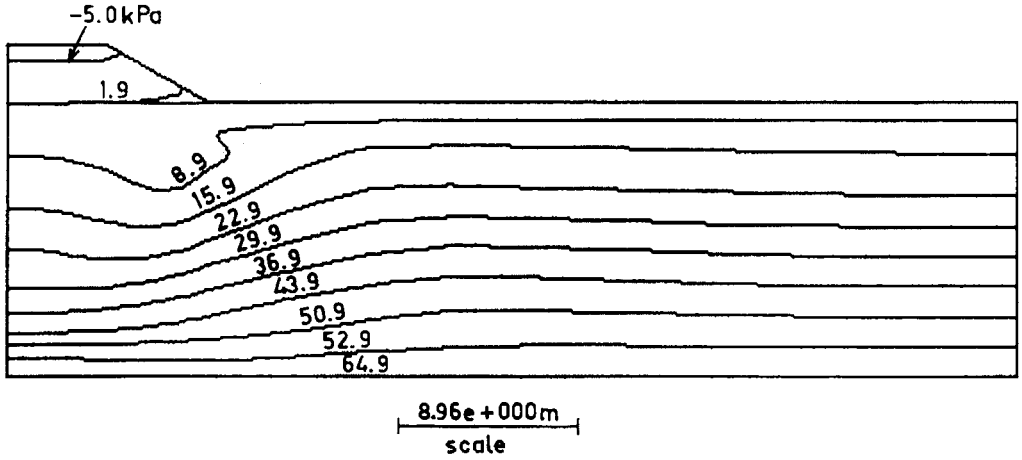

Fig. 62. Minimum effective principal stress contours immediately after construction. Z-soil.

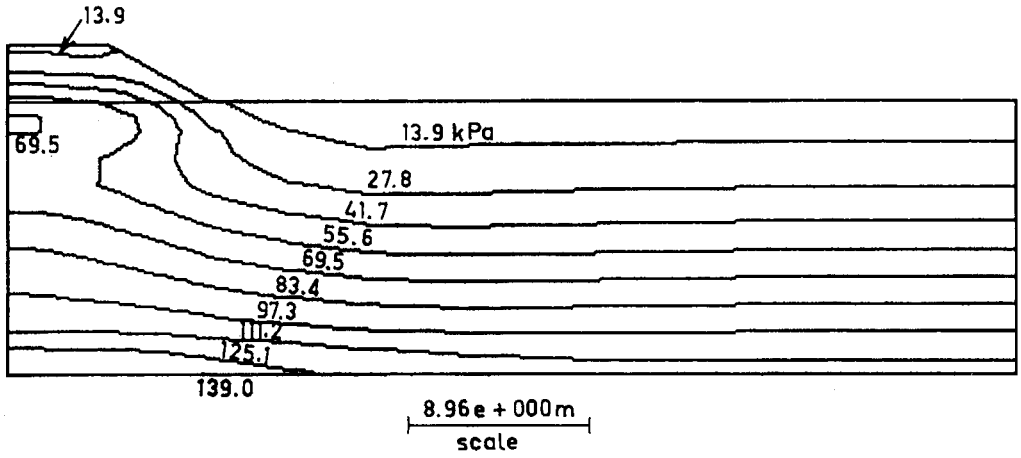

Fig. 63. Maximum effective principal stress contours one year after construction. Z-soil.

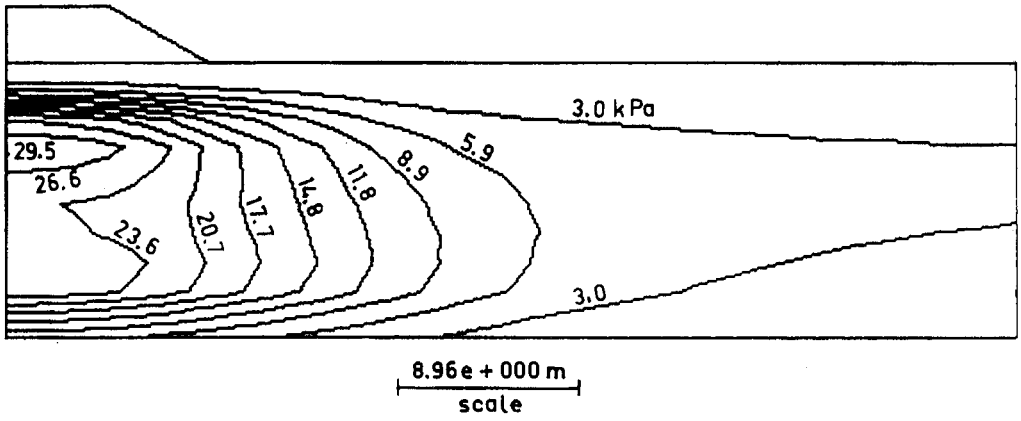

Fig. 64. Excess pore water pressure one year after construction. Z-soil.

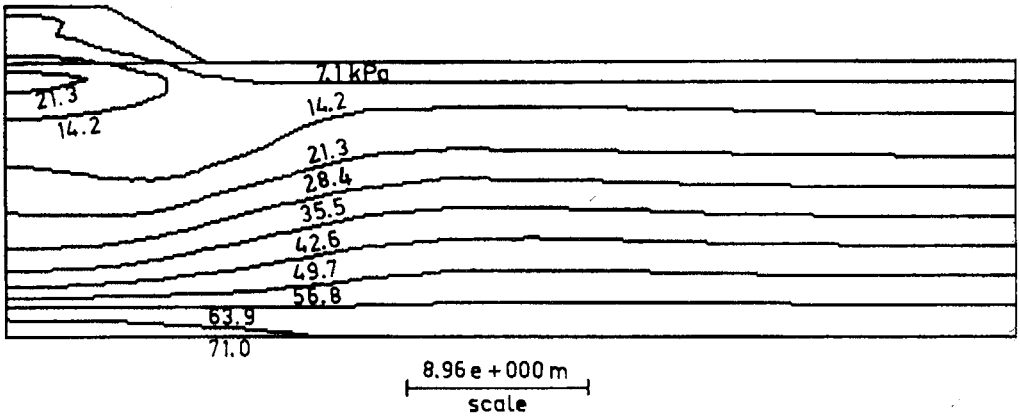

Fig. 65. Minimum effective principal stress contours one year after construction. Z-soil.

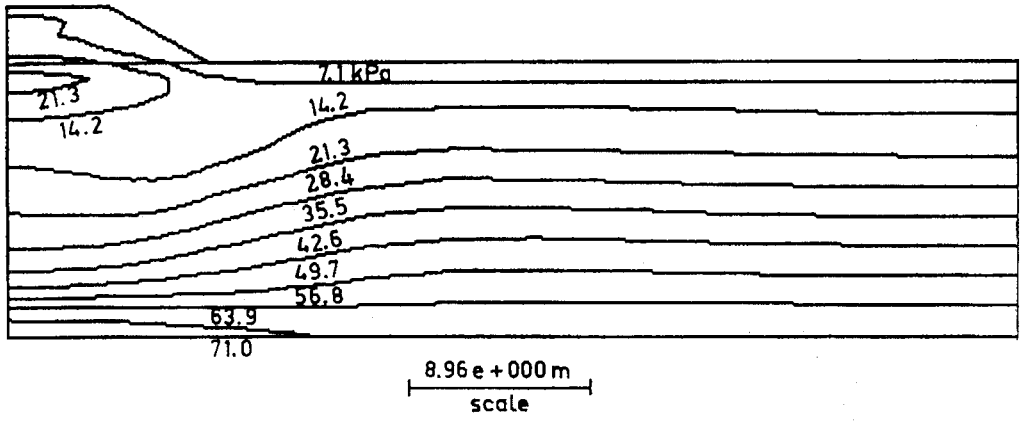

Fig. 66. Maximum effective principal stress contours 10 years after construction. Z-soil.

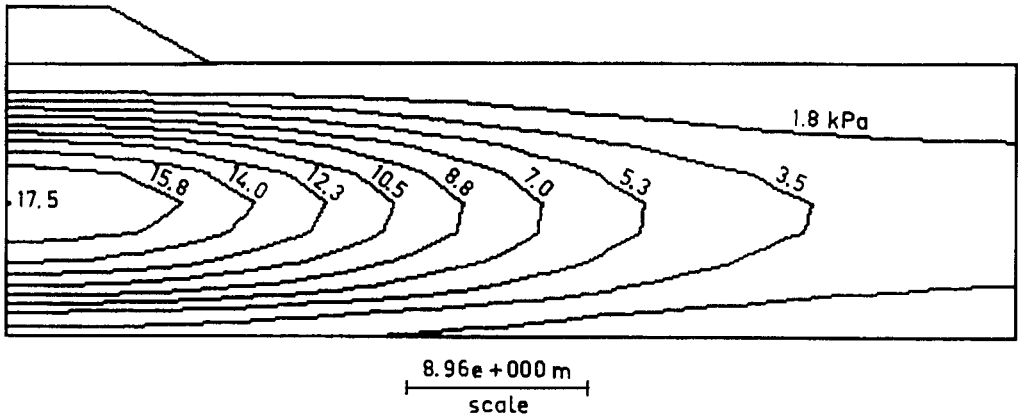

Fig. 67. Excess pore water pressure 10 years after construction. Z-soil.

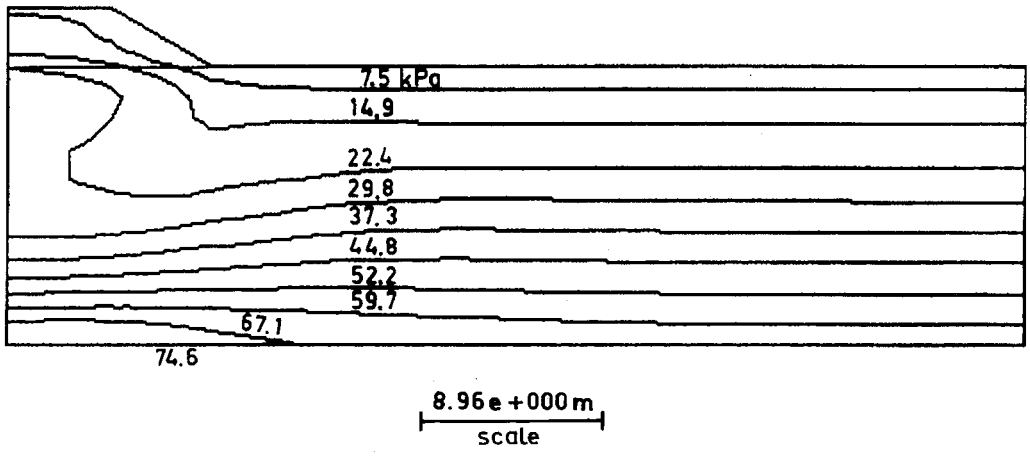

Fig. 68. Minimum effective principal stress contours 10 years after construction. Z-soil.

5.5 Calculations with the CRISP-94 program

The CRISP-94 program is a modified version of CRISP-90. Quadrilateral elements were used in the calculations performed with CRISP-94 (Fig. 72). The sensitivity analysis was conducted with 180–210 elements and 60-80 time increments. In the final calculation 180 elements and 120 time increments were used. Calculations for a period of one month consisted of 52 time increments, for one year of 77 time increments, for ten years of 100 time increments and for 100 years of 120 time increments. The sensitivity analysis was made with the initial data (Table 9). The effect of p_o' was calculated by changing the p_o'-values in Table 9. The data of the final calculation are given in Table 14. The final calculation included more exact pore pressure fixities and provided more information about the stress paths in the normally consolidated state. Some difference in the permeability ratio was assumed because the structure of the deep clay layer had been re-estimated. The p_o'-values were taken as the lowest possible estimates.

Table 14. Initial parameters of simulation calculation with CRISP-94 program (layers in Fig. 36)

Material layer	E_h kPa	E_v kPa	ν_{hh}	ν_{vh}	G_{hv} kPa	γ KN m^{-3}	k_x m s^{-1}	k_y m s^{-1}	K_o
5	3,000	3,000	0.35	0.35	2,000	18	$5x10^{-9}$	$5x10^{-9}$	0.67
	κ	λ	e_{es}	M	ν'	γ $kN\,m^{-3}$	k_x $m\,s^{-1}$	k_y $m\,s^{-1}$	K_o
4	0.01	0.30	2.65	1.2	0.40	18	$3x10^{-9}$	$3x10^{-9}$	0.67
3	0.01	0.60	4.25	1.0	0.35	15	$3x10^{-10}$	$1x10^{-10}$	0.6
2	0.01	0.50	3.80	1.0	0.35	17	$3x10^{-10}$	$1x10^{-10}$	0.6
1	0.01	0.30	3.15	1.0	0.35	17	$3x10^{-10}$	$1x10^{-10}$	0.6
		p_o' Modified Cam Clay model							
	at ground level	200 kPa							
	at level 33.9 m	200 kPa							
	at level 32.9 m	100 kPa							
	at level 31.9 m	70 kPa							
	at level 29.9 m	57 kPa							
	at level 27.4 m	57 kPa							
	at level 22.9 m	86 kPa							
	at level 22.8 m	150 kPa							
	at level 16.5 m	150 kPa							

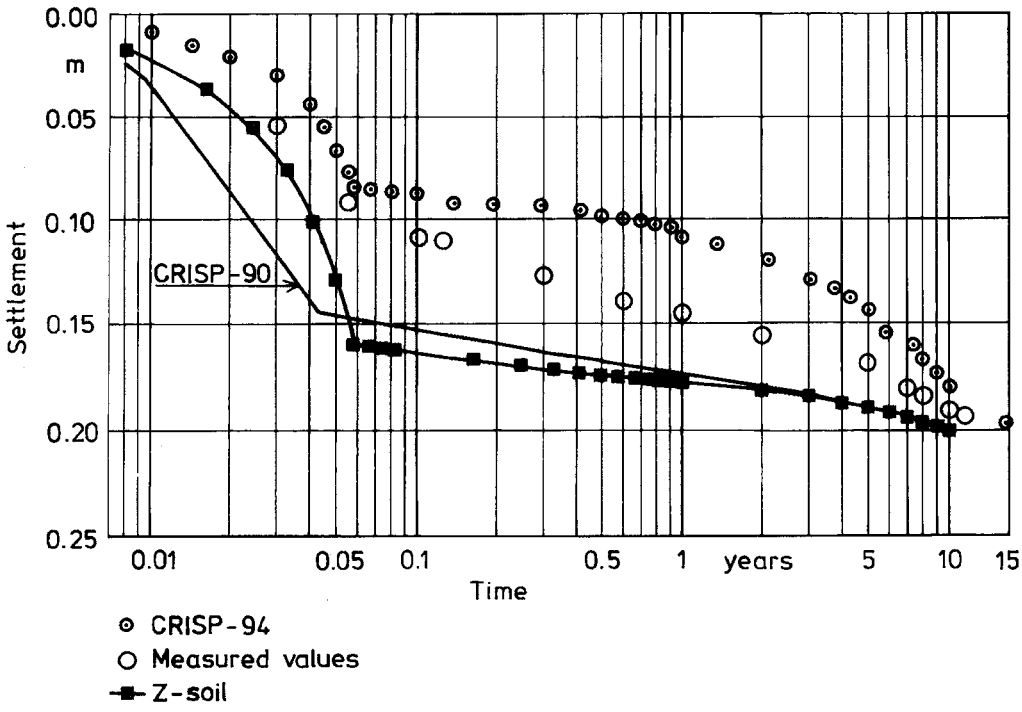

Fig. 69. Settlement at ground surface in middle of test embankment.

5.6 Calculation results with the CRISP-94 program

The results obtained with the CRISP-94 program are referred to as settlement values and final maximum pore pressures. Special attention is paid to the stress paths in the normally consolidated state. The settlement of the ground surface in the middle of the test embankment is presented in Fig. 69. The development of stresses in different elements under the centre of the test embankment is shown in Fig. 73.

6 Discussion

6.1 Simulation with different models

The stress distributions and displacements at different times as given by the Modified Cam-Clay model and the Schofield model are very alike (Figs 37–58, 74–75). During the early years settlements as calculated from the Schofield model are slightly larger than those deduced from the Modified Cam-Clay-model (Fig. 46). In the first year both are somewhat larger than the measured settlement but are still rather similar. The bulk of the excess pore water pressure disappears within about one year, in accordance with the measurements. The maximum pore water pressure (4.8 m) is of the same order of magnitude as the water-level drop in piezometers no. 4 and 23 B (Figs 9, 10 and 15).

The development of stresses at the centre of element 114 (at the level of the settlement plates) (Fig. 50) is similar in different models. The stress is distributed under the test embankment so as to keep the stress state of element 114 elastic. The shear strains given by the program are rather large. The situation is the same in element 118 (Fig. 51). In the Modified Cam-Clay model the stress state under the dry crust at the centre of element 77 (Fig. 52) reaches the yield locus and follows it, ending at

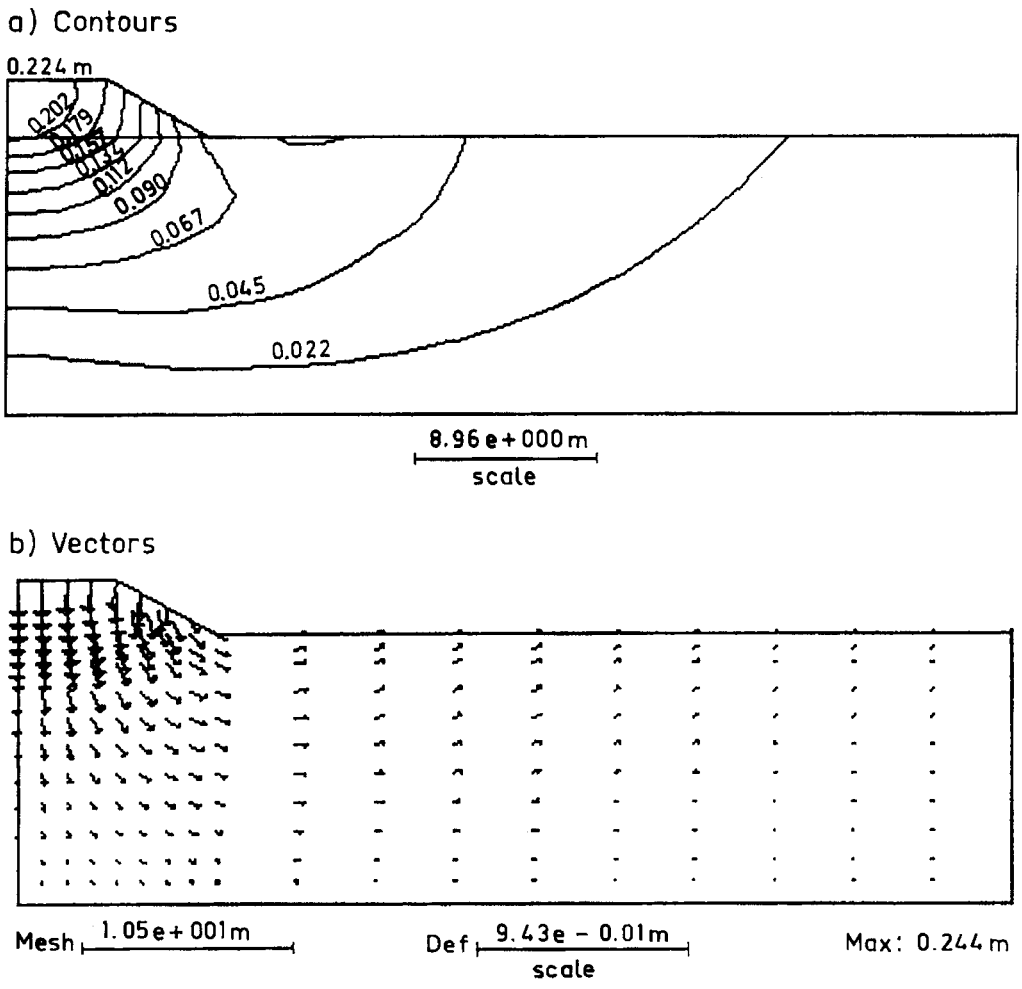

Fig. 70. Displacements 10 years after construction. Z-soil.

the critical state. In the Schofield model the stress state reaches Hvorslev's line, follows it to the critical state and continues along the yield locus to the normally consolidated region. The shear strains are smaller than those in the dry crust. At the centre of element 45 (Fig. 53) the stresses develop as in element 77.

Although the stress distributions given by the models are very alike, the elements in different models approach the critical state at different times (Fig. 54). In the Modified Cam-Clay model the first element approaches the critical state at increment 48, 7.5 years after construction. In the Schofield model the same element approaches the critical state at increment 40, two years after construction. The order of elements approaching the critical state is very similar in the two models.

As shown by Fig. 74, the critical state models give similar increases in vertical stresses under the test embankment to those calculated from Boussineq's equations. A comparison is made between the classical calculation methods and the calculation by finite element methods with critical state models. At the end of construction, the pore water pressure increase is largest in the middle of the dry crust clay layer. The increase in maximum principal effective stress is largest in layer 3 under the dry crust. Ten years after construction the pore

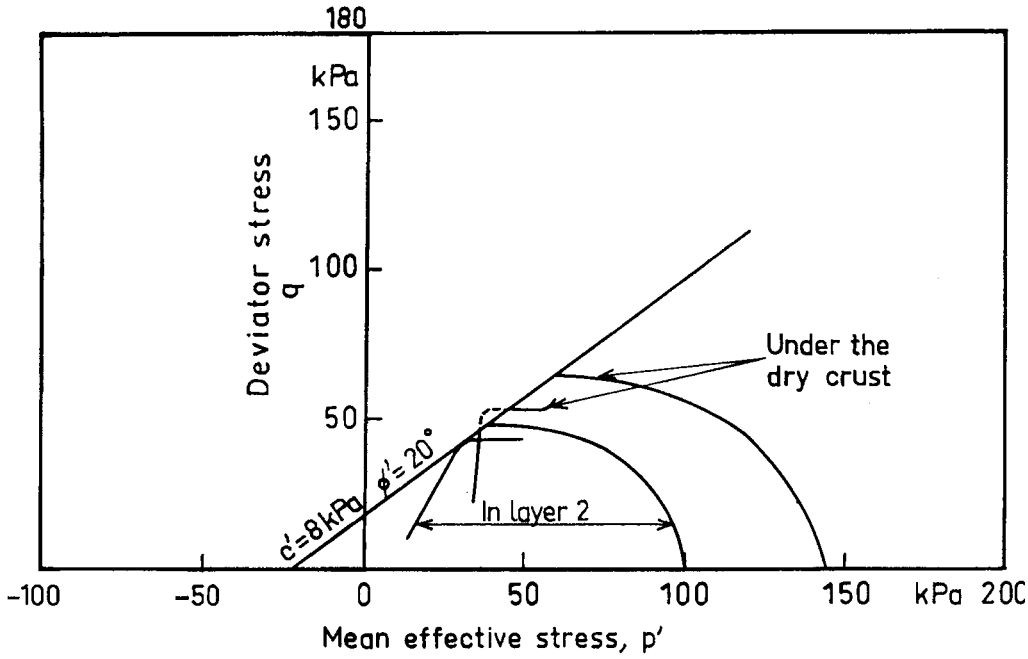

Fig. 71. Development of stresses under centre of test embankment in first element under dry crust and in uppermost element of material 2 layer. Z-soil.

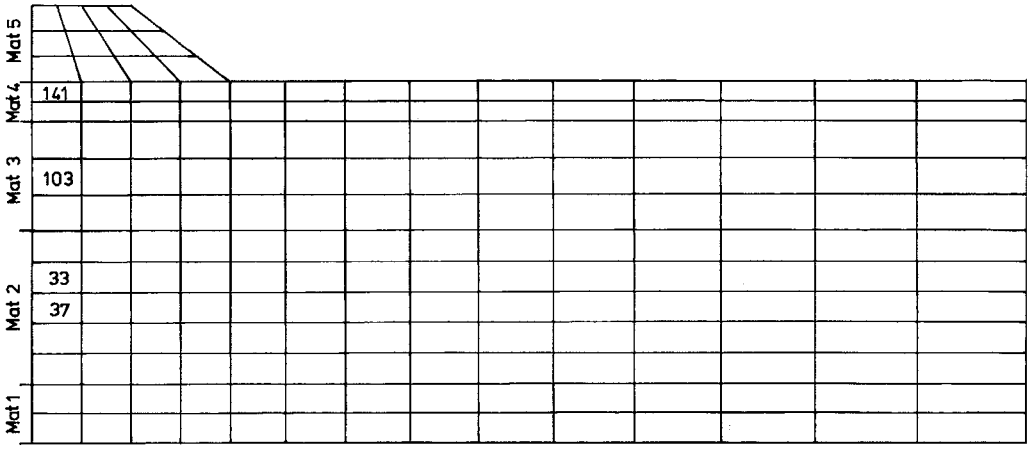

Fig. 72. Calculation cross-section of test embankment with element mesh for CRISP-94 program. Parameters used in calculation are listed in Table 14. Elements referred to are numbered.

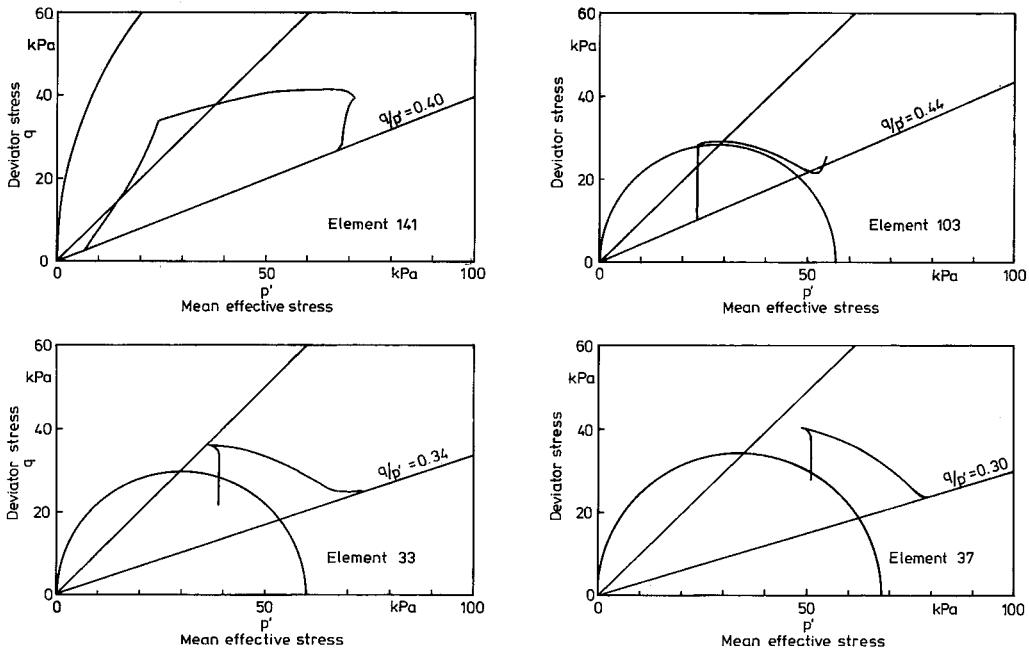

Fig. 73. Development of stresses under centre of test embankment. CRISP-94 program. Positions of elements referred to are shown in Fig. 72.

pressure increase is at its maximum (about 10 kPa) in the middle of the deep clay layer. In the dry crust layer the pore pressure increase is about 5 kPa. The total principal stresses are somewhat larger than those obtained with the Boussinesq calculation. Fig. 75 gives the distribution of mean effective stress ten years after construction. Figs. 50–53 show that the mean effective stresses in the dry crust clay correspond to points inside the yield surface; the assumption of preconsolidation pressure has no effect on that behaviour. The mean effective stresses in the deep clay layer are situated roughly on the yield surface; thus the preconsolidation pressure estimation is very important in the calculation.

The alternative modelling (Table 10) showed that the dam body can be modelled with the elastic isotropic model or the elastic, perfectly plastic model using the Mohr-Coulomb failure criterion. The results of calculations with the elastic, perfectly plastic model are given in Section 5.2.

When applied to the dry-crust clay layer, the elastic, perfectly plastic model did not describe the consolidation phenomenon properly, and even less so when it was used for modelling the whole cross-section.

Calculations with the Z-soil program were very similar to those with the Modified Cam-Clay and Schofield models and so the results, too, are similar. The stress distributions and settlements at different times are shown in Figs. 60–70. Fig. 71 illustrates the development of stresses under the centre of the test embankment in the first element under the dry crust and in the uppermost element of the material 2 layer.

The decrease in pore water pressure calculated with the Z-soil program is somewhat slower than that measured. The calculated settlement values are similar to the corresponding values obtained with the CRISP calculation.

The calculations with the CRISP-94 program were made with boundary conditions, where the possibility of a normally consolidated state in the soft layer under the dry crust was taken into account. A lower κ-value was chosen in view of the results of ten years of settlement observations. The

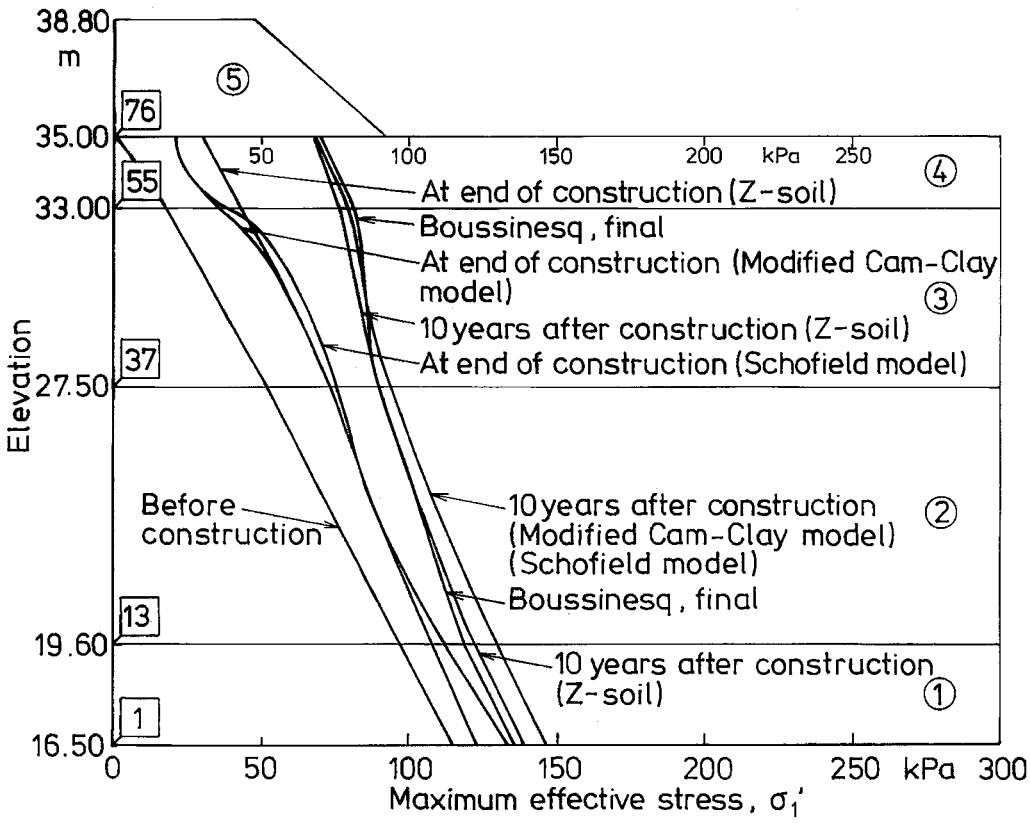

Fig. 74. Distribution of maximum principal stress under centre of test embankment. CRISP-90 and z-soil programs.

results of the calculations gave a somewhat different rate for settlements, as the calculated settlements for up to ten years after construction are lower than those measured and the rate of settlements over the period from 1 to 15 years is higher than those measured. The value for total settlement (100 years) calculated with the CRISP-94 program is 35 cm (22 cm with the CRISP-90 program).

In the final calculation with the CRISP-94 (data as in Table 14) the mean preconsolidation pressure p_o' was given as low a values as could reasonably be assumed. The calculation described well the behaviour of the clay layer in the normally consolidated state.

The stress paths at the elements under the centre of the test embankment (Fig. 72) are presented in Fig. 73. Element 141 is in the dry crust and remains continuously in the over-consolidated state. The value of the stress ratio q / p' increases with the increase in pressure during construction of the test embankment. After construction of the test embankment, the deviator stress q remains nearly constant during the increase in the mean effective stress p'. Five months after construction of the test embankment has started, p' begins to decrease while q remains nearly constant. In the end, the value of q / p' is about 0.5, which corresponds to a K_o -value of 0.68; thus the value σ_3' / σ_1' is almost the same as initially.

The stress path in element 103 goes straight up to the initial yield surface and follows it to the q / p'-value 0.44, which corresponds to a K_0-value of 0.66. The final value of K_o is thus about the same as initially and not the value of K_o calculated with equation (49), which gives a q / p'-value of 0.3, corresponding to a K_0-value of 0.75. The stress path in element 33 goes straight up to the critical state line, follows the yield surface and turns to the line with a q / p'-value of 0.34, which is close to the value 0.3. The stress path in element

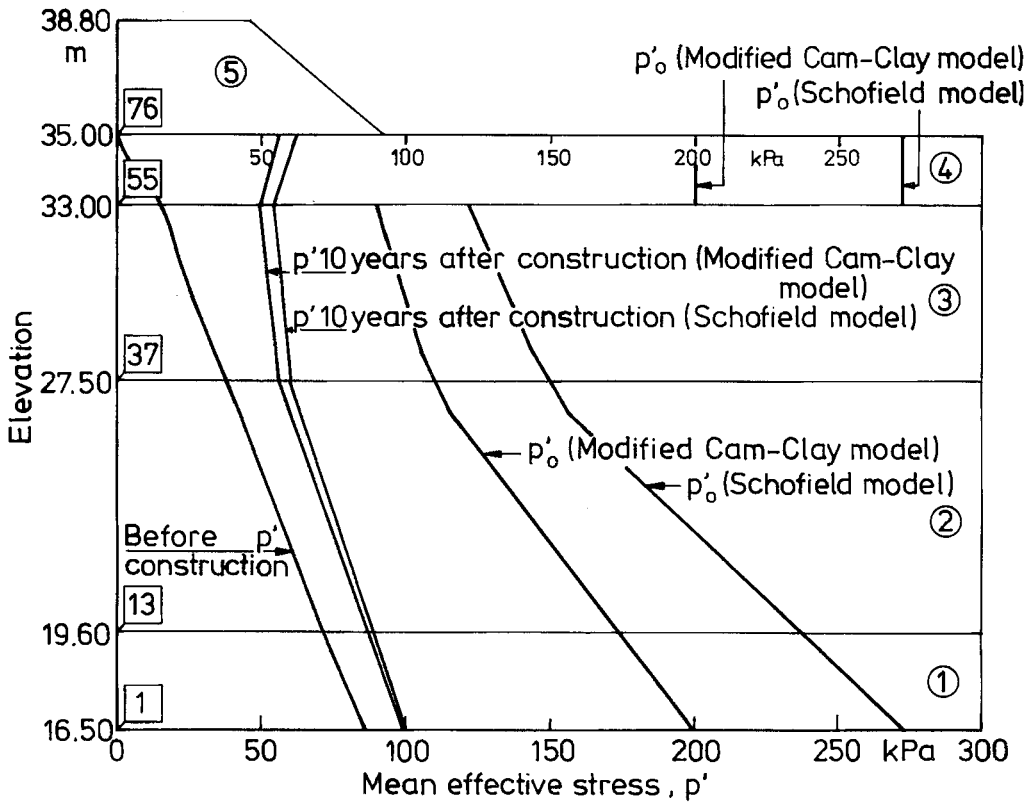

Fig. 75. Distribution of mean effective stress under centre of test embankment. CRISP-90 program.

37 goes straight up to the q-value 40 kPa, follows the yield surface and turns to the line with a q / p'-value of 0.3.

The stress path calculations show that the K_o-value of equation (49) was reached in the lower part of the clay layer. In the upper part of the clay layer the condition is not exactly the K_o-condition, because the load of the test embankment is only on a small area.

As shown in Fig. 69 the lowest p_o'-values gave a too large settlement increase after four years. The κ-value 0.01 used here is not the most probable one.

The foundation of the test embankment is not in the normally consolidated state to the extent assumed in the calculation with the lowest p_o'-values.

6.2 Sensitivity analysis

The effect of different parameters on the calculated settlement of the test embankment was studied by varying the values of the parameters one at a time while keeping the others constant (Tables 11 and 12). Some of the parameters are related to each other. To start with, the independent parameters of critical state models in the CRISP-90 program ($\kappa, \lambda, e_{cs}, M, k$ and ν') were considered. The effect of some parameters is obvious but systematic calculations were made to detect computational effects as well.

First, the effect of the parameter κ was studied. In the reference calculation (no. 11 in Table 11), its value was 0.03. The sensitivity calculations were made using κ-values of 0.02 and 0.04, which are within the range measured in laboratory tests. These values gave 15 cm and 29 cm for total

settlement in comparison to 22 cm with the reference calculation. Thus the correct choice of κ-value has a marked effect on the calculated settlement of the test embankment. As the effect of the κ-value focuses on the over-consolidated stress region, it has less influence on the settlement of the 15-m high embankment under design than on that of the test embankment.

The effect of the parameter λ on the calculated settlements of the test embankment was studied by increasing and decreasing the λ-values of different layers. In the second group of sensitivity analysis calculations (Table 11) the λ-values of the deep clay layers were increased by 0.1 and those of the dry crust by 0.01, which is within the detection limits. These changes gave 24 cm as the value of settlement in comparison to the 22 cm obtained in the reference calculation (no. 11 in Table 11). When the λ-values were decreased by the same amounts, 20 cm was obtained for settlement. Thus, the λ-values had a rather minor effect on the calculated settlement of the test embankment. For the embankment under design, the influence of λ is more marked because it lasts as long as the soil layers are in the normally consolidated state.

The different λ-values for the dry crust had no effect on the settlement, as the dry crust remains continuously in the over-consolidated state.

The influence of the parameter e_{cs} was studied by increasing and decreasing the value of the parameter for the deep clay layer (second group of analyses in Table 11). When the e_{cs}-values were increased by 1.0, the calculated settlement became 20 cm in comparison to the 22 cm obtained in the reference calculation (no. 11 in Table 11). A decrease of the same magnitude in the e_{cs}-values resulted in a calculated settlement of 26 cm. Thus the proper choice of parameter e_{cs} is important for reliable results. The value of e_{cs} is chosen according to the λ-value.

The effect of the parameter M on the calculated settlement was studied by increasing the value of M in the deep clay layer from 0.9 to 1.0 and in the dry crust from 1.15 to 1.25. The altered values of the parameter resulted in a calculated settlement of 21 cm in comparison to the 22 cm obtained in the reference calculation (no. 11 in Table 11). Therefore, the change in the parameter M has very little impact on the result of the calculation, and the parameter can be determined accurately enough with strength tests in the laboratory.

In the case of the dam embankment, M has a greater effect. As the test embankment had to be built at the site of the proposed dam, it could not be used to model all aspects pertinent to construction of the actual dam, e.g. failure of the test embankment foundation. The test embankment could, however, be monitored over a long period.

The effect of the hydraulic conductivity was investigated by varying the hydraulic conductivity of the dry crust and the test embankment. If these layers are given values higher than those used in the reference calculation by a factor of ten, the rate of settlement increases during construction. The calculated settlement during construction is 21 cm, whereas in the reference calculation (no. 11 in Table 11) it was 19 cm. The increase in hydraulic conductivity has, however, no effect on total settlement in either theory or practice. When the hydraulic conductivities of the dry crust and the test embankment used in the reference calculations were divided by five, the settlement rate was reduced during construction, resulting in settlement of 17 cm during that period. Thus, variation in the hydraulic conductivity of the dry crust and the test embankment has only a small effect on the rate of settlement in the model calculation.

The effect of the value of the Poisson ratio ν' was calculated by changing ν' (in the calculation with parameters in Table 9) in the deep clay layers from 0.35 to 0.25 and in the dry crust from 0.4 to 0.35. The resulting settlement ten years after construction was 13.2 cm in comparison to 18.3 cm in the original calculation. When the ν' values were further lowered to 0.20 and 0.30, respectively, the resulting settlement ten years after construction was 11.4 cm. Thus, the ν'-value has a considerable effect on the settlement.

When the calculated settlement is compared with the measured settlement it is possible that the value of ν' is too high and that of κ too low. This possibility cannot be excluded in the present study. With a κ-value of 0.03 and ν'-values for the deep clay layers and dry crust of 0.25 and 0.35, respectively, the results are almost the same as those obtained with the original data (Table 9), and are even slightly closer to the measured values.

The differences in K_o-values have the largest effect through the ν'-values, the influence of which was considered above.

The results of the sensitivity analysis using the elastic, perfectly plastic model with the Mohr-Coulomb failure criterion are given in Table 15. According to the calculations, the elastic-plastic

model with the Mohr-Coulomb failure criterion can be used for the embankment but not for the dry crust and especially not for the clay layer under the dry crust. Many of the difficulties were encountered in determining the pore water pressures.

Table 15. Calculated settlement of test embankment under centre line of test embankment and corresponding maximum pore water pressure. Elastic, perfectly plastic model + Modified Cam Clay/Schofield model, plane strain.

Data of models 1, 3 and 6 [x] as in Table 8 Data of model 5 [x] as in Table 9 (Changes of E_o and k given)	Total settlement cm	Max. pore pressure 10 years after construction kPa
Mat 1-4 model 3, mat 5-6 model 5 E_o = 3,000 kPa	20.4	27.5
Mat 1-4 model 6, mat 5-6 model 5 E_o = 3,000 kPa	20.1	26.5
Mat 1-4 model 3, mat 5-6 model 5 E_o = 5,000 kPa	20.0	24.5
Mat 1-3 model 6, mat 4-6 model 5 E_o = 3,000 kPa	15.1	18.0
Mat 1-3 model 3, mat 4 model 5, mat 5-6 model 1 E_o = 2,000 kPa	13.7	44.1
Mat 1-6 model 5 E_o (1-3) = 4,000 kPa, E_o (4-6) = 5,000 kPa k (4-5) = 5 x 10^{-8} m/s	21.7	
Mat 1-3 model 6, mat 4 model 5, mat 5-6 model 1 E_o = 5,000 kPa	22.2	28.5
Mat 1-3 model 6, mat 4 model 5, mat 5-6 model 1 E_o = 2,000 kPa	24.0	42.5
Mat 1-3 model 6, mat 4 model 5, mat 5-6 model 1 E_o = 3,000 kPa	23.5	36.2
Mat 1-3 model 3, mat 4 model 5, mat 5-6 model 1 E_o = 3,000 kPa	14.6	35.0

Mat = Material layer

[x] Model 1 = Elastic model
Model 3 = Modified Cam Clay model
Model 6 = Schofield model
Model 5 = Elastic perfectly plastic model with Mohr-Coulomb yield criterion

The results of the sensitivity analysis with the Z-soil program are given in Table 16. When the vertical permeability was multiplied by a factor of 5 ($k_h / k_v = 2$), the increase in settlement was about 5%. Had the horizontal permeability also been multiplied by 5, the increase in settlement would have been about 15%. As to the correct value of Young's modulus E, the comparison was made with a value E = 4,000 kPa for all material layers. According to the calculations, the correct value of E is very important in Z-soil calculations.

Table 16. Calculated settlement of test embankment under centre line of test embankment. Z-soil, plane strain.

Data	Settlement 10 years after construction top of embankment cm	 earth surface cm
As in Table 10	22.40	20.45
As in Table 10 but k_y=5x $k_{y\,initial}$	23.30	21.34
As in Table 10 but k=5x $k_{initial}$	25.20	23.40
As in Table 10 but E=4,000 kPa	17.70	16.08

The development of stresses under the centre of the test embankment was similar in the Z-soil analysis (Fig. 71) and in the CRISP analysis (Figs 50-53). The maximum pore pressures after ten years were 17.5 kPa in the Z-soil calculation (Fig. 67) and 18.7 kPa in the CRISP calculation (Fig. 44); the difference was, therefore, quite small.

The effect of the element mesh and the time increments were finally checked with the 1994 CRISP version using the 8-noded quadrilateral elements. The data given in Table 9 were employed. The initial mesh included 180 elements and 210 nodes. The time increments were as shown in Fig. 50. The results of the calculations are given in Table 17.

To establish the effect of the time increments, the next calculation was made with 100 time increments. The results were similar to those obtained in the reference calculation.

The effect of the element mesh was determined by performing the third calculation with 270 elements and 306 nodes. No considerable difference in results was found.

In the fourth calculation the effect of the value of the mean preconsolidation pressure p_o' was tested using the element mesh and the time increments of the second calculation. The data differed in the p_o'-value of the soft clay layer as shown in Table 17. As the minimum p_o'-value was reduced from 90 kPa to 70 kPa and in the whole soft layer correspondingly, settlement after ten years increased from 19 cm to 23 cm. The total settlement increased from 20 cm to 32 cm. The calculation showed that the determination of p_o' is important for proper results.

6.3 Effect of the error factors

The first group of error factors is caused by the variability in topography and soil layers in the test area. The length of the test embankment is finite (and thus does not exactly meet the two-dimensional – plane strain – conditions). The values of the soil parameters also vary. Those used were tested with the aid of the test embankment. It is, however, possible that the values used for the parameters and those prevailing in the soil differ in various combinations. The order of magnitude of any deviation was determined with sensitivity analyses of the parameters.

Another source of error lies in the difficulty of determining reliable boundary conditions for the pore water pressures. As the initial pore pressure

Table 17. Calculated settlement of test embankment under centre line of test embankment and corresponding pore water pressure. Elastic, perfectly plastic model + Modified Cam Clay model, plane strain. Element mesh with 8 noded quadrilateral elements. Calculation with CRISP-94 program.

	Total settlement cm	Settlement after 10 years cm	Max. pore pressure after 100 years kPa	Max. pore pressure after 10 years kPa
Data as in Table 9 180 elements, 210 nodes 60 time increments	20.3	18.7	0.2	15.4
180 elements, 210 nodes 80 time increments	20.5	18.9	0.1	15.3
270 elements, 306 nodes 60 time increments	20.7	19.1	0.2	15.4
180 elements, 210 nodes 80 time increments p_o' at level 35.00 m 200 kPa at level 33.10 m 200 kPa at level 33.00 m 70 kPa at level 30.00 m 75 kPa at level 27.50 m 80 kPa at level 23.00 m 100 kPa at level 22.90 m 150 kPa at level 26.60 m 150 kPa	31.7	23.3	1.9	17.5
Data as in Table 14 180 elements, 210 nodes 120 time increments	34.7	17.7	4.2	19.8

condition is obtained in the final measurements the difficulty arises when it is assumed that the chosen conditions represent the whole phenomenon. Since average values were used for the settlement of the settlement plates, the difficulty of determining the boundary condition did not affect the level of the results. The standard deviation of the settlement of the plates in the centre of the test embankment was about 20% of the average value. The determination of p'_o is also a source of error. The p_o'-value affects the stress state changes and is one of the most important parameters.

Yet another source of error is the difficulty of measuring pore pressure reliably in the field. The average values given by different piezometers were, therefore, used to compare the measured values with the calculated values. Hence the level of accuracy is similar to that of the boundary conditions.

The properties of the deep clay layers and dry-crust clay were studied in triaxial tests and oedometer tests in which the cylindrical sample and the results obtained correspond to axi-symmetry. The parameters were applied to plane strain with the aid of invariants. The settlement was observed under the centre of the test embankment,

where the conditions best correspond to those of the laboratory tests. The values calculated on the basis of axi-symmetry (Table 12) did not differ markedly from those of plane strain (Table 11).

A further possible source of error is the finite element method used. The program resulted in deviations of up to 3% when different initial values were employed. The maximum error in the initial values of some data combinations in Tables 11 and 12 was 5%. The stress fields calculated showed slight local deviations. The calculation also gave some erroneous results outside the influence of the load of the test embankment, such as minor uplift far from the embankment. These errors do not, however, seem to have had a significant effect on the calculated settlement value of the test embankment or the calculated development of pore water pressure under the test embankment and in its immediate vicinity.

The finite element method causes numerical errors due to the mesh and the iteration processes in the calculations. The influence of the element mesh and the time increments was calculated (Table 17). Checking showed that the method used gives fairly correct results. The simplicity of the solving method causes notable errors.

Errors also arise from the difference between the behaviour of the soil samples in the laboratory tests and that predicted by the critical state theory. For example, the shear of the over-consolidated samples does not obey the critical state theory exactly. The deviations are due to the variation in the properties of the insitu soil, anisotropy and desiccation cracks, and, in the compacted samples, the variation in compaction technique and in layering due to compaction. As the compaction of the test embankment resulted in a higher preconsolidation pressure than that in the insitu layers, the test embankment and the dry crust do not behave in exactly the same way. The K_o-values in the compacted test embankment and in the dry-crust layer may differ.

The value of K_o measured in the laboratory is lower than that obtained in other studies. It was, nevertheless, used in the calculations to compare the settlement calculated from the measured parameters with the measured settlements of settlement plates.

The laboratory tests also revealed differences in the build-up of the critical state in normally consolidated samples. The volume change did not stop during the tests, and it seems that the critical state was not reached. It might be reached with a ring shear apparatus permitting large displacements; such a test apparatus was not, however, available. The critical state parameter M approximated with the ratio of increments in volumetric strain and shear strain gave a reliable result.

The difficulty of determining the amount of contact surface in a shear plane at high strain also causes errors in the interpretation of the triaxial tests. Yet another source of error is the too high shear rate used in undrained and drained triaxial tests. During rapid shear in an undrained test the pore water pressure in the centre of the sample is higher than in the gauge. According to British criteria (Bishop and Henkel 1964), with the strain rates used in this project, the error showed generally disappear by the time of yield. In a drained test, too rapid shear generates pressure in pore water which cannot be measured, thus causing error. In the present study, the samples of the drained tests were drained through one end of the sample, and any pore water pressure was measured at the other end. The only source of error is then the difference between the pore water pressures inside the sample and at its ends.

As to the calculation with the elastic, perfectly plastic model, the elastic parameters were difficult to deduce from laboratory tests.

Errors also arise because the models applied do not take all the soil properties into account. One of these errors is the non-linearity of the elastic response. As a whole, the elastic parameters were difficult to test with the methods available. Nonetheless, the models were good enough for the accuracy of the parameters. If more reliable parameters could be devised, for instance, with in situ methods, it would be possible to take more features into account in the models.

In the modelling of the test embankment, the elastic effects were mainly deduced from the initial calculation results. In the final calculation with the CRISP-94 program, plastic effects were also considered. For the proposed earth dam, a greater number of plastic effects would have to be included. The laboratory tests and the parameters estimated cover these effects.

For the consolidation analysis, it was initially assumed that the horizontal permeability in clay layers under the dry crust was ten times the vertical permeability. This assumption was made because of the layered structure of clay sediments. The measurements made on site thus refer almost en-

tirely to the horizontal permeability. In sensitivity analysis the ratio of horizontal permeability to vertical permeability was taken as 2 (vertical permeability was increased 5 times).

The calculation gave an increase in settlement of about 5% compared with the initial calculation ($k_h / k_v = 10$). The increase in settlement was not very large, and so an error in the value of the permeability ratio does not significantly affect the level of settlement values. In the final calculation with the CRISP-94 program, a permeability ratio of 3 was used for the deep clay layer.

It is assumed that permeability in the dry-crust clay and the embankment material is similar both horizontally and vertically. As the dry-crust clay can be fractured vertically, it is difficult to know the ratio of permeabilities in different directions. However, this ratio in the embankment has only a minor effect on the settlement calculations and so the permeabilities in different directions are assumed to be equal.

The permeability measurements cannot be very accurate; they can only show the order of magnitude. Measurements on site are preferable to measurements in the laboratory. As the measurements of settlement agree with the calculations, the permeability measurements were acceptable.

Because the consolidation equations were originally developed for a homogeneous isotropic and fully saturated medium, the case analysed is not perfect in terms of any of the assumptions. The consolidation theory is nowadays applied to nonhomogeneous and unisotropic cases by having different permeabilities in different layers and different directions.

The possibility of unsaturation in the dry-crust clay was taken into account in the permeability value of the dry crust clay. A more exact analysis was not possible within the limits of the investigations.

The accurate measurement of the elastic modulus E in the laboratory needed for the Z-soil calculation is difficult and its value also affects the calculations of settlement. Compared with the test embankment settlements, the values are reasonable.

The element mesh also caused some errors in the Z-soil calculation, as immediately after construction two areas of maximal pore pressure were obtained (Fig. 61). Too small time increments can also be reason of that error.

6.4 Comparison with the results of other investigations

In the first part of this project the settlement of the test embankment was predicted with classical methods and the finite element method of non-linear elasticity. In the classical calculation (Pitkänen 1982) monitoring data on the test embankment were available for only one year. The calculation gave 70 cm for the test embankment settlement, which, at present, seems to be about 20 cm. In the non-linearly elastic FE-calculations (Loukola 1985) monitoring data on the test embankment were available for three years. The calculated final settlement of the test embankment was then 45 cm. The problems encountered in the calculation were mainly due to the difficulty of combining laboratory test data with test embankment data. No such problems occurred in the calculations with the critical state models.

The critical state theory was initially developed from laboratory data on some well tested soils, e.g. Weald Clay. According to Henkel (Henkel 1956), the properties of this clay are as follows: liquid limit = 43%, plastic limit = 18%, plasticity index = 25%, clay fraction = 40% and activity = 0.6. The plasticity index is similar to that in the Taasia clay (Table 3).

Fig. 76 (Roscoe et al. 1958) shows the undrained loading paths of the clay with a water content of 20.7% and various values of the over-consolidation ratio (OCR). The stress curves with $OCR > 3$ becomes tangential to Hvorslev's line. All the loadings end on the critical state line at point Q in Fig. 76.

In Fig. 16 the Taasia Clay is tested with a water content of 84-92%. The stress path with the original OCR = 4.5 turns to the right, parallel to the Hvorslev surface; OCR was calculated by dividing the preconsolidation pressure by the isotropic cell pressure applied. In Fig. 29, in the undrained tests on the dry-crust clay, the water content was 30–34%. As the clay was heavily over-consolidated, the p', q-curves turn to the right. These samples were taken from the test embankment while it was being built.

Fig. 77 (Graham et al. 1988) shows normalised yield envelopes of different clays. Classification data on the same clays are given in Table 18. The yield envelope of the Taasia clay is known thanks to the consolidation tests made with the oedometer and the shear tests with the triaxial apparatus. The

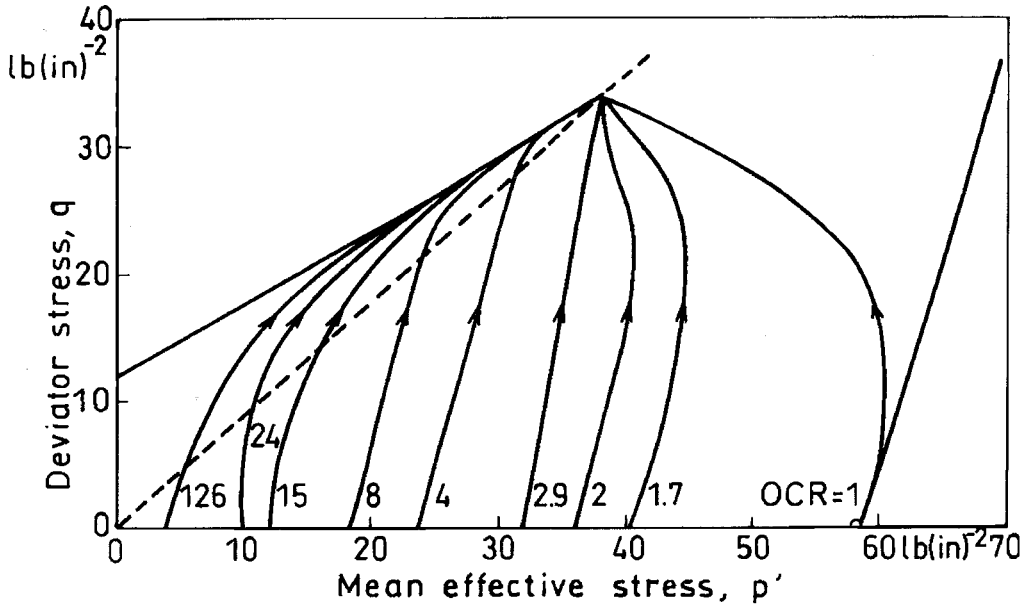

Fig. 76. (Roscoe et al. 1958) Section of yield domain for undrained tests on Weald Clay showing loading paths for various values of overconsolidation ratio. w = 20.7%.

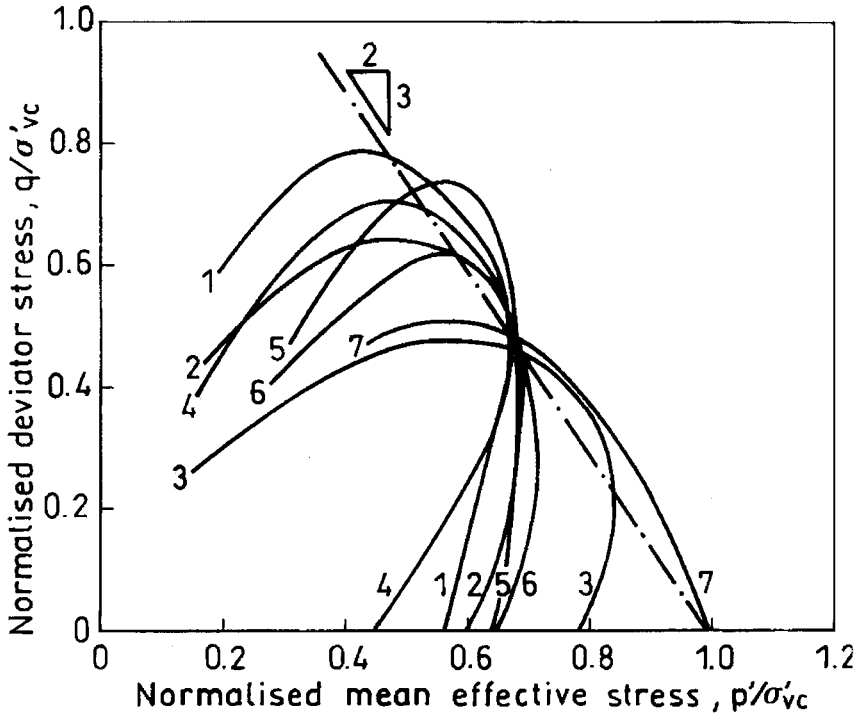

Fig. 77. (Graham et al. 1988) Examples of normalised yield envelopes from various sites: curve 1, Rang de Fleuve; curve 2, Belfast; curve 3, Winnipeg; curve 4, St Albans; curve 5, Lyndhurst; curve 6, Mastemyr, curve 7, Taasia (added).

Table 18. Classification data for yield envelopes of clays in Fig. 77 (Graham et al. 1988) (Taasia added 1993).

Site	w %	w_L %	I_p %	Activity	OCR
Rang de Fleuve	80	70	50	-	1.0-1.2
Belfast (a)	35–55	40-60	20-40	0.6	1.6-2.0
Belfast (b)	60-80	75-110	50-70	1.5	1.2-1.8
Winnipeg	54-63	65-85	35-60	0.67	2.4
St Albans	90	50	23	0.38	2.2
Lyndhurst	45	36	13-16	0.25	1.5
Mastemyr	40	26	5-13	-	1.2
Taasia					
dry crust	34	59	27	0.77	5.0
clay under dry crust	76	86	28	0.39	2.0

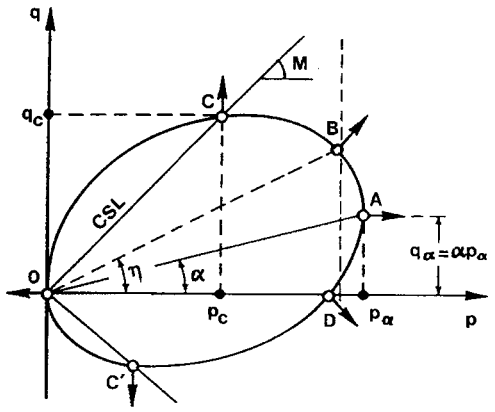

Fig. 78. Schematic illustration of anisotropic yield surface in triaxial space (Dafalias 1987).

curves determined for the Taasia clay are also given in Fig. 77 and the parameters of Taasia clay in Table 18.

The amount of anisotropy in different Finnish clays has been tested at Helsinki University of Technology. Some of the results are given in Table 19 (Karstunen et al. 1995). A schematic illustration of the anisotropic yield surface in the triaxial space is shown in Fig. 78 (Dafalias 1987).

Table 19 shows that the anisotropy parameter α (explained in Fig. 78) is zero in Taasia clay and of the order of 0.45–0.75 in other Finnish clays. The K_o-value in different clays does not differ accordingly. The K_o-values were calculated with Jaky's formula [equation (65)].

The yield envelope of the Taasia clay differs from that of the other clays. A recent experiment

Table 19. Parameters of anisotropic yield surface and calculated K_o-values (Karstunen et al. 1995).

Site	Depth z, m	M	α	K_o Jaky	Reference
Perno clay	4	0.90	0.45	0.609	Korhonen & al. 1987
Otaniemi clay	2	1.00	0.57	0.571	Lojander 1988
Riihimäki clay	4	1.06	0.58	0.550	Lojander 1988
Lahti silt	1	1.00	0.75	0.571	Lojander 1988
Taasia clay	4	1.05	0	0.553	Näätänen & al. 1994
Vaasa clay	5	1.50	0.57	0.400	Näätänen & al. 1994
Paimio clay	6	1.20	0.45	0.500	Korhonen & al. 1991
Paimio clay	1	1.10	0.625	0.535	Näätänen & al. 1994

on the Upper Pisa Clay in Italy (Berardi et al. 1991) gave curves very similar in shape to those for the Taasia clay. The Upper Pisa Clay had *OCR* = 1.6, LL = 65% and PI = 40%.

The yield curve for the critical state is much like that of the Winnipeg Clay. The results of the laboratory tests made here refer mostly to the part of the yield curve around the critical state. In Fig. 79 (Graham et al. 1988) the data on Winnipeg clay are normalised by the equivalent pressure of the one-dimensional normal consolidation line. The similarly normalised data on Taasia clay are included. The data on the two natural clays are similar and compatible with a yield surface of the Modified Cam Clay model type of yield surface.

Table 20 depicts the soil parameters of Rio de Janeiro soft clay (Almeida and Ramalho-Ortigão 1982). The parameters are similar to those for Taasia clay. Unlike the Taasia clay, the deposits of Rio de Janeiro soft clay contain allmost no dry crust.

An embankment on soft clay was studied by Almeida (1984) with a centrifuge model. The studied section is shown in Fig. 80 with model and prototype dimensions. Fig. 81 depicts the vertical effective stresses and the over-consolidation ratio modelled with a centrifuge. Fig. 82 illustrates the loading steps in the centrifuge. The critical state parameters are listed in Table 21. The finite element mesh is given in Fig. 83. Fig. 84 shows the initial specific volume, permeability and stress distribution used in the calculations.

Some of the results of the studies of Almeida are illustrated in Figs. 85–87. The displacements are distributed as in the Taasia test embankment (Fig. 57).

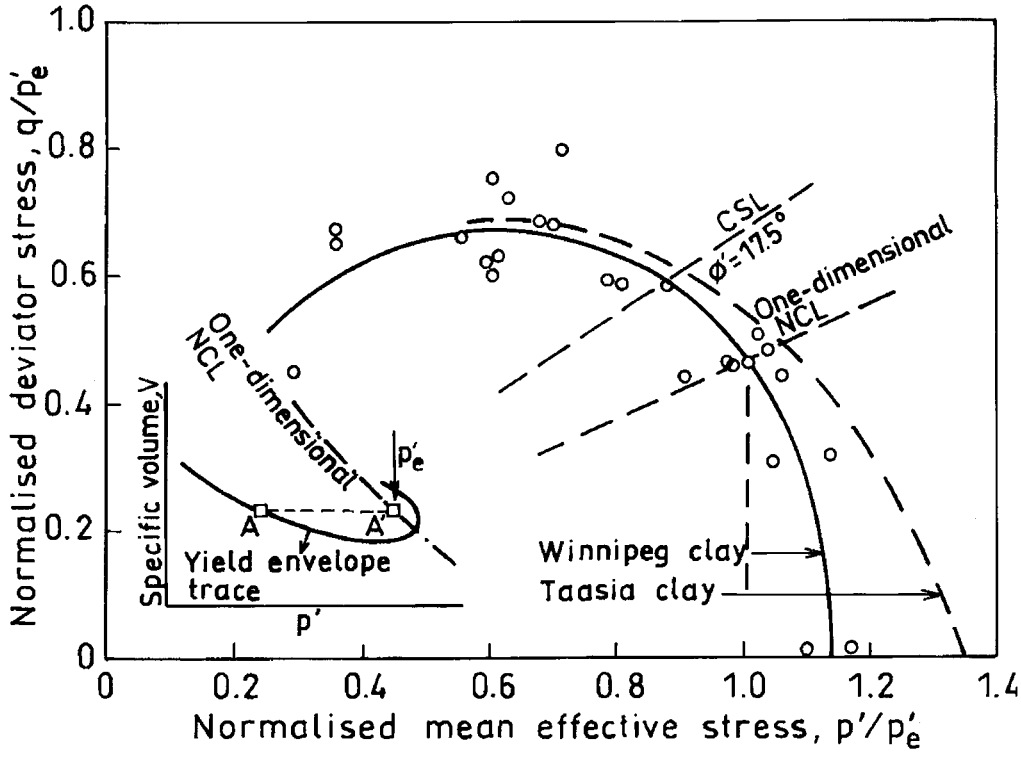

Fig. 79. (Graham et al. 1988) Yield envelope for natural Winnipeg clay normalised by equivalent pressure p_e on one-dimensional NCL for field deposit. Yield envelope for Taasia clay added.

Table 20. Soil parameters for in situ Rio de Janeiro soft clay used in finite element analyses (Almeida and Ramalho-Ortiqao 1982).

Depth (m)	λ	κ	e_{cs}	M	G (kPa)
0–3	0.90	0.13	5.8	1.14	350
3–5	0.83	0.13	5.8	1.14	550
5–7.5	0.83	0.11	5.3	1.14	700
7.5–11	0.70	0.10	4.6	1.14	900

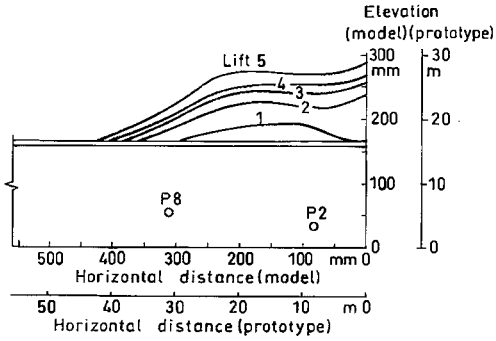

Fig. 80. Section through centrifuge model of embankment on soft clay, constructed in five lifts (after Almeida 1984, Wood 1990).

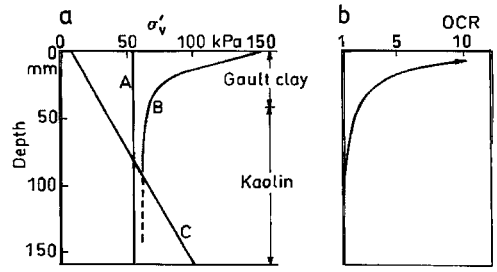

Fig. 81. (a) Vertical effective stresses and (b) overconsolidation ratio for clay in centrifuge model: (A) initial consolidation at 1 g; (B) partial consolidation at 1 g with top drainage only; (C) consolidation at 100 g (Almeida 1984). OCR = overconsolidation ratio

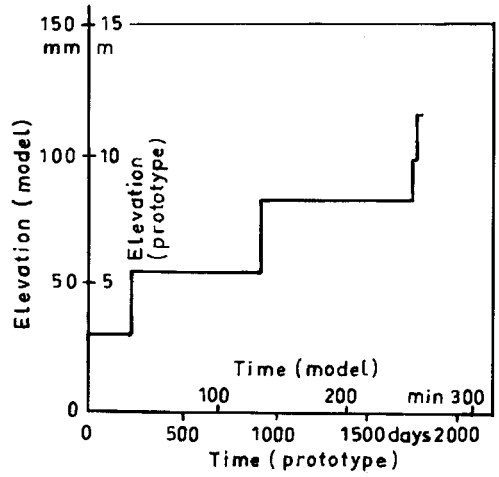

Fig. 82. Loading history for centrifuge model (Almeida 1984).

Table 21. Critical state parameters of Kaolin and Gault clay (Almeida, 1984).

	Kaolin	Gault clay
λ	0.25	0.219
κ	0.05	0.035
V	3.44	2.96
M	0.9	1.0

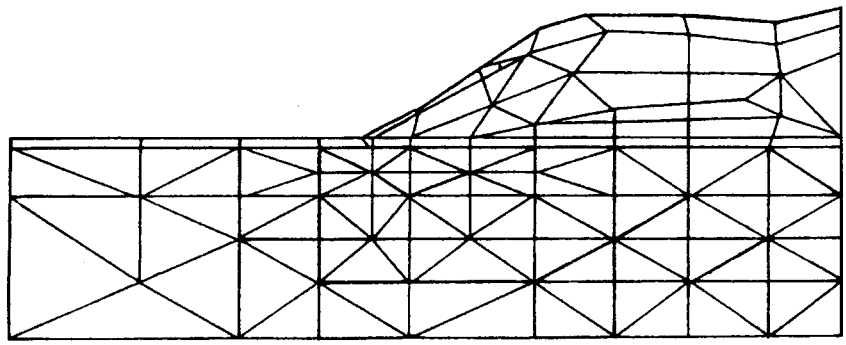

Fig. 83. Finite element mesh for analysis of model embankment on soft clay (Almeida 1984).

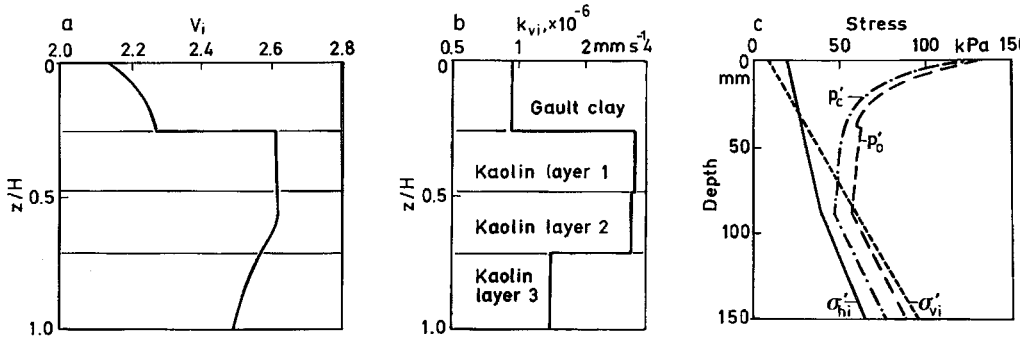

Fig. 84. Profiles of (a) initial specific volume, (b) permeability, and (c) vertical and horizontal stress and size of initial yield locus for clay beneath embankment (Almeida 1984).

6.5 Special features revealed by this study

The laboratory tests performed here showed that the dry-crust layer and the underlying clay have stress-strain characteristics that can be combined into the same normal consolidation line. Testing the dry-crust clay with undisturbed samples and samples from the test embankment permits the representativeness of the compacted samples to be assessed for the undisturbed dry-crust layer.

The undisturbed samples of the dry crust exhibited higher failure strengths than the test embankment samples. The K_o-value determined for the samples from the test embankment may not represent the dry-crust clay layer. The ageing undergone by the dry-crust layer is lost in compaction. The test results agree with the results of other investigators (Burland 1990, Leroueil and Vaughan 1990), as the intact clay fails at greater deviator stress values than does the restructured clay. Consequently, the different layers must be tested, if possible, in situ or with laboratory tests on undisturbed samples.

Owing to the great number of site and laboratory tests, the modelling of the behaviour of the test embankment succeeded well with a coupled consolidation type of procedure. Previous calculations (Pitkänen 1982, Loukola 1985), the elastic calculation in the present part of the research project and the calculation with the critical state models all show that the results of the critical state models are most reliable for the settlement analy-

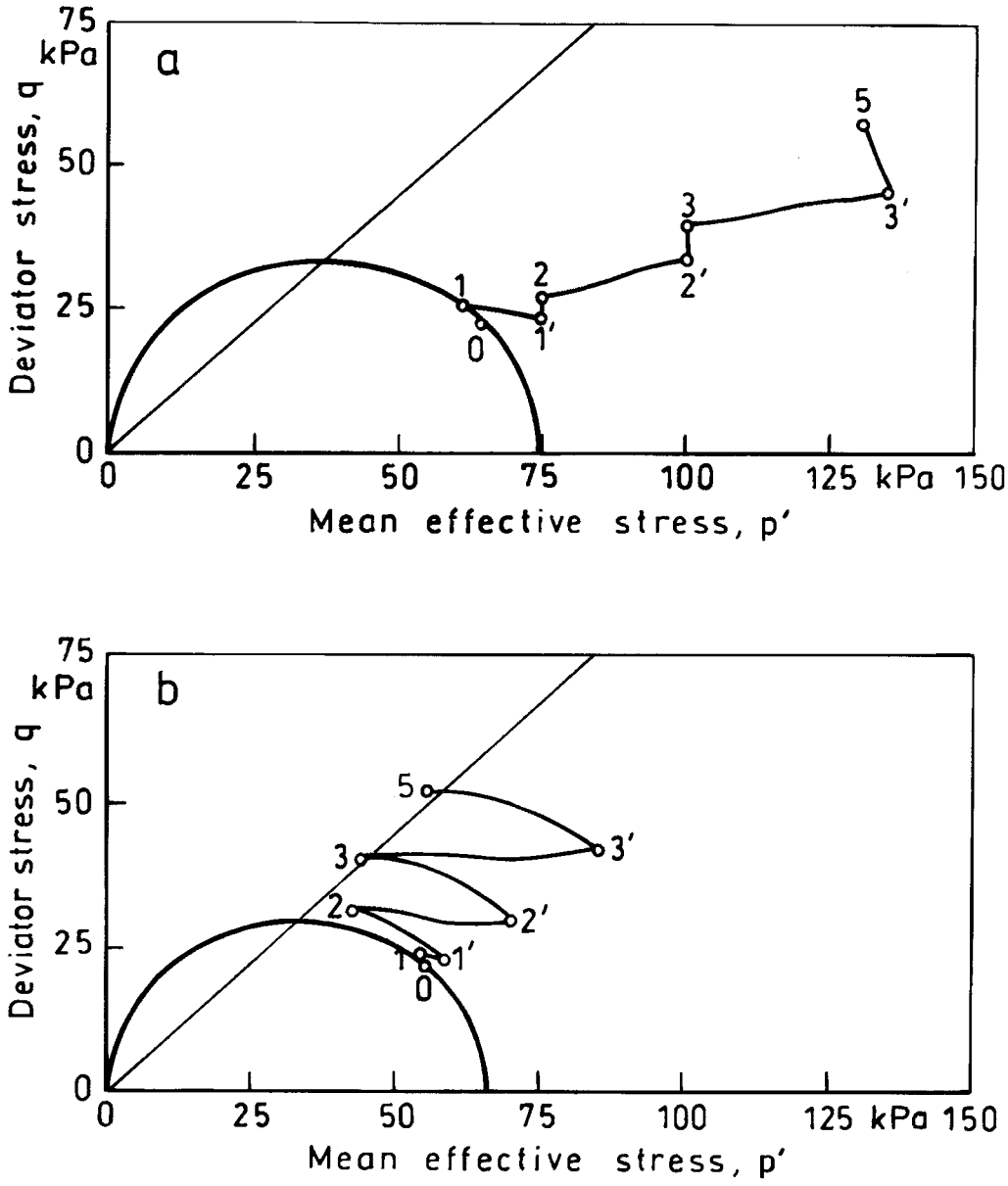

Fig. 85. Computed effective stress paths for elements of soil at positions of piezometers (a) P2 and (b) P8 (Almeida 1984).

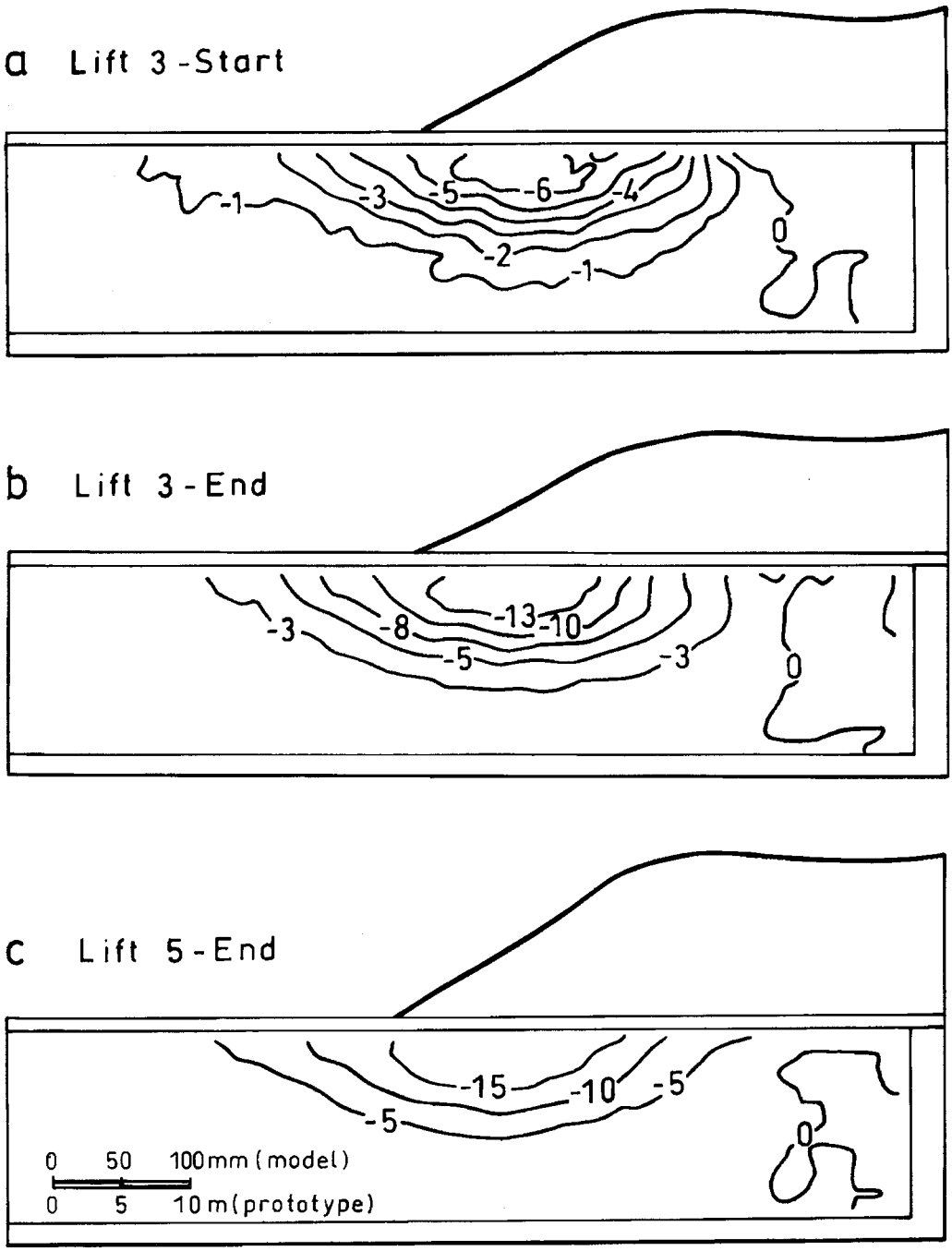

Fig. 86. Horizontal displacements, test MA3 (Almeida 1984).

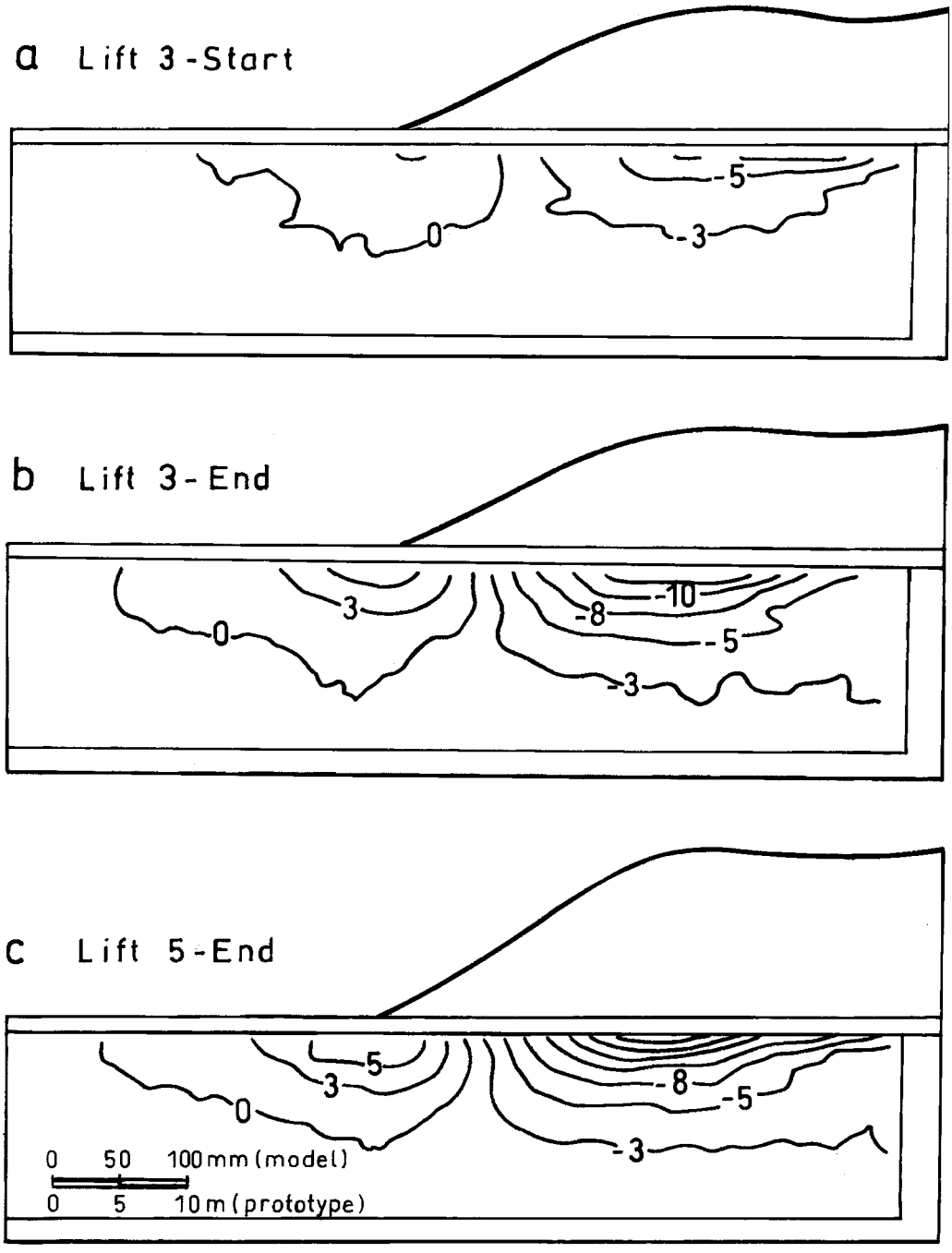

Fig. 87. Vertical displacements, test MA3 (Almeida 1984).

sis when the parameters are derived from site and laboratory tests. The calculation is not too sensitive to the errors in parameters. Moreover, the parameters for the elastic analysis are difficult to test with conventional laboratory tests.

Calculation with the lowest possible p_o'-values showed that the Modified Cam Clay model is suitable for calculation of deformations in the normally consolidated state.

The critical state models can be used to monitor stresses in the foundation of large dams and to draw up a construction schedule appropriate to the foundation. It is, however, difficult to calculate the conditions prevailing in the embankment, e.g. the location of cracks and the tensional stresses. The latter can be investigated with special models that take better account of tensile stresses. Smaller dams, where cracking is not a problem, can well be planned with the aid of critical state models.

7 Conclusions

The project revealed that critical state methods were effective for calculating the coupled consolidation of the Taasia test embankment. Although the critical state models could not describe all the features of the different clay layers, they were sufficiently accurate in relation to the accuracy of the parameters.

The outcome of the non-linear elastic calculation (Loukola 1985) with the methods developed in Canada (Eisenstein and Krishnayya 1972, Krishnayya 1973a, 1973b) was no better at explaining the behaviour of the test embankment. For the design of the dam body it was, however, an advantage that the tensional strength characteristics were included. In the CRISP-90 and CRISP-94 programs the critical state models cannot be used for the simulation of the embankment construction because of computational difficulties.

The conventional calculation methods failed to assess test embankment settlement. Some progress has been made in this respect since 1982.

One objective of this thesis was to define the critical state parameters for the design of a proposed dam and its construction schedule. The laboratory tests and simulation calculations showed that the value of the parameter κ is in the range 0.01–0.03. The parameter λ is in the range 0.6–0.8 for the most frequently tested layer (3) under the dry crust. The parameter λ for the dry crust could be analysed with the I_p-value, but it had no effect here.

The parameter M is in the range 0.9–1.1 for normally consolidated samples and in the range 1.1–1.2 for over-consolidated samples. The parameter e_{cs} is in the range 4.0–6.0. The best way to choose a reliable value for e_{cs} is to ensure from the combined results of the consolidation tests and drained triaxial shear tests (Figs. 33 and 34) that the level of the stresses at the critical state is correct. The range of hydraulic conductivities used in the calculations is recommended for use in the design of the proposed dam. A K_o-value of 0.67 would be best for the test embankment. As the value of K_o for the clay under the dry crust is somewhat lower, the value 0.6 was used instead. More tests are necessary to find a reliable value of K_o. The parameter values of the elastic model were chosen from the drained triaxial tests. They are sufficiently reliable for the simulation made here. The final calculations with the CRISP-94 program gave a K_o-value of 0.75 for the deep clay layer, which conforms with the CRISP theory.

The values of p_o' were chosen from the consolidation experiment made with the triaxial tests and the oedometer test. Some oedometer results were taken from previous investigations (Lojander 1980, Kallio 1980). In the final calculations at the lowest values of p_o' with the CRISP-94 program, the normally consolidated state was considered.

The value of the slope of Hvorslev's line is about 0.7 with a range from 0.5 to 0.9. The choice of design value depends on the circumstances, and the effect on the safety margin must be analysed.

The two sets of different models (the elastic model for the test embankment and the Modified Cam-Clay and the Schofield models for the foundations) gave almost identical results, which are compatible with those measured.

When the elastic, perfectly plastic model with the Mohr-Coulomb failure criterion was used instead of the elastic model for the test embankment, the two sets of models gave similar results to those obtained with the initial combinations. If the models are used in the design of an actual dam, calculations must be made with the parameters chosen and with some variations of these parameters (sensitivity analysis).

As the laboratory results supported the Modified Cam Clay type of yield surface, the preconsolidation pressure in the Schofield model

must be adjusted to ensure that the yield surface is compatible with the measured laboratory values on the critical state line. In other respects, both the Modified Cam Clay and the Schofield models could be used. In the Taasia case, the failure surface of over-consolidated clay can be simulated with Hvorslev's failure surface or with the Modified Cam Clay yield surface.

Another objective was to test the Taasia clay at stages of different over-consolidation ratios. As shown in Fig. 33, the combined isotropic consolidation line permits the proper preconsolidation pressure value to be estimated for the over-consolidated clay, which, in this case, is higher than the values calculated without combining the different test results. The critical state line calculated from the combined isotropic normal consolidation line (Fig. 33) was used for soil layer 3 and for estimating the critical state pressure levels of the other layers. Fig. 34 shows that the critical state line calculated from the combined results of the consolidation test agrees with the shear test results if the fact that the critical state was not always reached is taken into account.

According to the combined results of triaxial tests in the p',q-coordinate system (Fig. 35), the M-value for the over-consolidated clay is higher than that for normally consolidated clay. Cohesion is also higher for over-consolidated clay. There is also a difference between over-consolidated clays, as intact clay has higher cohesion than reconstituted clay.

The laboratory and field tests and simulations undertaken demonstrate that the critical state methods are useful in:

- developing an integrated method to monitor stresses and strains;
- giving an overall picture of the development of stresses and strains and their relationships in a foundation composed of clay deposits under an earth dam;
- interpreting laboratory test data;
- designing small dams; and
- simulating the conditions in the foundation of large dams and choosing their construction schedule.

Compared with the classical methods in which stability and strains were treated separately and limit state analysis was the only stability analysis, the critical state methods permit a more versatile computational approach.

Although the laboratory tests for the present study did not always strictly obey the critical state theories available as computer programs, the behaviour of the samples was in general compatible.

The programs based on the critical state theory are sensitive to special situations, e.g. large differences in properties between the embankment and the foundation and between the dry crust and the underlying layers. In the present case, the differences were not too marked and the program gave fairly reliable results. Use of the programs is rather laborious if applied to more complicated cases.

Calculations with the Z-soil program gave similar results to those obtained with the CRISP program. The sensitivity of the Z-soil program to special situations was not tested. It permits non-associative models to be used, but the need for these did not arise here.

Calculations with the CRISP-94 program demonstrated the importance of the values of the average preconsolidation pressure p_o'. Calculations with the lowest possible p_o'-values gave a κ-value of 0.01, which in the other calculations was in the range of 0.02 to 0.03. No other effects on the parameters were found.

The Taasia test embankment was one of the first where critical state models were applied in Finland. Consequently, there is a shortage of comparative data, particularly on the parameters of the critical state models for Finnish clays. Once data have accumulated, and the laboratory methods are reduced to a reasonable number of oedometer tests, triaxial tests and other studies, the method will be economically viable. As the critical state methods were still being developed during the study, the costs of the research project were high for the planning and design of only one dam. The main outcome of the project lies in its contribution to our knowledge of Finnish clays. It would also have been useful in the final planning of the proposed dam. As it seems, however, that the dam is not to be constructed, the instrumentation of the test embankment can be checked and the plastic behaviour of the clay layers more effectively studied by raising the test embankment.

8 Summary

This report presents the second part of a study aimed at solving the problems involved in building a flood control dam on a thick clay deposit.

The emphasis is on application of the critical state theory to the study of clay deposits.

The calculations were tested by comparing the calculated settlement and pore water pressure values of the test embankment constructed in the study area with the measured values. The test embankment was constructed using local dry-crust clay. The behaviour of the 4.5-m-high test embankment was monitored over a period of 15 years.

At the site of the proposed earth dam, the clay deposit is from 0 to 35 m thick. Under the test embankment the clay deposits are 17 m thick. The site was studied with weight sounding and vane tests.

Numerous soil samples were taken from the test site and studied in the laboratory. The studies, which included the determination of index properties, undrained shear strength, and other strength and strain properties, were conducted on clay samples from deposits under the dry crust and on dry-crust clay.

Various triaxial compression tests played a key role in the investigations. The triaxial tests were performed both isotropically and anisotropically using consolidated samples. In the anisotropic tests the ratio of principal stresses was given values of 0.8 and 0.6. Both drained and undrained shear strengths were determined. Dry-crust material was submitted to the K_o-test. The test technique corresponded to that used in the UK, on the basis of which the theory of the critical state was developed.

As shown by the laboratory tests, the different materials largely obey the models of the critical state theory. The values of the soft layers differed from those predicted by the models, because the samples showed continuous volumetric strain in triaxial compression. The dry-crust clay and the embankment material differed in terms of failure stress. The anomalous values of the dry-crust clay and the embankment material are due to differences between intact and restructured clays and to the considerable scatter. Owing to insitu drying, the dry-crust clay was cracked and thus difficult to study.

The settlement of the test embankment was calculated with the finite element program, CRISP, using the Modified Cam-Clay model and the Schofield model in which Hvorslev's failure surface was applied to over-consolidated clay and the original Cam-Clay model to normally consolidated clay. Calculations were also made with the Z-soil program. The model used is similar to the Roscoe-Hvorslev model, which was not included in the CRISP-program. The Z-soil program gave similar results to those obtained with the CRISP-program. In the final analysis with the latest version (94) of the CRISP-program the Modified Cam-clay model was used.

The CRISP models studied gave almost identical results when the model calculations were adjusted to correspond with each other at the critical state.

The errors due to the calculation method were assessed by printing out the pressures and displacements as a compound presentation covering the whole cross-section. The calculated values are about the same as those measured. The investigations and calculations permitted probable values of the parameters of the critical state to be established for the Taasia clay. These parameters can be applied in the dam design and as reference data in studies on other similar clays in Finland.

As a result of this project, critical state models can be applied to calculate the settlement of the proposed dam. Non-linear elastic models with tensile effects can be used in attempts to prevent the dam from cracking.

If, however, the dam is not constructed, the plastic behaviour of the clay layers can be studied by raising the test embankment.

Acknowledgements

This study was conducted at the technical research office of the Water and Environment Research Institute during planning for the construction of an earth dam to regulate the River Taasianjoki. In the course of the work I received much encouragement from my superiors, Professor Seppo Mustonen, Dr Hannu Laikari and, in the final stage, Ilkka Manni.

Professor Kalle-Heikki Korhonen and, in the final stage, Professor Eero Slunga supervised the work, providing constructive criticism. Matti Lojander made many valuable suggestions and put his material on Taasia clay at my disposal. Anu Näätänen provided useful advice and assisted me with the final calculations. Pauli Vepsäläinen gave useful advise in the final stage.

Professor David Muir Wood from UK, professor Kenneth Runesson from Sweden and professor Kennet Axelson from Sweden have performed

careful examination of the manuscript. Numerous comments and recommendations have been considered. It has considerably improved the value of the study.

Jukka Airila assisted me in calculations with the CRISP-90 program and Markus Sjöholm with the Z-soil program. Tuula Rytkönen and Markku Liponkoski helped with the development of the programs. Tuulikki Suokko assisted in geological questions. Berit Bergström assisted in the laboratory and Marjatta Sorsa in the calculation of laboratory results. The field work was done by Heikki Jyllilä.

The figures were drawn by Raili Korkiakangas, Anneli Vehviläinen and Katri Salmela. The manuscript was typed by Meri Kostian, Päivi Laaksonen, Minna Wasenius, Tuula Alanko and Anja Tarhonen. The original version was translated into English by Gillian Häkli. Marja-Liisa Poikolainen assisted in checking the references.

I express my greateful thanks to all the above persons.

Helsinki, May 1996

Erkki Loukola

Yhteenveto

Julkaisussa esitetään jälkimmäinen osa tutkimuksista, joilla pyrittiin selvittämään paksun savikerroksen varaan perustetun tulvasuojelupadon rakentamiseen liittyvät geotekniset ongelmat. Julkaisu keskittyy kriittisen tilan teorian soveltamiseen savikerrosten mallintamisessa.

Käytetty ohjelmisto ja kriittisen tilan teoria on esitetty tutkimuksessa käytetyiltä osiltaan. Ohjelmistossa on kriittisen tilan laskentaan yhdistetty konsolidaation aiheuttamien muodonmuutosten laskenta. Julkaisussa on esitetty myös kriittisen tilan parametrien ja indeksiominaisuuksien vuorosuhteet.

Kriittisen tilan laskennan testaus on suoritettu vertaamalla tutkimusalueelle rakennetun koepenkereen laskettuja painuma- ja huokosvesipainearvoja mitattuihin arvoihin. Koepenger on rakennettu tutkimusalueen kuivakuorisavesta. Sen korkeus on noin 4,5 m. Koepenkereen käyttäytymistä on seurattu 15 vuoden ajan.

Savikerrosten kokonaispaksuus vaihtelee suunnitellun maapadon alueella 0–35 m. Koepenkereen alla on savikerrosten kokonaispaksuus 17 m. Alue on tutkittu painokairauksin ja siipikairauksin.

Koealueelta on otettu lukuisia maanäytteitä, jotka on tutkittu laboratoriossa. Tutkimukset ovat käsittäneet indeksiominaisuuksien, suljetun leikkauslujuuden, muiden lujuusominaisuuksien ja painumaominaisuuksien tutkimuksia. Tutkimukset on jaettu paksujen savikerrosten tutkimuksiin ja kuivakuorisaven tutkimuksiin.

Keskeisiä tutkimuksia ovat erilaiset kolmiaksiaaliset puristuskokeet. Kolmiaksiaalikokeet on suoritettu sekä isotrooppisesti että anisotrooppisesti konsolidoiduilla näytteillä. Anisotrooppisessa konsolidoinnissa on käytetty pääjännitysten suhteena arvoja 0,8 ja 0,6. Näytteet on leikattu avoimina tai suljettuina kokeina. Lisäksi on suoritettu kuivakuorimateriaalille ns. K_o-koe. Koetekniikka vastaa Isossa Britanniassa tehtyjä kokeita, joiden avulla kriittisen tilan teoria on kehitetty.

Laboratoriokokeiden perusteella eri materiaalit noudattavat pääosin kriittisen tilan teorian mukaisia malleja. Suurimmat poikkeamat ko. malleista on todettu pehmeiden kerrosten osalta näytteiden jatkuvana tilavuudenmuutoksena kolmiaksiaalisessa puristuksessa sekä kuivakuorisaven ja pengermateriaalin poikkeamina murtumajännityksen osalla. Kuivakuorisaven ja pengermateriaalin tulosten poikkeavuudet johtuvat maakerrosten häiriintymättömän ja sullotun saven ominaisuuksien erilaisuudesta ja suuresta hajonnasta. Kuivakuorisavikerros on luonnossa kuivumisen johdosta halkeillutta ja siksi vaikeasti tutkittavissa.

Koepenkereen painuma on määritetty Modified Cam Clay -mallilla ja ns. Schofield-mallilla, jossa ylikonsolidoituneen saven osalla käytetään Hvorslevin teoriaa ja normaalikonsolidoituneen saven osalla alkuperäistä Cam Clay -mallia. Laskelmat suoritettiin myös Z-soil-ohjelmalla. Käytetty malli vastaa Roscoe-Hworslev-mallia, jota ei ollut käytettävissä CRISP-ohjelmistossa.

Tutkituilla CRISP-malleilla on saatu lähes identtiset tulokset kun mallilaskennat on sovitettu siten, että ne vastaavat toisiaan kriittisen tilan kohdalla. Z-soil-ohjelmalla saadut tulokset vastaavat CRISP-ohjelmilla saatuja tuloksia. Viimeinen tarkistuslaskenta suoritettiin CRISP-ohjelman parannetulla versiolla (94) Modified Cam Clay mallia käyttäen.

Tulostamalla paineet ja siirtymät koko poikkileikkauksen käsittävinä yhdistelmäkuvina on saatu

esille myös laskentamenetelmän aiheuttamat virheet.

Laskennan tulokset vastaavat suuruusluokaltaan mitattuja tuloksia. Tutkimusten ja laskennan avulla on saatu määritettyä Taasian savelle todennäköiset kriittisen tilan parametrit, joita voidaan käyttää padon mahdollisessa suunnittelussa ja vertailutietona vastaavia muita suomalaisia savia tutkittaessa.

Tutkimusprojektin tuloksena kriittisen tilan malleja voidaan käyttää mahdollisen padon painumien laskennassa. Padon halkeilun estämisen suunnittelussa voidaan käyttää epälineaarisia elastisia malleja, joissa voidaan ottaa huomioon myös vetojännitykset.

Tehtyä tutkimusta voidaan tarkentaa korottamalla koepengertä, jolloin savikerrosten plastiset ominaisuudet tulisivat paremmin esille.

List of Symbols

a_ϕ	material parameter in Drucker-Prager criterion
c	cohesion (kPa)
c_L	shear strength at liquid limit (kPa)
c_P	shear strength at plastic limit (kPa)
c_u	unconfined shear strength (kPa)
c_o	cohesion at y = y_o (Table 1) (kPa)
c'	cohesion intercept in terms of effective stresses (kPa)
d	standard deviation
e	void ratio
f	yield function
h	height of water level in gauge tube (m)
h	head of pore water pressure (m)
k	hydraulic conductivity (ms^{-1}), material parameter in Drucker-Prager criterion
k_h	horizontal hydraulic conductivity (ms^{-1})
k_v	vertical hydraulic conductivity (ms^{-1})
k_x	hydraulic conductivity in x-direction (horizontal) (ms^{-1})
k_y	hydraulic conductivity in y-direction (ms^{-1})
m	mean value
m_c	rate of increase in shear strength with depth
m_e	rate of increase in Young's modulus with depth
p'	mean effective stress (kPa)
p_e'	equivalent stress: value of p' at the point on the isotropic normal compression line or the one dimensional compression line at the same specific volume
p_o'	average preconsolidation pressure, intersection of the stable state boundary surface and axis in the p',q coordinate system (isotropic test) (kPa)
p_{Ko}'	preconsolidation value for p' in oedometer test (kPa)
p_{cs}'	mean effective stress in critical state (kPa)
p_T'	intersection of the Drucker-Prager line and the p' axis in the p',q coordinate system (kPa)
p_u'	mean effective stress at the intersection of the swell curve and critical state line (kPa)
q	deviator stress (kPa)
q_f	deviator stress in failure state (kPa)
q_{cs}	deviator stress in critical state (kPa)
r	radius of tube attached to sensor tip (m)
s	undrained shear strength (kPa)
s_1	stress deviation in direction of maximum principal stress (kPa)
s_2	stress deviation in direction of intermediate principal stress (kPa)
s_3	stress deviation in direction of minimum principal stress (kPa)
s_{ij}	deviatoric stress tensor
t	time (s, a)
u	pore water pressure (kPa)
$\bar{u}$	excess pore water pressure (kPa)
v_x	flow rate in x-direction (ms^{-1}) (horizontal)
v_y	flow rate in y-direction (ms^{-1}) (vertical)
w	water content (%)
w_L	liquid limit (%)
y	elevation (m)
y_0	elevation (initial) (m)
z	height (m)
E	modulus of elasticity, Young's modulus (kPa)
E_o	modulus of elasticity in elevation y_o (kPa)
E_h	horizontal modulus of elasticity (kPa)
E_v	vertical modulus of elasticity (kPa)
G_{hv}, G	shear modulus, modulus of rigidity (kPa)
G_s	specific gravity of soil grains
H	slope of Hvorslev surface
I_1'	first effective stress invariant (kPa)

I_p plasticity index (%)
J number of failure criteria (Table 1)
J_2 second invariant of stress deviation (kPa)
J_3 third invariant of stress deviation (kPa)
K' bulk modulus (effective stresses) (kPa)
K_{nc} coefficient of earth pressure at rest of normally consolidated soil
K_o coefficient of earth pressure at rest
K_w bulk modulus of water (kPa)
L length of sensor tip (m)
M slope of critical state line
M_f slope of Drucker-Prager line
N specific volume of isotropically compressed soil at p'=1 kPa, number of samples
OCR over-consolidation ratio
P direction of plastic flow
Q normal to yield surface (Z-soil program)
R radius of sensor tip (m), ratio of unconfined compression strengths at plastic and liquid limit
S slope of tensile crack
V specific volume
V_f specific volume at failure
V_λ specific volume of soil at anisotropic compression with p'=1 kPa
V_κ specific volume of soil in over-consolidated state with p'=1 kPa
V_u specific volume at intersection of swell curve and critical state line
δV change in specific volume
δV^e elastic change in specific volume
δV^p plastic change in specific volume
δW dissipated work
α anisotropy parameter
δ_{ij} Kronecker delta
γ unit weight $(kN\,m^{-3})$
γ_w unit weight of water $(kN\,m^{-3})$
ε_1 strain in direction of maximum principal stress (%)
ε_2 strain in direction of intermediate principal stress (%)
ε_3 strain in direction of minimum principal stress (%)
ε_x strain in x-direction (horizontal) (%)
ε_y strain in y-direction (vertical) (%)
ε_z strain in z-direction (horizontal) (%)
ε_x^e elastic strain in x-direction (%) (horizontal)
ε_y^e elastic strain in y-direction (%) (vertical)
ε_z^e elastic strain in z-direction (%) (horizontal)
ε_s second deviatoric strain invariant (shear strain) (%)
$\varepsilon_{s(xy)}$ shear strain in xy-plane (%)
$\varepsilon_{s(yz)}$ shear strain in yz-plane (%)
$\varepsilon_{s(zx)}$ shear strain in zx-plane (%)
ε_s^p plastic shear strain (%)
ε_v volumetric strain (%)
$\delta\varepsilon_v^p$ plastic change in volumetric strain
ε_v^p plastic volumetric strain (%)
η ratio of deviator stress to mean effective stress
κ slope of settlement line of over-consolidated clay in $\ln(p')$, V-plane
λ parameter of total volumetric strain
$d\lambda$ positive scalar defining amplitude of plastic flow (Flow rule in Z-soil program)
ν Poisson's ratio
ν_{hh} Poisson's ratio (horizontal strain due to horizontal force)
ν_{hv} Poisson's ratio (horizontal strain due to vertical force)
ν_{vh} Poisson's ratio (vertical strain due to horizontal force)
ν' effective Poisson's ratio
σ_1 maximum principal stress (kPa)
σ_2 intermediate principal stress (kPa)
σ_3 minimum principal stress (kPa)
σ_x' effective stress in x-direction (horizontal) (kPa)
σ_y' effective stress in y-direction (vertical) (kPa)
σ_z' effective stress in z-direction (horizontal) (kPa)
σ_1' maximum effective principal stress (kPa)
σ_2' intermediate effective principal stress (kPa)
σ_3' minimum effective principal stress (kPa)
σ_v' vertical effective stress (kPa)
σ_{vc} maximum vertical effective stress = preconsolidation stress (kPa)
τ_{xy} shear stress in xy-plane (kPa)
τ_{yz} shear strain in yz-plane (kPa)
τ_{zx} shear strain in zx-plane (kPa)
ω_x body force in x-direction $(kPa\,m^{-1})$ (horizontal)
ω_y body force in y-direction $(kPa\,m^{-1})$ (vertical)
ϕ angle of friction (radians or degrees)
ϕ' angle of friction in terms of effective stresses (radians or degrees)

ϕ_{cs}'	angle of friction between soil grains at critical state
Ψ	angle of non-associativity (°), plastic-strain increment ratio
Γ	specific volume of soil at critical state with p' = 1 kPa
θ	Lode angle (°)
θ_f	angle of orthotrophy (°)

Abbreviations

AP	arboreal pollen
CAD	consolidated anisotropic test
CID	consolidated isotropic test
CADC	consolidated anisotropic drained compression test
CAUC	consolidated anisotropic undrained compression test
CC	Cam Clay
CIDC	consolidated isotropic drained compression test
CIUC	consolidated isotropic undrained compression test
DP	Drucker-Prager
EGAR	eastern gateway access road
HOCS	highly over-consolidated stress
INCL	Isotropic normal consolidation line
LOCS	lightly over-consolidated stress
MCC	Modified Cam Clay
MIT	Massachusetts Institute of Technology
NCC	normally consolidated clay
NAP	non-arboreal pollen
NCS	normally consolidated state
OCC	over-consolidated clay
SCH	Schofield model

References

Almeida, M.S.S. 1984. *Stage Constructed Embankments on Soft Clay*, PhD thesis, Cambridge University, Cambridge 142 pp., app.

Almeida, M.S.S. & Ramolho-Ortigáo, J.A. 1982. *Performance and Finite Element Analysis of a Trial Embankment on Soft Clay*, Cambridge University, Engineering Department, Cambridge, 11 pp.

Atkinson, J.H. 1981. *Foundation and Slopes. An Introduction to Applications of Critical State Soil Mechanics,* McGraw-Hill Book Company Ltd, London, 382 pp. ISBN 0-07-084118-7.

Atkinson, J.H & Bransby, P.L. 1978. *The Mechanics of Soils. An Introduction to Critical State Soil Mechanics*. McGraw-Hill Book Company Ltd, London, 375 pp. ISBN 0-07-084077-6.

Berardi, G., Caroti, L., Giunto, G., Jamiolkowski, M. & Lancellotta, R. 1991. Mechanical properties of Upper Pisa Clay. In: *Proceedings of the Tenth European Conference on Soil Mechanics and Foundation Engineering,* Florence 26–30 May 1991, Volume 1, A.A. Balkema, Rotterdam, pp. 1–10. ISBN 905410 0028.

Biot, M.A. 1941. General Theory of Three-Dimensional Consolidation. *Journal of Applied Physics* 12: 155–164.

Bishop, A.W. & Henkel, D.J. 1964. *The Measurements of Soil Properties in the Triaxial Test*, Second Edition, Reprint, Edward Arnold (Publishers) Ltd, London, 228 pp.

Bishop, A.W. & Wesley, L.D. 1975. A Hydraulic Triaxial Apparatus for Controlled Stress Path Testing. *Géotechnique* 25: 657–670.

Bjerrum, L. 1967. Engineering Geology of Norwegian Normally Consolidated Marine Clays as Related to Settlements of Buildings. *Géotechnique* 17: 81–118.

Borja, R.I. 1984. *Finite Element Analysis of the Time-dependent Behavior of Soft Clays*, PhD thesis, Stanford University, Stanford, xiii, 224 pp.

Britto, A.M. & Gunn, M.J. 1987. *Critical State Soil Mechanics via Finite Elements,* Ellis Horwood Ltd, Chichester, 486 pp. ISBN 0-85312-937-1.

Britto, A.M. & Gunn, M.J. 1990. *CRISP 90, User's and Programmer's Guide* 1/6/90, Cambridge University, Engineering Department, Cambridge, several pagenumber sequences.

Burland, J.B. 1990. On the Compressibility and Shear Strength of Natural Clays, The 30th Rankine Lecture. *Géotechnique* 40: 329–378.

Casagrande, U. 1980. *Taasian saven mekaaniset ominaisuudet* (The Mechanical Behaviour of Taasia Clay), MSc thesis, Helsinki University of Technology, Department of Civil Engineering, Espoo, 62 pp. (In Finnish.)

Cedergren, H.R. 1967. *Seepage, Drainage and Flow Nets*, John Wiley & Sons, New York, 489 pp.

Dafalias, Y.F. 1987. An Isotropic Critical State Clay Plasticity Model. In: *Proceedings of the 2nd International Conference on Constitutive Laws for Engineering Materials*, Arizona 5–8 January 1987, Volume 1, Elsevier, New York, pp. 513–521.

Davis, E.H. & Poulos, H.G. 1963. Triaxial Testing and Three-dimensional Settlement Analysis. In: *Proceedings of the Fourth Australian-New Zealand Conference on Soil Mechanics and Foundation Engineering,* Adelaide 1963, pp. 233–243.

Eisenstein, Z. & Krishnayya, A.W.G. 1972. *Analysis of Cracking of Earth Dams*, University of Alberta, De-

partment of Civil Engineering, Edmonton, xxi, 140 pp.

Graham, J., Crooks, J.H.A. & Lau, S.L.K. 1988. Yield Envelopes: Identification and Geometric Properties. *Géotechnique* 38: 125–134.

Henkel, D.J. 1956. The Effect of Overconsolidation on the Behaviour of Clays During Shear. *Géotechnique* 6: 139–150.

Houlsby, T.T. 1985. The Use of a Variable Shear Modulus in Elastic-Plastic Models for Clays. *Computers and Geotechnics* 1: 3–13.

Houlsby, T.T., Wroth, C.P. & Wood, D.M. 1982. *Predictions of the Results of Laboratory Tests on a Clay Using a Critical State Model,* University of Oxford, Department of Engineering Science, Oxford, O.U.E.L. Report No. 1504/83, SMO42/83, 53 pp.

Hvorslev, M.J. 1937. *Über die Festigkeitseigenschaften gestörter bindiger Böden* (On Some Physical Properties of Remoulded Cohesive Soils), Danmarks Naturvidenskabelige Samfund, Copenhagen, 159 pp. (In German.)

Jaky, J. 1944. A nyugalmi nyomás tényezöje (The Coefficient of Earth Pressure at Rest). *Magyar Mérnök és Epitész Egglet Közlönye* 78: 355–358. (In Hungarian).

Jamiolkowski, M., Leroueil, S. and Lo Presti, D.C.F. 1991. *Theme Lecture: Design Parameters from Theory to Practice*, Paper presented at Geo-Coast '91 – Yokohama, Université Laval, Département de génie civil, Quebec, 40 pp.

Janbu, N., Bjerrum, L. & Kjaernsli, B. 1964. *Veiledning ved løsning av fundamenteringsoppgaver*, Norwegian Geotechnical Institute, Oslo, Publication no. 16, 93 pp. (In Norwegian).

Kallio, T. 1980. *Taasian saven painumisominaisuudet* (The Settlement Behaviour of Taasia Clay), MSc thesis, Helsinki University of Technology, Espoo, 73 pp. (In Finnish.)

Karstunen, M., Näätänen, A. & Lojander, M. 1995. The Effect of Natural Anisotropy of Clays. In: *Proceedings of the Eleventh European Conference on Soil Mechanics and Foundation Engineering*, Copenhagen 28 May – 1 June 1995, Volume 6, Danish Geotechnical Society, Aalborg, Bulletin 11, pp. 6.83–6.88. ISBN 87-89833-00-7.

Korhonen, K-H. & Lojander, M. 1987. Yielding of Perno Clay. In: *Proceedings of the 2nd International Conference on Constitutive Laws for Engineering Materials*, Volume 2, Elsevier Science Publishing Co., New York, pp. 1249–1255.

Korhonen, K-H., Karstunen, M. & Lojander, M. 1991. The Yielding of Anisotropic Cohesive Soils. In: *Proceedings of the Tenth European Conference on Soil Mechanics and Foundation Engineering,* Florence 26–30 May 1991, Volume 1, A.A. Balkema, Rotterdam, pp. 237–241. ISBN 905410 0028.

Krishnayya, A.W.G. 1973a. *Finite Element Non-linear Analysis for Two Dimensional Problems (FENA 2D), Users Manual*, University of Alberta, Department of Civil Engineering, Edmonton, Soil Mechanics No. 19, 27 pp., app.

Krishnayya, A.W.G. 1973b. *Finite Element Consolidation Program for Two Dimensional Problems (FECP 2D), Users Manual*, University of Alberta, Department of Civil Engineering, Edmonton, Soil Mechanics No. 22, 21 pp., app.

Lambe, T.W. 1954. *Soil Testing for Engineers*, John Wiley & Sons, New York, 165 pp.

Leroueil, S., Magnan, J.-P. & Tavenas, F. 1990. *Embankments on Soft Clays*, Ellis Horwood Ltd, New York, 360 pp. ISBN 0-13-275736-2.

Leroueil, S. and Vaughan, P.R. 1990. The General and Congruent Effects of Structure in Natural Soils and Weak Rocks. *Géotechnique* 40: 467–488.

Lojander, M. 1980. *Taasian tekojärven maapadon painumien ja vakavuuden analysointia* (Studies of Settlements and Stability of the Earth Dam of Taasia Artificial Lake), MSc thesis, Helsinki University of Technology, Espoo, 86 pp. (In Finnish.)

Lojander, M. 1988. The Parameters of the Mechanical Model for Anisotropic Clay. In: *X Nordiske Geoteknikermøte, Artikler og Poster-sammendrag*, NGM-88, Oslo, 13–15 Mai, pp. 153–157.

Lojander, M. 1993. Maakerrosten mekaniikka (The Mechanics of Soil Layers). In: Korhonen, K-H., Lojander, M. & Karstunen, M. *Pehmeikölle maan varaan rakennettavan tiepenkereen geotekniset laskelmat* (Geotechnical Calculations of a Road Embankment on a Soft Foundation), Finnish National Road Administration, Geotechnics, Helsinki 1993. (In Finnish.)

Loukola, E. 1985. *Pehmeikölle perustettavan Taasian maapadon jännitykset ja muodonmuutokset* (The Stresses and Strains of the Taasia Earth Dam to be Constructed on Soft Foundation), National Board of Waters, Helsinki, 87 pp., app. (In Finnish with English abstract.) ISBN 951-46-8933-X.

Mesri, G. & Abdel-Chaffar, M.E.M. 1993. Cohesion Intercept in Effective Stress-Stability Analysis. *Journal of Geotechnical Engineering* 119: 1229–1249.

Näätänen, A. & Lojander, M. 1994. The Selection of the Parameters for the Modified Cam Clay Analysis. In: *Proceedings of the 3rd European Conference on Numerical Methods in Geomechanics*, Manchester UK 7–9 September 1994, A.A. Balkema, Rotterdam, pp. 105–110.

Nayak, G.C. & Zienkiewicz, O.C. 1972. Convenient From of Stress Invariants for Plasticity. *Journal of the Structural Division* 98:949-954.

Naylor, D.J. 1978. Stress-Strain Laws for Soil. In: Scott, C.R. (ed.) *Developments in Soil Mechanics-1*,

Applied Science Publishers Ltd, London, pp. 39-68. ISBN 0 85334 7719.

Parry, 1982. Private Communication with Britto, A.M. and Gunn, M.Y. (Ref. Britto & Gunn 1987.)

Pickles, A.R. 1989. *The application of critical state soil mechanics to predict ground deformations below an embankment constructed on soft alluvium,* PhD thesis, City University, Civil Engineering Department, London, 131 pp., app.

Pitkänen, H. 1982. *Taasian maapadon rakennusalueen maaparametrit ja pystyojitussuunnitelma* (The Soil Parameters and Vertical Drainage of the Construction Area of the Taasia Earth Dam), MSc thesis, Helsinki University of Technology, Espoo, 69 pp. (In Finnish.)

Rankama, K. (ed.) 1964. *Suomen geologia* (Geology of Finland), Kirjayhtymä, Helsinki, 414 pp. (In Finnish.)

Roscoe, K.H, Schofield, A.N. & Wroth, C.P. 1958. On the Yielding of Soils. *Géotechnique* 8: 22–53.

Roscoe, K.H, Schofield, A.N. & Wroth, C.P. 1959. Correspondence. On the Yielding of Soils. *Géotechnique* 9: 72–83.

Roscoe, K.H. & Poorooshasb, H.B. 1963. A Theoretical and Experimental Study of Strains in Triaxial Tests on Normally Consolidated Clays. *Géotechnique* 13: 12–38.

Roscoe, K.H, Schofield, M. A. & Thurairajah, A. 1963. Yielding of Clays in States Wetter than Critical. *Géotechnique* 13: 211–240.

Roscoe, K.H. & Burland, J.B. 1968. On the Generalized Stress-Strain Behaviour of "Wet" Clay. In: *Engineering Plasticity*, Cambridge University Press, Cambridge, pp. 536–609.

Schofield, A. & Wroth, P. 1968. *Critical State Soil Mechanics*, McGraw-Hill, London, xx, 310 pp.

Singh, A. & Mitchell, J.K. 1968. General stress-strain-time function for soils. *Journal of Soil Mechanics and Foundations Division* 94: 21–46.

Skempton, A.W. 1957. *Discussion on Planning and Design of the New Hong Kong Airport.* Proceedings of the Institution of Civil Engineers 7: 305–307.

Vepsäläinen, P., Arkima, O., Lojander, M. & Näätänen, A. 1991. The trial embankments in Vaasa and Paimio, Finland. In: *Proceedings of the Tenth European Conference on Soil Mechanics and Foundation Engineering,* Florence 26–30 May 1991, Volume 2, A.A. Balkema, Rotterdam, pp. 633–640. ISBN 905410 0028.

Wood, D.M. 1984. Choice of Models for Geotechnical Predictions. In: *Mechanics of Engineering Materials.* John Wiley & Sons Ltd, New York, pp. 633–654.

Wood, D.M. 1985. Index Properties and Consolidation History. In: *Proceedings of the 11th International Conference on Soil Mechanics and Foundation Engineering,* San Francisco 12–16 August 1985, A.A.2 Balkema, Rotterdam, pp. 703–706.

Wood, D.M. 1986. *Index Properties and Critical State Soil Mechanics. Recent Developments in Laboratory and Field Tests and Analysis of Geotechnical Problems*, A.A. Balkema, Rotterdam, pp. 309–331.

Wood, D.M. 1990. *Soil behaviour and critical state soil mechanics*, Cambridge University Press, Cambridge, 462 pp. ISBN 0-521-33249-4.

Wroth, C.P. 1975. *In-situ Measurement of Initial Stresses and Deformation Characteristics*, Cambridge University, Engineering Department, Cambridge, CUED/C-SOILS TR 23, 51 pp.

Wroth, C.P. 1977. The Predicted Performance of Soft Clay Under a Trial Embankment Loading Based on the Cam-Clay Model. In: *Finite Elements in Geomechanics*, John Wiley & Sons, Chichester, pp. 191–208. ISBN 0-471-99446-4.

Wroth, C.P. 1984. The Interpretation of In Situ Soil Tests. The 24th Rankine Lecture. *Géotechnique* 34: 449–489.

Wroth, C.P. & Wood, D.M. 1978. The Correlation of Index Properties with Some Basic Engineering Properties of Soils. *Canadian Geotechnical Journal* 15: 137–145.

Yong, R.N. & Townsend, F.C. eds. 1980. *Laboratory Shear Strength of Soil*, American Society for Testing and Materials, Philadelphia, 717 pp.

Zace Services Ltd 1993. *Z-soil PC User manual*, Version 2.1, Zace Services Ltd, Lausanne, several page number sequences.

Zienkiewicz, O.C. & Taylor, R.L. 1989. *The Finite Element Method*, McGraw-Hill Book Company (UK) Ltd, London, 648 pp. ISBN 0-07-084174-8.

Appendices 1–4

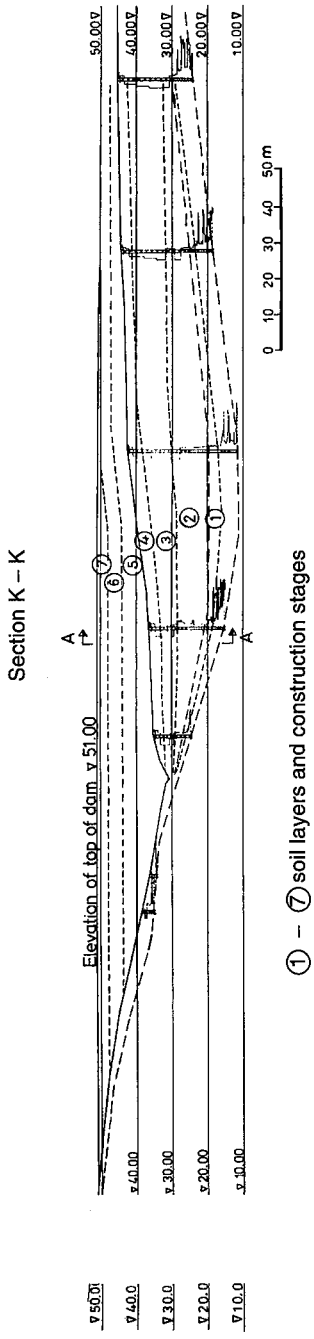

Appendix 1. Longitudinal section of proposed earth dam (Fig. 1).

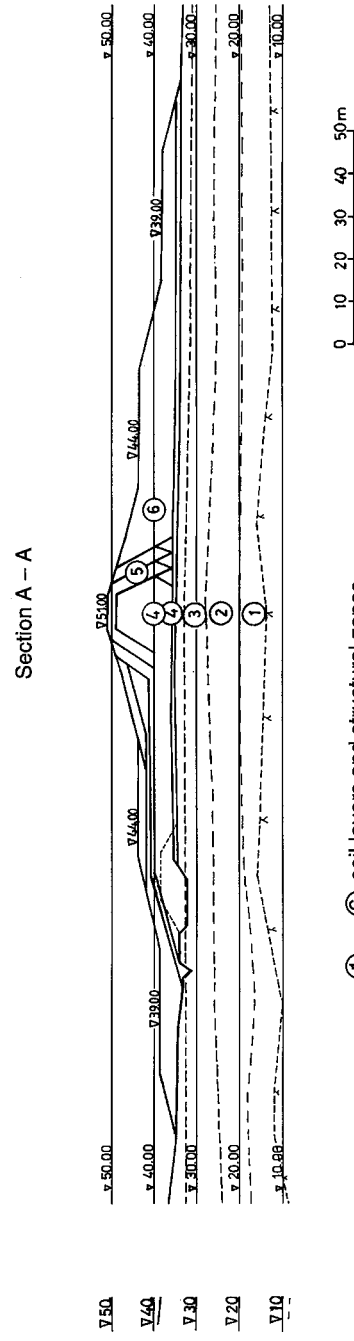

Appendix 2. Cross-section of proposed earth dam (Fig. 1).

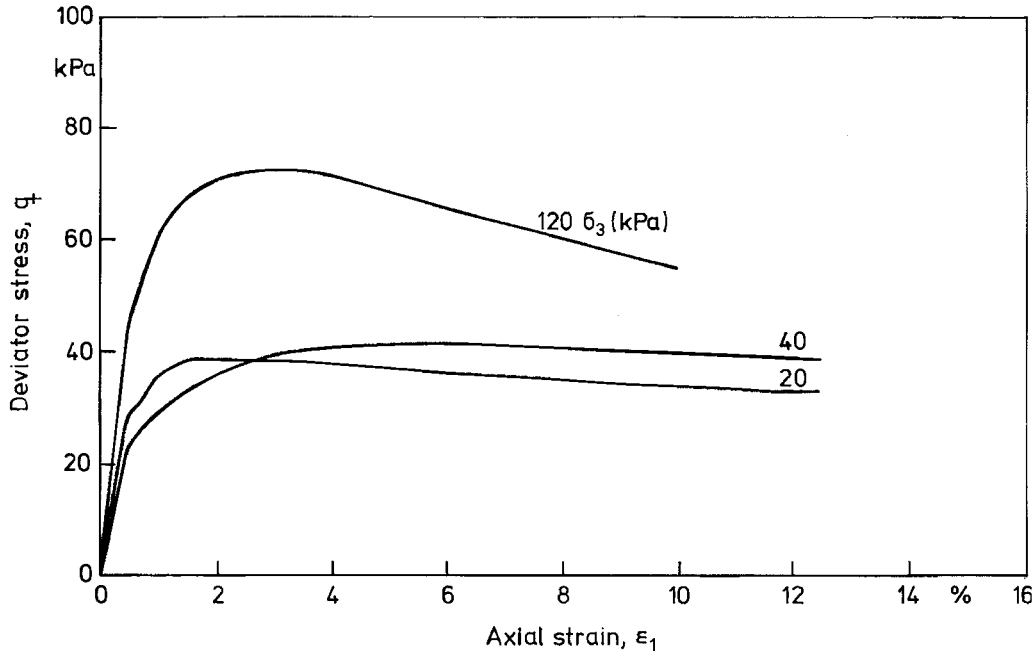

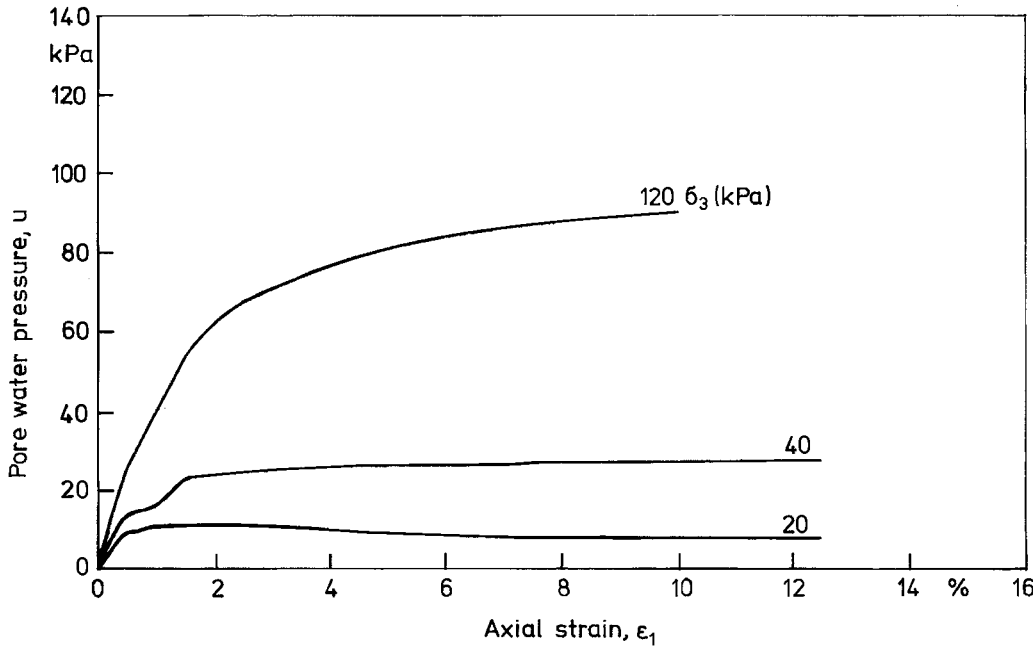

Appendix 3. Foundation of Taasia test embankment. Layer 3. Sample set 1. w = 84–92%. Triaxial CIUC test. Sampling depth 2.47–2.96 m. σ'_{vc} = 90 kPa.

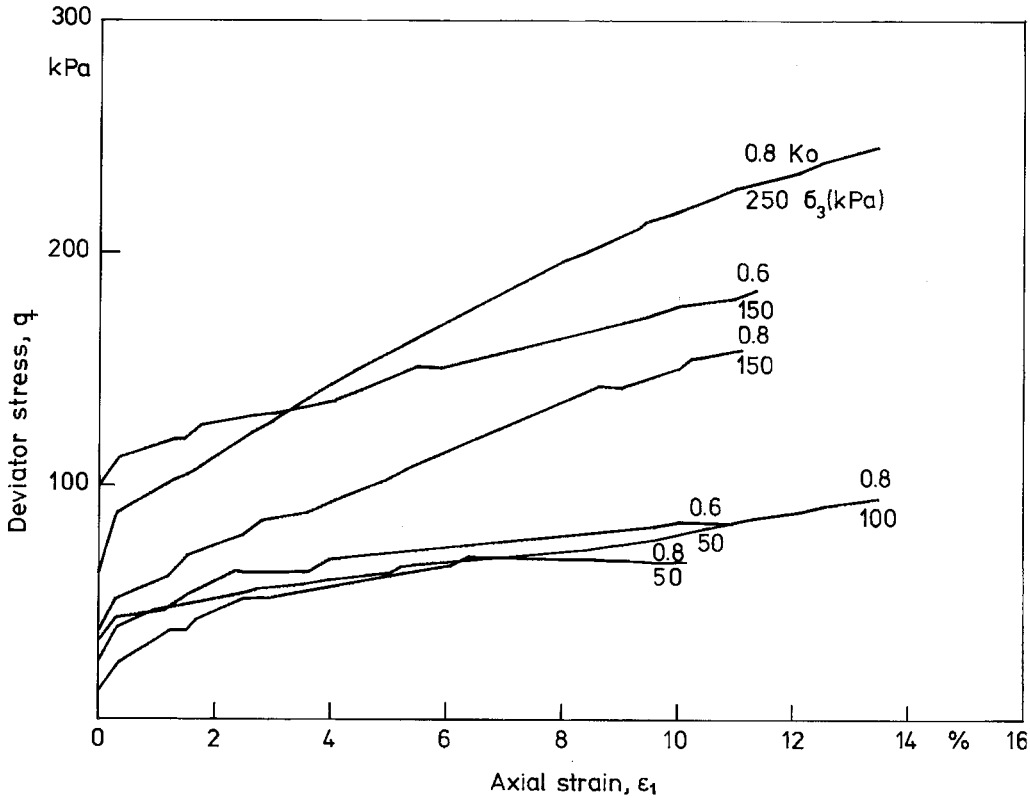

Appendix 4. Foundation of Taasia test embankment. Layer 3. Sample sets 4, 5 and 6. Triaxial CADC test. Samples from level 31.75 m. w = 60–79%. σ'_{vc} = 85 kPa. ε_1 / t = 1.2% d^{-1}.

ISSN 1239-1875
ISBN 952-11-0097-4